high-value products from agricultural residues through sustainable chains

Project number: 101081776

Deliverable D4.1

End-products formulation and end-usages specifications

Workpackage(s) concerned: WP4
Workpackage leader: David Bolzonella (UNIVR)
Deliverable Leader: Hélène Angellier-Coussy (UM)
EC Version: 1.0

Planned delivery date (as in DoA): 30/11/2025 (M36)
Actual submission date:

Funded by the European Union
UK Research and Innovation
中华人民共和国科学技术部
Ministry of Science and Technology of the People's Republic of China

1. Table of content

This project has received funding from the European Union's Horizon Europe research and innovation programme under the grant agreement No. 101081776, the UK Research and Innovation (UKRI) fund under the UK government's Horizon Europe funding guarantee, the Swiss State Secretariat for Education, Research and Innovation (SERI) and from the National Key Research and Development Program supported by the Ministry of Science and Technology of the People's Republic of China (No. 2023YFE0104900). Views and opinions expressed are however those of the author(s) only and do not necessarily reflect those of neither of the aforementioned Funding authorities. Neither the European Union, the United Kingdom, the Swiss Confederation or the People's Republic of China nor the European Commission, UKRI, SERI or NKRDPC can be held responsible for them.

© 2025. This work is openly licensed via a CC-BY-NC-ND

Dissemination Level

P	**Public**	☒
CO	Confidential, only for members of the consortium (including the Commission Services)	☐
CI	Classified, as referred to Commission Decision 2001/844/EC	☐
SEN	Sensitive	☐

Type

R	Document, Report	☒
DEM	Demonstrator, Pilot, Prototype	☐
DEC	Websites, Patent Fillings, Videos, etc	☐
Other	(Please describe the type)	☐

Project Number: 10108176

Project: AgriLoop : pushing the frontier of circular agriculture by converting residues into novel economic, social and environmental opportunities

Topic: HORIZON-CL6-2022-CIRCBIO-01-05

Duration: 48 Months

Start date of Project: 1st December 2022

End date of the Project: 30 November 2026

Coordinator: INRAE

Deliverable: D4.1

Due date of deliverable: 30/11/2025

Actual submission date:

Work package number: WP4

WP Leader (name and organisation): University of Verona (UNIVR)

Person in charge of the deliverable (name and organisation): Hélène Angellier-Coussy (UM)

Author(s): Hélène Angellier-Coussy (UM), Diana Molina Delgado (FCAC), Rita Escórcio (ITQB), Natasha Bizzotto (UNIBO), Bénédicte Bakan (INRAE), Tommaso Barbieri (TOMAPAINT), Giovanna Pesante (UNIVR), Lars Stegemüller (Avecom), Yuexin Yu (HBNACOL), Shi Wang (SDIC), Xiaowei Fei (SJCOF), Chao Liu (SCRG), Linling Fan (SYBT), Ying Wang (BJAMS)

Contributor(s): Hélène Angellier-Coussy (UM), Tatiana Coutand (UM), Stéphane Peyron (UM), Diana Molina Delgado (FCAC), Marius Simon (FCAC), Rita Escórcio (ITQB), Cristina Silva Pereira (IRQB), Natasha Bizzotto (UNIBO), Annamaria Celli (UNIBO), Laura Sisti (UNIBO), Bénédicte Bakan (INRAE), Denis Lourdin (INRAE), Giovanna Pesante (UNIVR), David Bolzonella (UNIVR), Marianna Villano (UNIROMA), Gaia Salvatori (UNIROMA), Lars Stegemüller (Avecom), Laetitia Van Wonterghem (Avecom), Kim Windey (Avecom), Martin Struk (UGent), Korneel Rabaey (UGent), Yuexin Yu (HBNACOL), Lei Qi (HBNACOL) Lanju Xu (HBNACOL), Shi Wang (SDIC), Nan Jiang (SDIC), Xiaoyu Wang (SDIC), Xiaowei Fei (SJCOF), Yunfu Sun (SJCOF), Minghua Zhang (SJCOF), Qincai Sun (SJCOF), Chao Liu (SCRG), Shumiao Zhao (SCRG), Linling Fan (SYBT), Lihui Song (SYBT), Lihui Song (SYBT), Ying Wang (BJAMS), Hao Wei (SYBT)

Version: 1.0

As outlined in the Grant Agreement, deliverable 4.1. is related to the work performed in Tasks 4.1. and 4.2. It reports the relationships between formulation, processing, structure and performance of biopolyester-based materials produced at laboratory-scale. Three strategies have been investigated: blending, composites and multilayers. It also delivers the first results on the production of plant molecules, MPs and PHAs at pilot scale (T4.1, T4.2).

A technical mission in Catalonia, coordinated by FCAC, enabled the **collection of end-user needs** from agricultural cooperatives. Conventional plastics remain dominant. Key barriers to shift towards biodegradable plastics include high costs**,** limited technical knowledge, and retailer resistance. Priority applications for frugal innovation were identified: mulching films, seedling bags, horticultural pots, tree protectors, plant support ropes, labels, and pest control clips.

On the technical side, the work demonstrated that **PHBV purity is critical for film processing**. Only samples with ≥50% PHA content yielded usable films. PHBV-based blends with PBSA, PBAT, and MI3 were successfully developed by BIOMI and tested at pilot scale for the production of **mulching films**. The best-performing films showed mechanical properties comparable to fossil-based (LD-PE) and commercial bio-based (MI3) benchmarks, with elongation at break exceeding 600%.

PHBV/cutin blends were developed by UNIBO, showing a plasticizing effect at low cutin content (≤10%), but reduced mechanical performance at higher concentrations due to poor interfacial compatibility. **Hydrophobic cellulosic papers** were obtained by INRAE using cutin-based coatings, with improved water contact angle and mechanical properties, without significant changes in water vapor or oxygen permeability.

Finally, **PHBV/lignocellulosic biocomposites** were produced by UM using peanut shells. Up to 20 wt% filler was incorporated without major loss in mechanical performance, thanks to good interfacial adhesion promoted by surface roughness and biochemical composition of the fillers.

Plant molecules extraction at pilot-scale progressed both in Europe and in China. **Cutin** was extracted by TOMAPAINT from tomato pomace, with a process yield of 15%, obtaining 250 kg of cutin paste with a solid content of over 60%. SDIC applied **high-efficiency apple polyphenol extraction technology** to green apple pomace, reaching purity up to 81% and a total of 14.1 kg of polyphenol-rich powder. **Proanthocyanidins were extracted from peanut red skins** by SJCOF, with a final product purity up to 99.9%, allowing their future use in the health care, food, medicine or cosmetic markets.

MP production at pilot-scale is underway. AVECOM and UGENT in Europe have finalised lab-scale trials and have set up pilot production to hydrolyse **grey starch from the potato industry leftovers into bacterial proteins** (Cupriavidus necator), yielding up to 88% COD solubilization, a biomass concentration up to 12 g/L and a protein content of 50-66%. The pilot-scale production of **yeast MP** (Saccharomyces cerevisiae) **from fresh distiller's grains** by SCRG in China started in September '2024. However, yields were lower compared to lab-scale production, probably due to the inefficient spray drying process, a problem that is under investigation.

Pilot-scale PHB production by UNIVR **from mixed microbial cultures** allowed the obtaining of PHBV with a purity up to 86.4% when using a combined NaOH & enzymes purification, and an HV content of

18.3-26.2%; the feedstock initially consisted of a synthetic mix of VFAs and then switched to a **real substrate of cow manure and corn leftovers**. HBNACOL utilised **pure cultures** (Cupriavidus necator) and a **feedstock of glucose** to obtain PHB production, whose results were linearly scalable from the initial 5 L volume up to 50 and 800 L, and with PHB content stabilising at around 40%.

Tests in close-to-real conditions are planned for the products under development:

- Feeding trials are planned with **cows and chickens for yeast proteins in China** and with **shrimps and chickens for bacterial proteins in Europe**.
- Field trials of **PHBV-based mulching films** will be performed on **salad and onion crops** in Europe.
- **Biocomposite-based vineyard clips** are at present being tested in vineyards in France.

1. Introduction

How to overcome the reluctance of industry for waste-based products as alternatives to effective usual products from well-functioning value chains with primary resources, knowing how expensive is the pathway to reach equivalent performances from low quality raw materials (Johansson and Krook 2021)? To better tackle this challenge, it has been recently advocated to forget blind mimicking of over-dimensioned oil-based (or primary resource) counterparts, preferring “open eyes” tailored and just necessary performances to fit targeted applications, taking great care of the end-of-life stages as a novel essential driving functions especially in the agri-food sector (Guillard et al. 2018; Doineau et al. 2022). For that purpose, early interactions with the end-users are expected to help to translate their needs into functional properties and then adjust the processing conditions to the just necessary performances.

Three types of end-products were targeted in WP4 of **AgriLoop:**

- **A portfolio of biodegradable materials based on PHBV and/or cutin** to replace conventional plastics in agriculture (e.g., mulching films, clips) and packaging. These lab-scale developments build on knowledge from WP2 (cutin extraction from tomato pomace) and WP3 (production of PHAs with controlled monomer composition and purity).
- **Microbial proteins derived from grey starch or fresh distiller’s grains** for feed applications, with work spanning from lab scale to upscaling.
- **Polyphenols extracted from peanut red skins** for use in healthcare, food, pharmaceutical, and cosmetic markets, also progressing from lab scale to upscaling.

2. First step towards a frugal design mindset for the development of alternatives to conventional plastics: collection of end-users needs regarding the use of plastics in the farming sector (FCAC)

First step towards a frugal design mindset for the development of alternatives to conventional plastics: collection of end-users needs regarding the use of plastics in the farming sector (FCAC)

2.1. Objective of the technical mission

Rather than merely mimicking existing plastics, the frugal design approach seeks to redefine product functionalities (for example, focusing on soil protection, moisture retention, or plant growth enhancement) while minimizing material complexity, processing, and costs. For that purpose, the technical mission organized by FCAC in Catalonia (10–12 June 2024), in collaboration with INRAE and UM, aimed to collect end-users' needs and practical insights regarding the use of plastic materials in agricultural production and packaging. The main objective was **to establish a knowledge base for the frugal design of bio-based and biodegradable materials,** by identifying where, how, and why plastics are used in real farming conditions.

This mission therefore represents the first operational step towards user-centered, frugally designed bio-based products. By engaging directly with farmers and cooperative technical staff, the activity ensured that future PHA-based materials developed within WP4 will directly respond to functional needs and local use conditions, supporting practical adoption and contributing to environmentally sustainable substitution of fossil-derived materials.

. The visits included four cooperatives located in the Maresme and Girona regions:

- **CORMA** – Ornamental plant sector
- **Agrícola El Progrés-Garbí SCCL** – Horticultural sector
- **Conca de la Tordera SCCL** – Horticultural sector
- **Girona Fruits SCCL** – Fruit sector (mainly apple production)

Interviews were held with seven farmers and technical staff (including agronomists) across these cooperatives, and the CEOs or representative staff of each cooperative. The information collected focused on current practices and materials used, the potential for substitution with biodegradable or bio-based materials, and perceived barriers to change.

2.2. Description of the questionnaire

The interviews followed the structured "AgriLoop farmer questionnaire" template (Annex 1), jointly developed under WP1 (Task 1.3 – End-user requirements and safety needs). This ensured consistency in data collection across different regions and user groups.

The questionnaire covered five key areas:

1. Farm profile and production systems (sector, scale, type of crops)
2. Current use of plastics (types, quantities, lifetime, reasons for use)
3. Perceived problems related to plastics (environmental, economic, operational)

4. Experience with alternatives (biodegradable, recycled, or bio-based materials)
5. Expectations and needs for new bio-based materials (functional priorities, cost tolerance, degradation rate, handling)

The main aspects related of each area are:

Section 1. Farm description

- Name / Cooperative
- Sector (fruit, horticulture, ornamental, etc.)
- Cultivated area (ha)
- Main crops / products
- Number of members

Section 2. Use of plastics

- What types of plastics are used (films, pots, nets, ropes, packaging, etc.)?
- Approximate quantities or surface covered?
- Average lifetime of materials?
- Main reasons for choice (price, availability, performance)?

Section 3. Alternatives and experience

- Have you tested biodegradable or bio-based products?
- If yes, what were the results (durability, handling, performance)?
- What are the barriers to wider adoption?

Section 4. Future needs and expectations

- Which functions are most important (protection, growth support, packaging, etc.)?
- What would you expect from a bio-based alternative (degradation time, mechanical strength, cost)?
- Are you interested in collaborating in field trials or co-design activities?

Section 5. Waste and end-of-life management

- How are plastics currently managed after use?
- Is there an existing recycling or collection system?
- Any particular difficulties (cost, regulations, logistics)?

2.3. Main observations

Conventional plastics remain the dominant material used in both field applications (e.g. mulching films, irrigation pipes, protective structures) and post-harvest packaging. Their widespread use is largely justified by their robustness, cost-effectiveness, and compliance with commercial standards.

Alternative materials, such as biodegradable mulching films or seedling bags, have been tested or adopted to a limited extent. In particular, the ornamental and horticultural sectors have carried out small-scale trials with some success.

Packaging innovations using paper, cardboard box or bio-based components (e.g. wrappers with plastic windows) were mentioned, though the adoption of fully transparent biodegradable materials remains very limited due to high cost and lack of suitable commercial biodegradable products.

Market chain dynamics, especially those dictated by supermarket buyers, play a critical role in packaging decisions. Retailers tend to resist changes that affect appearance, shelf-life, or consumer expectations regarding packaging.

Material use snapshot. An indicative overview of material use (from interviews and field observations) highlights the predominance of conventional plastics, with limited but growing interest in alternatives (Table 1).

Table 1. Type of plastics used and corresponding applications.

Material Type	Applications (examples)	Observations
Conventional	Mulching films, irrigation, labels, packaging	27 mentions
Biodegradable	Mulching films, seedling bags, some packaging	4 mentions
Bio-based	Some packaging formats	2 mentions
Other	Experimental materials	1 mention

Visual examples documented during the visits include biodegradable seedling bags (CORMA – Novaplant 2000) (**Figure 1a**), biodegradable mulching film (Conca de la Tordera – Hora Soms) (**Figure 1b**) and bio-based packaging trials (Conca de la Tordera) (**Figures 1c and 1d**).

Figure 1. Examples of plastic products.

Challenges and opportunities. The interviews allowed to highlight that the transition towards bio-based or biodegradable solutions is blocked primarily by **higher prices**, often triple that of conventional materials, **limited technical knowledge** and mixed past experiences, and **lack of consumer and retailer acceptance**, especially in export markets**.** Nonetheless, cooperative staff showed a **willingness to collaborate with research institutes** and participate in further knowledge exchange initiatives, such as those involving UM and INRAE, to explore viable, scalable alternatives.

Some of the most interesting examples as potential applications to be replaced by biobased and biodegradable materials were **plastic trellising ropes**: Used in horticulture greenhouses (Conca de la Tordera) (**Figures 2a and 2b**), **herbicide protection guards for newly planted trees**, as used in Fruit orchards (Girona Fruits) (**Figure 2c and 2d**), **corporate and traceability labels,** used by all cooperatives (**Figure 2e**), and **clips for pest control (e.g. Zeuzera pyrina)** – single-use (**Figure 2f**)

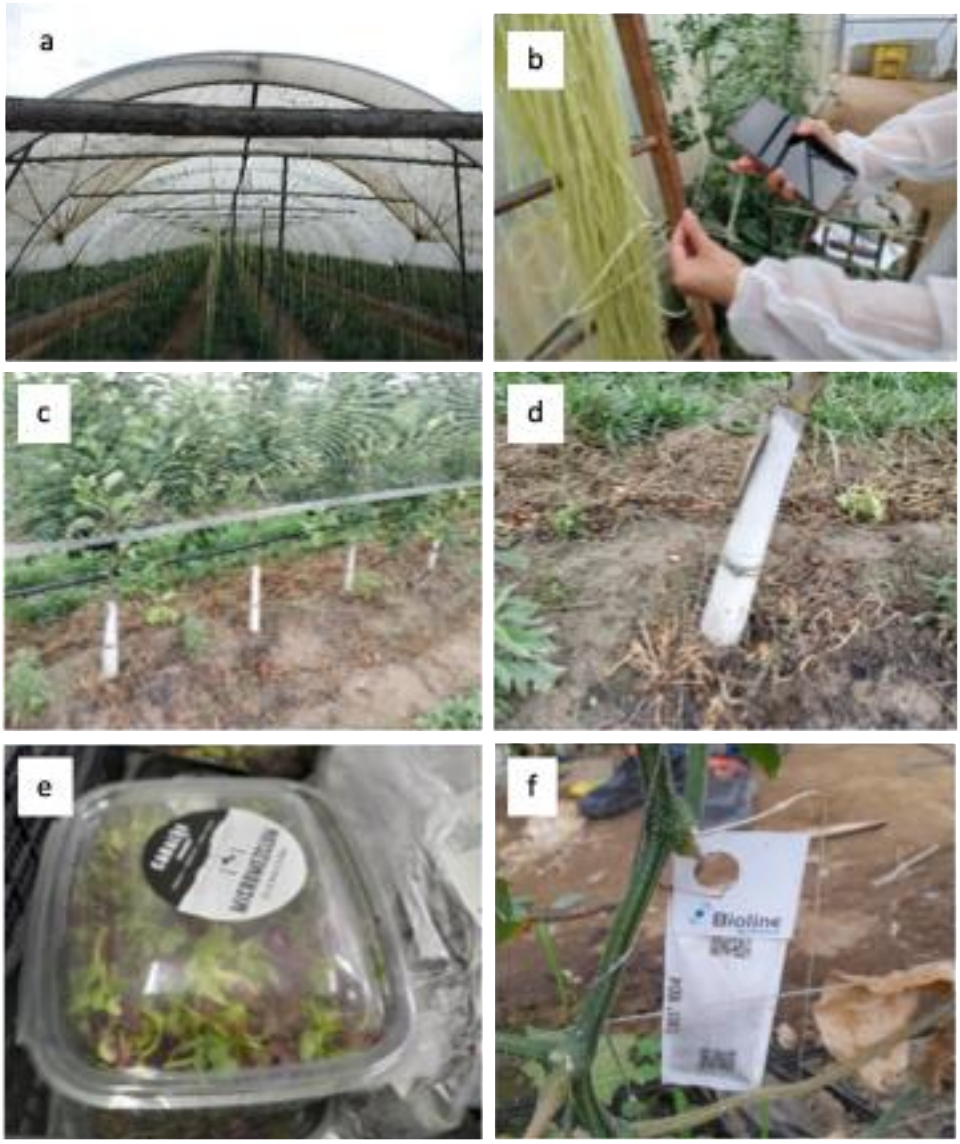

Figure 2. Identification of applications that could be replaced by by biobased and biodegradable materials.

Additional insights from stakeholder Interviews – CORMA and Girona Fruits. To complement the field observations, structured interviews were carried out with representatives from two cooperatives: **CORMA** (ornamental sector) and **Girona Fruits SCCL** (apple producers). These interviews followed the AgriLoop farmer questionnaire template and provide a more detailed view of the plastic applications in use, their service life, and the perceived challenges of switching to alternative materials.

CORMA (ornamental plant production). The operation produces approximately 10 million plants per year across 100,000 m² of cultivated area, with 42% under greenhouse and 58% outdoors. Plastics are mainly used for seedling bags and horticultural pots (around 18 million units annually), transport trays (about 1 million units), and labelling, which involves plastic-based labels and nets (approximately 25 million metres per year), all single-use. Most plastic waste is collected for reuse or recycling. The operation has taken part in EU R&D operational groups focused on biodegradable seedling bags, some

of which are still used by local councils, and has trialled labels and pots made from rice husk. Since the pandemic, there has been a noticeable increase in demand from European customers for recycled or recyclable materials. The company demonstrates strong awareness of sustainability challenges and is open to innovation, although adoption is often limited by functional and economic constraints.

Girona Fruits SCCL (fruit production – apples). The operation spans approximately 700 hectares, primarily focused on apple orchards. Plastics are used in several key areas: growth protectors for young apple trees made from conventional plastic, with a lifespan of up to 20 years; pest control clips (e.g., for Zeuzera pyrina), which are single-use and applied across around 50 hectares annually; and a wide variety of packaging materials, mostly conventional plastics, with some cardboard or wooden alternatives depending on market demands. Hard plastic boxes are reused multiple times, while other packaging is typically single-use. Additional materials include antistone nets with a 15-year lifespan and rubber bands lasting up to 20 years, with usage estimated at 8,000 to 10,000 metres per hectare. Disposal practices are mixed, involving reuse, recycling, and in some cases, leaving materials in the field. Alternatives have been explored, such as textile-based tree protectors, but these failed under field conditions due to exposure to radiation, temperature fluctuations, and humidity. The operation emphasizes the need for minimum resistance and durability in any new material. Packaging decisions are largely driven by supermarket and client specifications, which limits flexibility. While open to alternatives, the operation stresses that any new solution must offer technical performance equivalent to current materials.

2.4. Conclusion and recommandations

The Catalan field mission provided a detailed picture of current plastic uses in different agricultural systems and identified key leverage points for the transition towards bio-based and biodegradable materials. The findings confirm that:

- Functional needs (durability, resistance, cost) are more critical than simply replacing plastics by “green” copies.
- Several priority applications for frugal innovation have been identified: seedling bags, mulching films, horticultural pots, tree protectors, plant support ropes or twines, and labels.
- Stakeholders are open to collaboration with research partners (UM, INRAE, UNIBO, etc.) to test practical alternatives.

This first phase thus anchors the frugal design approach in real user contexts. It will directly inform the formulation and testing of PHA-based composites and coatings in the next stages of WP4 (Tasks 4.1 and 4.2), ensuring that future AgriLoop materials meet genuine field needs with efficient and simplified design strategies.

3. Development of a panel of biopolyester-based materials on a laboratory scale

The aim of Task 4.1 was to design lab-scale materials using microbial polyester (PHBV), plant polyester (cutin), or a combination of both, by exploring the relationships between processing, structure, and properties. The first step focused on assessing how PHBV purity influences its processability under thermomechanical treatment (part 3.1.). Subsequently, three development strategies were pursued for polyester-based materials: polymer blends, multilayer structures, and lignocellulose-reinforced biocomposites.

Blends:

- Blends of PHBV and either PBS, PBSA or PBAT (part 3.2.) for the development of flexible films
- Blends of PHBV and cutin for the development of rigid materials for food packaging (part 3.3.)
- Blends of cutin and carboxymethycellulose for the development of packaging materials with antimicrobial properties (part 3.4/)

Multilayers:

- Cutin-coated papers for the development of hydrophobic packaging materials (part 3.5.)
- Cutin-coated PHBV films for the development of hydrophobic packaging materials (part 3.6.)

Biocomposites:

- PHBV/peanut shells biocomposites for the development rigid items for agricultural application (part 3.7)

3.1. Impact of purity on PHBV processability and performance (UM, UNIROMA, UNIVR)

3.1.1. Introduction

The current high PHAs cost (3–15 times higher than oil-based polymers) and environmental impacts are principally due to the production, extraction and purification steps (Guimarães et al. 2022; Gahlawat et al. 2020). PHA granules are synthesized by bacteria as insoluble cytoplasmic inclusions in the presence of excess carbon when other essential nutrients are limited, such as nitrogen or phosphorous. The granule's core is surrounded by a mix of lipids and proteins, whose role is to regulate the interactions between the apolar polymeric center and its aqueous surrounding. The entire recovery of PHA granules from the cells is thus a necessary and tricky step and includes different successive steps: biomass concentration (using filtration and centrifugation), a pre-treatment to weaken the cell structure, disruption of the non-PHA cell mass (NPCM), the recovery and accumulation of PHAs, the purification and finally the drying. Today, the main challenges of the recovery method are to decrease the environmental impact (toxicity, solvent polluting, energy consumption etc.) and the economic cost, while preserving the physical-chemical properties of the polymer. The research hypothesis is that high purity is not necessary, depending on the target application, and that the degree of purity can be optimized according to the intended application.

In this context, the objective of the present work was **to get better knowledge about the effect of PHAs purity on their processability through thermomechanical treatments,** evaluated though in-depth thermal analysis by Differential Scanning Calorimetry (DSC) and by testing film production using heat pressing. For that purpose, different samples of PHBV (Polyhydroxybutyrate-co-hydroxyvalerate),

with different HV contents and purity levels, were produced in WP3 and provided by the University of Verona (UNIVR) and the University of Roma Sapienza (UNIROMA), and analyzed by the University of Montpellier (UM). A first series of analysis was carried out on samples provided by UNIVR, and a second one on samples provided by UNIROMA.

3.1.2. Materials and methods

3.1.2.1. Raw materials

Samples were codified as Supplier_PHA content_HV content (**Table 2**). For example, sample UVR_21.5PHA_38.3 means that it was supplied by the University of Verona, that the PHA content was 21.5% and the HV content was 38.3 mol%.

3.1.2.2. Pre-treatment by grinding

The received powders were heterogeneous in size, with sometimes extremely rigid blocks. To be able to characterize them by DSC and produce films, a grinding step was necessary to obtain a fine and homogeneous powder. It cannot be ruled out that this treatment could have altered the polymer's properties. For this purpose, a mild ball milling step was performed using a MM400 (Retsch) grinder. 50 mL steel jars were filled with 2 steel balls with a diameter of 15 mm and 1 steel ball with a diameter of 20 mm (grinding media) and PHA powder in the same volume as the balls.

Table 2. List of the PHBV samples considered in the present study

Sample code	PHA content (%)	HV content (mol%)	Quantity (g)
UVR_21.5PHA_38.3HV	21.5	38.3	10
UVR_22.4PHA_24.3V	22.4	24.3	42
UVR_48PHA_0HV	48	0	200
UVR_2.7PHA_17.5HV	2.7	17.5	300
UR_98PHA_27HV	98	27	22.9
UR_96PHA_20HV	96	20	5
UR_80PHA_40HV	80	40	10
UR_77PHA_22HV	77	22	33
UR_74PHA_48HV	74	48	15
UR_42PHA_33HV	42	33	16.7

The UVR_21.5PHA_38.3HV, UVR_22.4PHA_24.3V, UVR_48PHA_0HV, UVR_2.7PHA_17.5HV, UR_98PHA_27HV, UR_96PHA_20HV, UR_77PHA_22HV and UR_42PHA_33HV were easy to grind, and the 30-second 15 Hz setting was sufficient. For the UR_80PHA_40HV sample, several settings were tested, but none of them produced satisfactory results. The sample became a collection of dry agglomerates, most likely due to the heat in the grinder. To avoid the same phenomenon, UR_74PHA_48HV was sieved to 0.560 mm, which limits agglomerates and produces a homogeneous powder.

3.1.2.3. Differential Scanning Calorimetry (DSC)

DSC analyses were performed using a DSC 25 (TA Instruments) under nitrogen atmosphere, at a constant flow rate of 50 mL.min^{-1}. Samples (approximately 5–10 mg) were sealed in 40 µL aluminum pans with pierced lids. Heating and cooling rates were set to 10° C.min^{-1} for all tests, and each experiment was conducted in duplicate. Two different heating/cooling protocols were applied to PHBV pellets. In the first protocol, powders were heated from -50 °C to 220 °C at a rate of 10 °C.min^{-1} in order to define the processing temperature (noted Tp). In the second protocol, powders were first heated from -50 °C to Tp, held at this temperature for the duration required for film preparation (5, 7 or 12 min), then cooled down to -50 °C and held for 2 minutes, and finally heated up to 200 °C, at a rate of 10 °C.min^{-1}. Melting temperature (Tm), glass transition temperature (Tg), melt crystallization temperature (Tc) and cold crystallization temperature (Tcc) were determined from DSC curves. Melting and cold crystallization enthalpies were calculated by integrating the respective peaks, normalized by initial sample mass. Overall theoretical degree of crystallinity (Xc, in %) was calculated using Equation 1, based on the melting enthalpy (ΔHm) and enthalpy of cold crystallization (ΔHcc), where ΔHm0 is the melting enthalpy of a 100% crystalline PHBV, i.e., 146 J.g^{-1} (Barham et al. 1984b).

$$\mathrm{Xc}\ (\%) = \frac{\Delta \mathrm{Hm} - \Delta \mathrm{Hcc}}{\Delta \mathrm{Hm}_0} \mathrm{x}100 \quad \text{(equation 1)}$$

3.1.2.4. Production of films by thermopressing

The aim of this experiment is to analyse the ability of unpurified PHAs to form films (when the available quantity of polymers was sufficient, i.e. of at least 10 to 15g). Polymers were dried at 60 °C under vacuum during 24 hours and then shaped in films by compression molding using a heated hydraulic press (20T, Pinette Emidecau Industries). The processing temperature (Tp) has been selected from DSC analysis (**Table 3**). Five processing steps were followed: (1) contact with plates at Tp for 5 min, (2) then pressing at Tp for 30 s under 50 bar, (3) followed by pressing at Tp for 30 s under 100 bar, (4) then pressing at Tp for 60 s under 150 bar and (5) finally cooling during 10 minutes at room temperature. Produced films were then stabilized under vacuum at 25 °C and 50% HR for a minimum of 14 days before further characterization. Three mold thickness have been used, i.e. either 100, 200 or 300 µm, depending on the available quantity of polymer. The mass of polymers deposited in the mold was adjusted accordingly.

For UVR_22.4PHA_24.3HV, UVR_48PHA_0HV and UVR_2.7PHA_17.5HV sample, a plasticizing effect has been explored, using glycerol as plasticizer, at a content of 10, 20 and 30 wt%.

Table 3. Processing temperatures (Tp) tested for the production of films using a heating hydraulic press

Sample code	Tp (°C)
UVR_22.4PHA_24.3V	120, 125, 130 and 180
UVR_48PHA_0HV	160, 172, 175, 180 and 185
UVR_2.7PHA_17.5HV	170
UR_96PHA_20HV	-
UR_98PHA_27HV	170

UR_80PHA_40HV	170
UR_77PHA_22HV	170
UR_74PHA_48HV	170
UR_42PHA_33HV	170

3.1.2.5. Tensile tests

Nominal tensile properties (Young's Modulus, stress at break and strain at break) of thermoshaped films have been measured with two different devices. For the UVR_22.4PHA_24.3HV and UVR_48PHA_0HV samples, tests were conducted with a texture analyzer (TAXT+, Stable Microsystem Swantech). Given the poor mechanical properties of materials, a tensile tester (INSTRON 68SC-5) equipped with a 2 kN load cell was used for the other films. In both cases, measurements were performed on stripes 5 mm wide, with a crosshead speed set at 10 $mm.min^{-1}$.

3.1.3. Results and discussion

3.1.3.1. Thermal properties

The melting behaviour of the PHBV sample was analysed using Differential Scanning Calorimetry (DSC) to determine the appropriate processing temperature. During the first heating scan up to 200 °C, two distinct melting peaks were observed for some samples, indicating the presence of two populations of crystalline structures. For instance, in the UVR_48PHA_0HV sample (**Figure 3**), the first melting peak (Tm1) appeared broad, suggesting a less ordered or heterogeneous crystal population. The second peak (Tm2) was sharper and more defined, corresponding to the melting of more stable and well-organized polymer crystals.

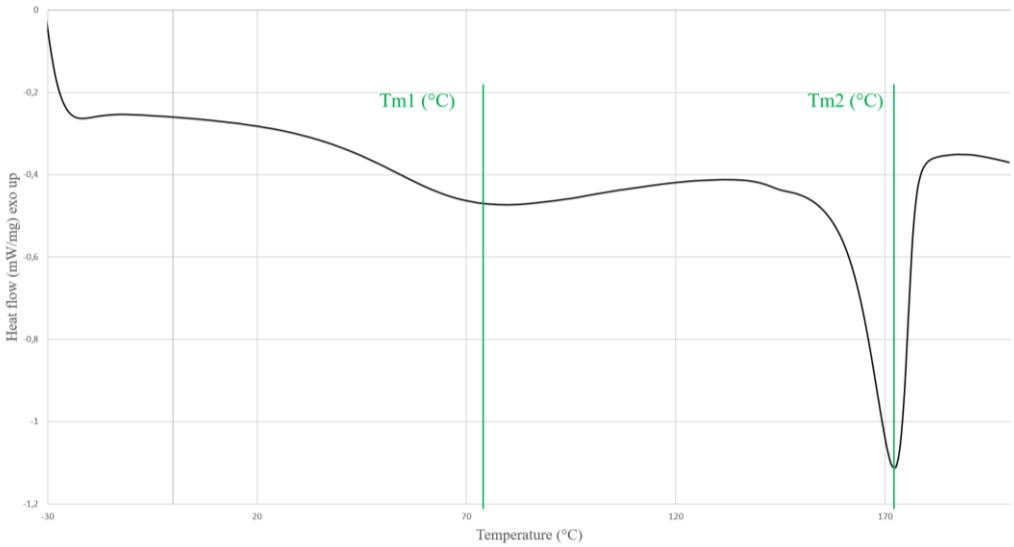

Figure 3. DSC thermogram obtained during the first heating scan of UVR_48PHA_0HV

For samples provided by UNIROMA, heating–cooling–heating cycles were conducted using various pre-heating temperatures (Tp) to determine the optimal processing temperature based on the crystallization behaviour of the copolymers. The optimal temperature was defined as the one that enables crystallisation from the molten state while minimizing cold crystallization. Based on prior results obtained during the initial heating ramp up to 200 °C, a specific range of Tp values was selected for each sample. This strategy aimed either to deliberately promote heterogeneous nucleation by completely erasing the thermal history of the copolymer (i.e., full melting of crystals), or conversely, to favour self-nucleation by partially melting the crystalline structures.

Different behaviours were observed depending on the HV content and purity, illustrated by the following sample-specific observations (**Table 4**).

- **UR_98PHA_27HV**: The sample exhibiting the highest purity showed a single melting peak around 104 °C during the first heating ramp. Initial crystallization tests conducted at pre-heating temperatures (Tp) of 130 °C and 150 °C revealed that increasing Tp enhances crystallization, as evidenced by a slight rise in crystallization temperature (Tc) and enthalpy values, from 25 ± 1 J/g to 32 ± 1 J/g, along with sharper crystallization peaks. This behaviour

was unexpected, as Doineau et al. (2023) had previously reported a progressive decrease in melt crystallization temperature with increasing Tp, culminating in its disappearance at 200 °C due to the inability of P(3HB-co-3HV) to reorganize into a crystalline structure once all nuclei are eliminated (Doineau et al. 2023). Surprisingly, a test at Tp = 170 °C—initially presumed to induce degradation and inhibit crystallization—revealed a well-defined crystallization peak at 66 ± 1 °C. This result led to the recommendation of 170 °C as the optimal pre-heating temperature for film production.

- **UR_96PHA_20HV**: During the first heating ramp, two distinct melting peaks were observed at approximately 100 °C and 152 °C, which justified the choice of a pre-heating temperature (Tp) above 170 °C. For this sample, the expected effect of Tp was confirmed: when Tp was set to 200 °C, no crystallization peak appeared during cooling, and surprisingly, no crystallization occurred at all—explaining the absence of a melting peak during the second heating ramp. In contrast, at Tp = 170 °C, melt crystallization was clearly observed at 96 ± 0 °C, indicating that this temperature is suitable for thermal processing using the press.

- **UR_80PHA_40HV**: This sample exhibited poor reproducibility, characterized by the presence of two to three melting peaks and significant variability in enthalpy values during the same heating ramp. This inconsistency is likely due to compositional heterogeneity within agglomerates formed during the grinding process. Thermal processing trials at 170 °C and 180 °C were conducted but proved unsuitable for pressing, as the material did not respond adequately to these conditions.

- **UR_77PHA_22HV**: This sample exhibited a behaviour similar to UR_96PHA_20HV, with cold crystallization occurring in the absence of melt crystallization, as expected.

- **UR_74PHA_48HV**: Two melting peaks were observed during the first heating ramp, around 71 °C and 147 °C, although these do not correspond to the polymer's melting behaviour, as it is expected to be amorphous. Thermal processing tests at 150 °C and 170 °C confirmed the absence of crystallization, supporting the amorphous nature of the material. Among these, Tp = 170 °C was preferred, as it allowed clear visualization of the second melting peak.

- **UR_42PHA_33HV**: This sample exhibited behaviour similar to the previous one. Both processing temperatures, 145 °C and 175 °C, were retained for press trials, as they were considered suitable for evaluating thermal behaviour and material response.

Table 4. Temperatures and enthalpies of thermal transitions (melting, crystallization, glass transition, and cold crystallization) of the samples according to Tp.

Sample code	First heating ramp				Tp (°C)	Cooling ramp		Second heating ramp						
	T_{m1} (°C)	T_{m2} (°C)	ΔH_{m1} (J/g)	ΔH_{m2} (J/g)		T_c (°C)	ΔH_c (J/g)	T_g (°C)	T_{cc} (°C)	ΔH_{cc} (J/g)	$T_{m1'}$ (°C)	$T_{m2'}$ (°C)	$\Delta H_{m1'}$ (J/g)	$\Delta H_{m2'}$ (J/g)
UR_98PHA_27HV	104 ± 2	-	55 ± 4	-	130	63 ± 0	25 ± 1	-7 ± 1	-	-	113 ± 1	-	28 ± 0	
UR_98PHA_27HV	104 ± 2	-	55 ± 4	-	150	68 ± 1	32 ± 1	-8 ± 1	-	-	117 ± 1	-	40 ± 1	
UR_98PHA_27HV	104 ± 2	-	55 ± 4	-	170	66 ± 1	32 ± 1	-8 ± 1	-	-	113 ± 0	-	44 ± 2	
UR_96PHA_20HV	100 ± 1	152 ± 1	28 ± 4	9 ± 2	170	96 ± 0	47 ± 2	-11 ± 0	-	-	136 ± 1	147 ± 1	51 ± 1	
UR_96PHA_20HV	100 ± 1	152 ± 1	28 ± 4	9 ± 2	200	-	-	-32 ± 0	-	-	-	-	-	-
UR_80PHA_40HV	73 ± 1	153 ± 9	19 ± 1	15 ± 15	170	89 ± 4	11 ± 0	-10 ± 2	-	-	145 ± 9	-	11 ± 2	-
UR_80PHA_40HV	73 ± 1	153 ± 9	19 ± 1	15 ± 15	180	79	9	-10 ± 2	-	-	144 ± 7	-	15 ± 6	-
UR_77PHA_22HV	109 ± 1	151 ± 2	23 ± 5	5 ± 1	170	81 ± 7	27 ± 8	-4 ± 1	-	-	132 ± 6	146 ± 6	34 ± 8	
UR_77PHA_22HV	109 ± 1	151 ± 2	23 ± 5	5 ± 1	200	-	-	-14 ± 4	66 ± 1	11 ± 2	106 ± 4	126 ± 3	16 ± 2	
UR_74PHA_48HV	71 ± 1	-	19 ± 1	-	150	-	-	-14 ± 0	-	-	161 ± 8	-	4 ± 1	-
UR_74PHA_48HV	71 ± 1	147 ± 5	19 ± 1	8 ± 3	170	-	-	-15 ± 0	-	-	-	-	-	-
UR_74PHA_48HV	71 ± 1	147 ± 5	19 ± 1	8 ± 3	200	-	-	-11 ± 0	-	-	-	-	-	-
UR_42PHA_33HV	102 ± 2	-	25 ± 3	-	145	-	-	-15 ± 0	-	-	-	-	-	-
UR_42PHA_33HV	102 ± 2	-	25 ± 3	-	175	-	-	-19 ± 1	-	-	-	-	-	-
UR_42PHA_33HV	102 ± 2	-	25 ± 3	-	200	-	-	-28 ± 4	-	-	-	-	-	-

3.1.3.2. Processability of PHAs for the production of films

A first series of tests was conducted on the UVR_48PHA_0HV sample. The resulting films were heterogeneous and brittle, with a dark brown coloration, appearing almost black in some areas. These visual characteristics suggest thermal degradation during shaping, likely due to a Maillard reaction (**Figure 4**). Following this preliminary study, the idea of using glycerol as a plasticizer was proposed and mold thickness of at least 200 µm. to favour cohesion.

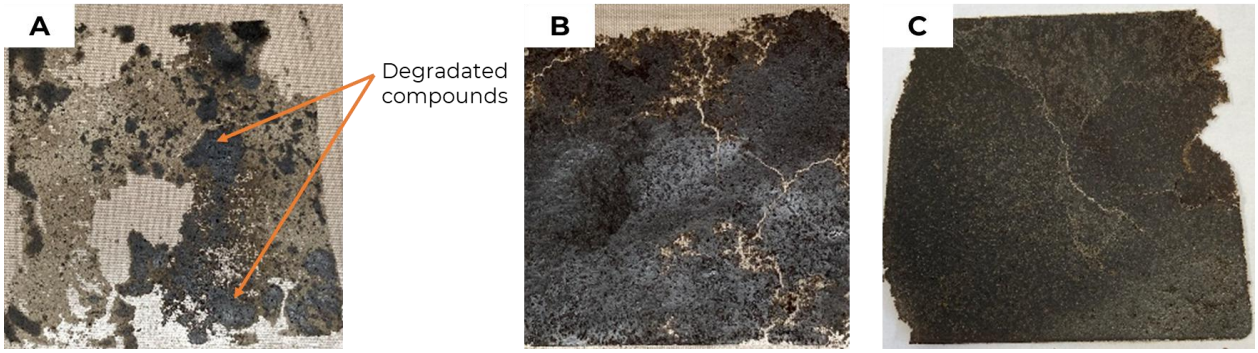

Figure 4. UVR_48PHA_0HV-based films obtained by thermopressing at 180 °C, using with a mold thickness of (A and B) 100 µm and (C) 200 µm.

The plasticizing effect of glycerol was investigated in a second phase. Initial tests were carried out with 20 wt% and 30 wt% glycerol on the UVR_22.4PHA_24.3HV and UVR_48PHA_0HV samples. However, phase separation led to glycerol exudation, compromising film integrity. At 20 wt%, the films appeared more homogeneous, although they remained very fragile and brittle. Based on these observations, a glycerol content of 10 wt% was selected for further testing on the three samples provided by UNIVR (UVR_22.4PHA_24.3HV, UVR_48PHA_0HV, and UVR_2.7PHA_17.5HV) (**Figure 5**). For UVR_22.4PHA_24.3HV, the resulting film was still brittle but homogeneous enough to allow mechanical testing. In contrast, the UVR_48PHA_0HV film remained highly brittle and heterogeneous, with holes that prevented any mechanical characterization. The UVR_2.7PHA_17.5HV sample yielded a film that was extremely brittle and lacked any mechanical integrity. These results highlight the need for non-purified PHAs with a minimum PHA content of 50% to achieve suitable film properties.

A third series of tests was conducted using samples provided by Sapienza University of Rome. Observations (**Figure 6**) revealed varying film properties depending on composition. The UR_98PHA_27HV sample produced a film with some heterogeneities but good mechanical integrity. The UR_96PHA_20HV film also showed heterogeneities, but was more brittle and less robust than UR_98PHA_27HV. The UR_77PHA_22HV sample yielded a film with good integrity, although it contained dispersed agglomerates, indicating that reduced purity negatively affects film homogeneity when compared to UR_96PHA_20HV. The UR_74PHA_48HV film had acceptable integrity but appeared more fragile and brittle than UR_77PHA_22HV, likely due to its high HV content. Finally, the UR_42PHA_33HV sample resulted in a brittle film with no mechanical integrity, confirming the previous conclusion that a minimum PHA content of 50% is required to achieve film-forming properties.

	UVR_2.7PHA_17.5HV		UVR_22.4PHA_24.3HV				UVR_48PHA_0HV			
Glycerol content (wt%)	0	10	0	10	20	30	0	10	20	30
Film picture	Impossible to shape		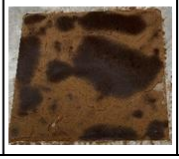		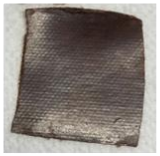			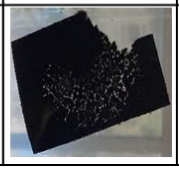	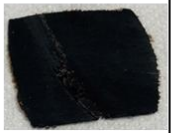	Impossible to shape

Figure 5. Pictures of thermopressed films obtained from UNIVERONA samples, with and without the addition of glycerol as plasticizer.

	UR_98PHA_27HV	UR_96PHA_20HV	UR_77PHA_22HV	UR_74PHA_48HV	UR_42PHA_33HV
Film picture					

Figure 6. Pictures of thermopressed films obtained from UNIROMA samples

3.1.3.3. Mechanical performance of films

Mechanical testing was performed whenever homogeneous films could be obtained. Measurements were carried out on the UVR_22.4PHA_24.3HV sample with glycerol contents of 10 wt% and 20 wt%, as well as on the UR_98PHA_27HV sample (**Table 5**). The materials exhibited low mechanical strength and high fragility, with stress at break values ranging from 3 to 13 MPa. Standard deviations were relatively high due to the presence of film heterogeneities, which acted as stress concentrators and initiated premature failure.

Table 5. Stress and strain at break, and Young's modulus of UVR_22.4PHA_24.3HV with 10 and 20wt% glycerol and UR_98PHA_27HV

Sample	Stress at break (MPa)	Strain at break (%)	Young's Modulus (MPa)
UVR_22.4PHA_24.3HV 10wt% glycerol	13 ± 6	4 ± 2	n.m.
UVR_22.4PHA_24.3HV 20wt% glycerol	6 ± 5	4 ± 1	n.m.
UR_98PHA_27HV	3 ± 1	0.5 ± 0.1	800 ± 100

3.1.4. Conclusion

In conclusion, this project highlights the importance of PHA composition and the role played by its various components, such as biomass and impurities. To enable film formation, the polymer must be grindable or sievable to obtain a fine and homogeneous powder. Additionally, if the PHA is semi-crystalline, it must be able to recrystallize during the cooling phase. So far, only two polymers—UR_98PHA_27HV and UR_74PHA_48HV— could successfully be converted to analyzable films. Of these, mechanical properties have only been assessed for UR_98PHA_27HV, revealing that it is highly brittle. Future work should explore blending these PHAs with other polymers to improve their processability and mechanical performance. Moreover, other shaping processes such as extrusion (compounding step) and injection molding for the production of bulk parts could prove more suitable than film pressing for certain applications.

3.2. PHBV-based blends for mulching films (BIOMI)

3.2.1. Introduction and overall methodology

Over 36 months, BIOMI performed a total of 8 trials. Trial 2 was specifically focused on evaluating the performance of the fossil-based benchmark (LD-PE), while the 3rd trial examined the performance of the bio-based and soil biodegradable MI3 benchmark. With trials 1, 4, 5, and 6, BIOMI worked on developing 13 different PHBV-based formulations for mulching films. These formulations were produced on a pilot scale equipment following the same process methodology in every trial. Initially, before processing, raw materials were characterized for their physical properties such as density (ASTM D792) and moisture (ASTM 6980), as well as their rheological properties including the melt flow index – MFR (ISO 1133), and their thermal properties using differential scanning calorimetry – DSC (ASTM D3418). To prevent degradation during processing, all materials were dried in hot air dryers. The production process involved compounding on a twin-screw extrusion line. The resulting granules underwent thorough characterization following aforementioned standards. The insights gained from this characterization were then used to make the necessary adjustments to the production process. Following that, blow extrusion lines were used to produce flexible mulching films, which were subsequently characterized for their mechanical properties under standard ASTM D882.

Based on the results of processability and characterization from these trials, the best 3 formulations were scaled up in the 7th trial using commercially available PHBV. During that trial, 3 formulations were obtained resulting in 7 different film samples. Two formulations selected from the 7th trial (PHBV(L)/PBSA and PHBV(L)/PBAT) and one additional backup (PHBV(L)/MI3) were scaled up in the 8th trial using PHBV produced and received by UNIVR, as well as PHBV from Paques Biomaterials. In this trial, 9 formulations were obtained and from them 8 different film samples.

3.2.2. 1st trial

In September 2023, the first trial was conducted, during which neat PHBV and blends with acetyltributylcitrate as plasticizer and/or PBS, were tested. A commercial grade of PHBV was considered. The formulations were successfully extruded using a twin-screw extruder and characterized according to their thermal, rheological, and physical properties based on relevant standards: ASTM D3418 (Differential Scanning Calorimetry – DSC), ISO 1133 (Melt Flow Rate – MFR), ASTM D792 (Density), and ASTM 6980 (Moisture content) (**Table 6, Figure 7**).

Table 6. Characterization of PHBV-based compounds – 1st trial

Formulation	Tm (°C)	MFR (g/10 min) (180 °C - 2.16 kg)	Density, ($g.cm^{-3}$)	Moisture content (%)
neat PHBV	171	10.9	1.191	0.458
PHBV/plasticizer	170	15.3	1.148	0.273
PHBV/PBS	116; 167	7.5	1.251	0.249
PHBV/PBS/plasticizer	108; 166	17.6	1.263	0.226

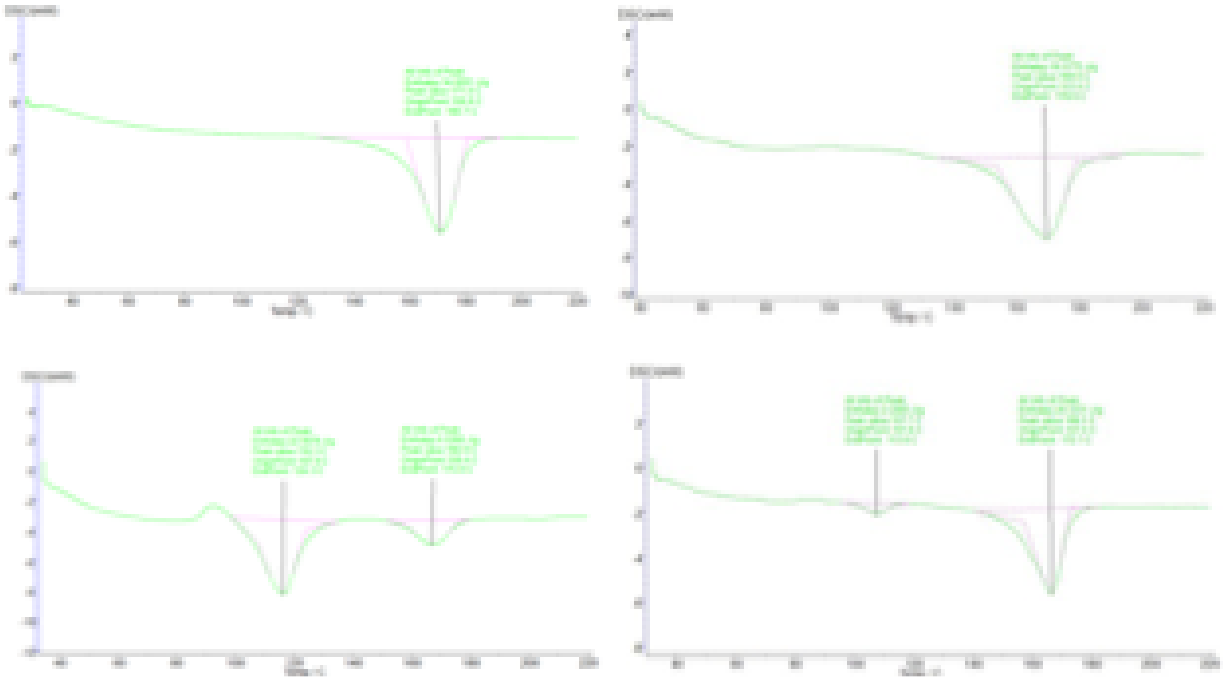

Figure 7. DSC thermograms of neat PHBV (top-left), PHBV/plasticizer (top-right), PHBV/PBS (bottom-left), PHBV/PBS/plasticizer (bottom-right)

The produced and characterized compounds were successfully extruded into films using a cast extruder, without any issues (**Figure 8a**). Some samples were sent to UNIBO, as substrates for the development of multilayer materials (**Figure 8b**).

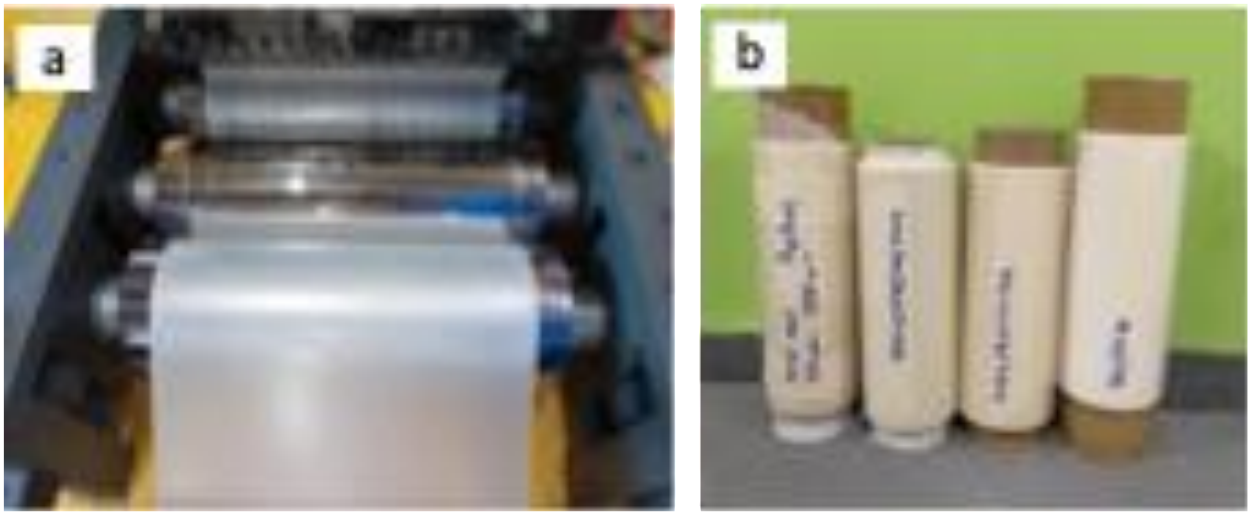

Figure 8. (a) Cast extrusion (1st trial) to obtain the (b) PHBV-based rolls that were sent to UNIBO.

In accordance with ASTM D882, the mechanical properties of the films were evaluated using a tensile testing machine. Results are presented in **Table 7**.

Table 7. Mechanical properties of PHBV-based films – 1st trial

	neat PHBV	PHBV/plasticizer	PHBV/PBS	PHBV/PBS/plasticizer
Tensile strength (break), MPa	29.2 ± 2.2	24.3 ± 1.1	26.2 ± 0.7	23.5 ± 0.5
Tensile strength (yield), MPa	28.9 ± 2.0	24.8 ± 0.4	23.9 ± 0.4	23.2 ± 0.2
Elongation (break), %	3.0 ± 0.5	3.2 ± 0.1	321.9 ± 3.0	4.5 ± 0.2
Elongation (yield), %	2.9 ± 0.5	3.3 ± 0.1	6.8 ± 1.1	4.5 ± 0.2
Elastic modulus, MPa	1650 ± 28	1363 ± 42	651 ± 43	2281 ± 287
Thickness, µm	153	153	64	145
Width, cm	38.5	29.0	30	29.5

3.2.3. 2nd and 3rd trial: benchmarks

The objective of the second and third trials was to establish reference benchmarks for evaluating the performance of the packaging materials developed during the project. The second trial, conducted with the fossil-based LD-PE, provided essential data on the behaviour of a conventional, non-biodegradable polymer, serving as a baseline for interpreting the performance of bio-based alternatives (**Table 8, Figure 9**). In parallel, the third trial focused on MI3, a commercial bio-based and biodegradable material, offering key reference data to assess the functional properties and behaviour of the newly developed bio-based materials. MI3 is one of the 15 formulations that holds the OK SOIL TÜV certificate for granulates and mulch films. In terms of composition, it should be similar to the formulations that are developed in the frame of the Agriloop project. Besides proven biodegradability and very good mechanical properties, the MI3 blend is easy to process due to balanced mixing, good density, and suitable MFI for blown film extrusion, which is the only technology used for producing mulch films. Together, these trials enabled a robust comparative evaluation framework.

Table 8. Characterization of LD-PE compounds (2nd trial) and MI3 compounds (3rd trial)

Formulation	Tm (°C)	MFR (g/10 min) (160 °C - 2.16 kg)	MFR (g/10 min) (190 °C - 2.16 kg)	Density, ($g.cm^{-3}$)	Moisture content (%)
Fossil-based benchmark LD-PE	112.5	0.8	2.2	0.930	0.153
Bio-based benchmark	110.6	1.8	-	1.241	0.425

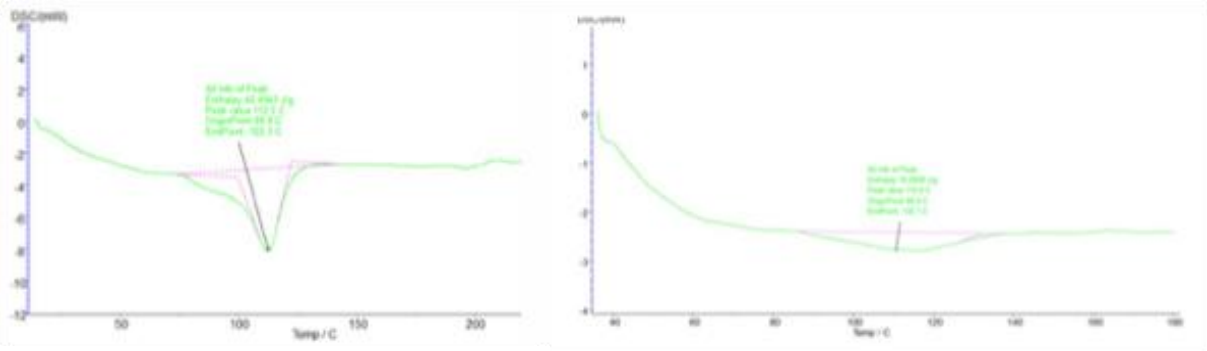

Figure 9. DSC thermograms of LD-PE (left) and MI3 (right).

Starch-based MI3 material was produced on twin screw extruder. To avoid thermal degradation, temperatures between 110 and 150 °C were applied. The process was stable (**Figure 10**). Films were then extruded on blow extruder (at temperatures between 175 and 190 °C for LD-PE) without issues (**Figure 11**). Films were characterized according to ASTM D882 and mechanical properties are presented in **Table 9**.

Figure 10. Compounding process of bio-based benchmark "MI3" – 3rd trial

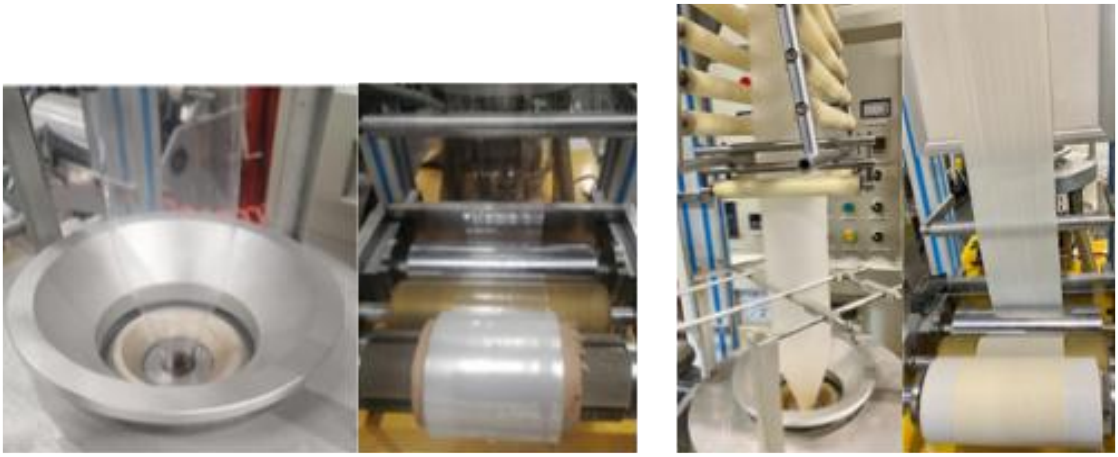

Figure 11. Film (blow) extrusion of LD-PE (left) and MI3 (right)

Table 9. Mechanical properties of LD-PE film (2nd trial) and MI3 film (3rd trial)

	Fossil-based benchmark LD-PE	Bio-based benchmark MI3
Tensile strength (break), MPa	20.8 ± 0.1	21.9 ± 1.3
Tensile strength (yield), MPa	9.5 ± 0.2	9.9 ± 0.7
Elongation (break), %	325.9 ± 39.7	580.3 ± 60.6
Elongation (yield), %	9.0 ± 0.8	7.2 ± 2.8
Elastic modulus, MPa	312.0 ± 9.5	133 ± 9
Thickness, µm	34	20
Width, cm	13.0	14.0

3.2.4. 4th trial: PHBV/PBSA blends

In the fourth trial, different ratios of PHBV (Tianan Enmat Y100P) and PBSA (BioPBS FD92PM) biopolymers were evaluated. Three formulations were tested, each containing low (L, i.e. between 10 and 30% of PHBV), medium (M), and high (H) levels of PHBV. During the compounding step, temperatures were maintained between 130 °C and 150 °C to prevent thermal degradation. The process was stable, and no issues were encountered (**Figure 12**). The produced materials were characterized according to the aforementioned standards, and the results are shown in **Table 10**. The melting behaviour is shown on **Figure 13**.

Figure 12. Compounding process (left) and film (blow) extrusion (right) of PHBV/PBSA formulations – 4th trial

Table 10. Results of the characterization of PHBV/PBSA compounds – 4th trial

Formulation	Tm (°C)	MFR (g/10 min) (160 °C - 2.16 kg)	MFR (g/10 min) (190 °C - 2.16 kg)	Density, ($g.cm^{-3}$)	Moisture content (%)
PHBV(L)/PBSA	89,3/168,3	No flow	9.3	1.222	0.151
PHBV(M)/PBSA	88,1/168,4	0.3	13.7	1.203	0.302

PHBV(H)/PBSA	87,3/169,4	No flow	17.5	1.218	0.377

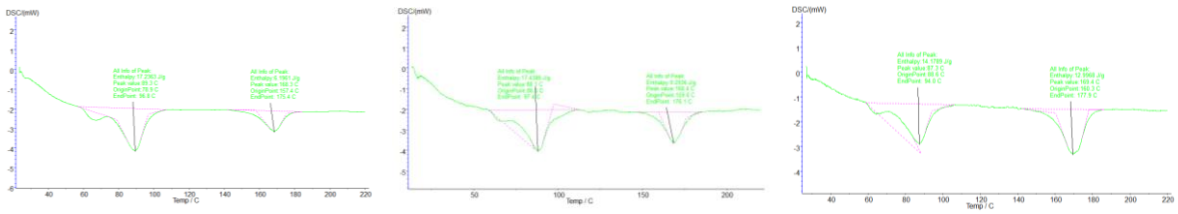

Figure 13. DSC thermograms of PHBV(L)/PBSA (left), PHBV(M)/PBSA (middle), PHBV/PBSA (right)

All three formulations were evaluated using a blow extruder (Figure 12). For formulations with a low amount of PHBV, lower temperatures (150–160 °C) were used, making it easier to extrude the films. In contrast, when extruding materials with a high percentage of PHBV, slightly higher temperatures (160–170 °C) were necessary. However, the resulting films were sticky and tacky, making them difficult to open. The mechanical properties of the produced films were tested in the same manner as in previous trials, and the results of the characterization are shown in **Table 11**.

Table 11. Mechanical properties of PHBV/PBSA films – 4th trial

	PHBV(L)/PBSA	PHBV(M)/PBSA	PHBV(H)/PBSA
Tensile (break), MPa	27.2 ± 1.4	26.6 ± 1.0	24.0 ± 2.2
Tensile (yield), MPa	11.4 ± 1.3	13.9 ± 3.1	12.1 ± 1.1
Elongation (break), %	341.3 ± 31.9	383.7 ± 61.7	225.7 ± 24.6
Elongation (yield), %	9.2 ± 0.6	1.8 ± 0.2	1.4 ± 0.7
Elastic modulus, MPa	424.7 ± 36.7	658.3 ± 33.1	1301.3 ± 52.8
Thickness, µm	25	30	80
Width, cm	9.5	6.0	6.0

3.2.4. 5th trial: PHBV/PBS blends

In this trial, three formulations with low (L), medium (M), and high (H) ratios of PHBV (Tianan Enmat Y100P) were compounded with PBS (BioPBS FZ91PM). The compounding process was stable, with temperatures set between 130 and 150 °C to prevent thermal degradation (**Figure 14**). The resulting compounds were thoroughly characterized for their thermal, rheological, and physical properties, as detailed in **Table 12** and **Figure 15** (DSC thermograms).

After characterizing the formulations, they were evaluated using a blow extruder (Figure 14). As in the previous trial, during film extrusion of the formulation with a low percentage of PHBV, lower temperatures were used (150 – 160 °C). In contrast, for the film extrusion of the formulation with a high percentage of PHBV, the temperatures were set between 175 and 190 °C. Films with a low amount

of PHBV were easier to extrude than those with a high content of PHBV, which tended to be sticky and tacky. The mechanical properties are presented in **Table 13**.

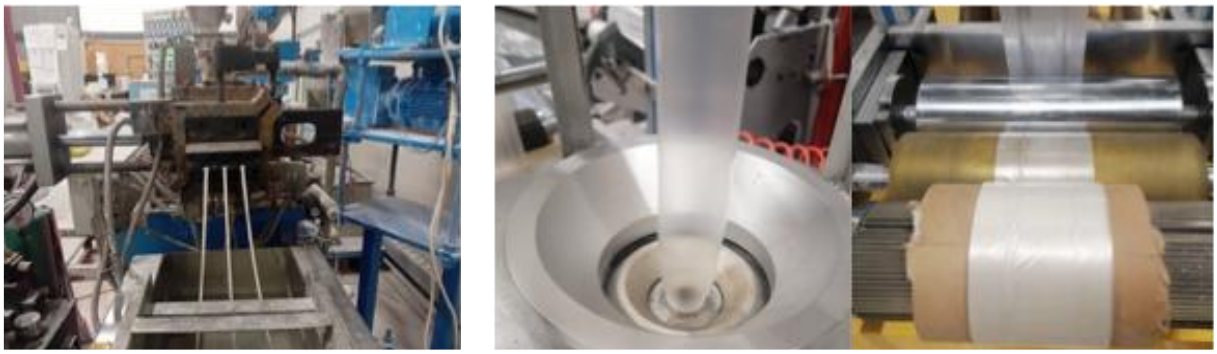

Figure 14. Compounding process (left) and (blow) extrusion (right) of PHBV/PBS formulations – 5th trial

Table 12. Characterization of PHBV/PBS compounds – 5th trial

Formulation	Tm (°C)	MFR (g/10 min) (160 °C - 2.16 kg)	MFR (g/10 min) (190 °C - 2.16 kg)	Density, ($g.cm^{-3}$)	Moisture content (%)
PHBV(L)/PBS	116,5/169,4	0.7	12.0	1.216	0.408
PHBV(M)/PBS	115,8/170,6	0.2	12.4	1.229	0.266
PHBV(H)/PBS	113,0/169,6	No flow	14.0	1.243	0.274

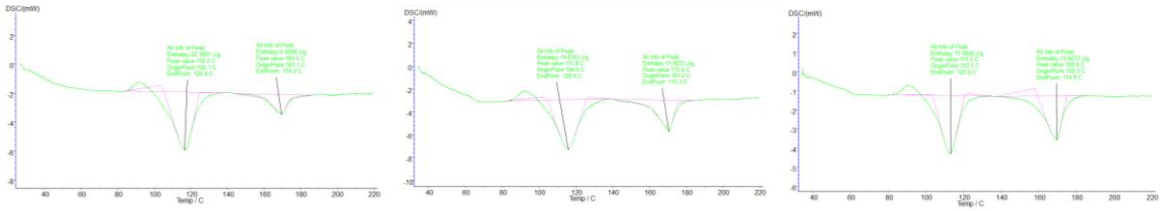

Figure 15. DSC thermograms of PHBV(L)/PBS (left), PHBV(M)/PBS (middle), PHBV/PBS (right).

Table 13. Mechanical properties of PHBV/PBS films – 5th trial

	PHBV(L)/PBS	PHBV(M)/PBS	PHBV(H)/PBS
Tensile (break), MPa	34.9 ± 6.0	25.3 ± 4.4	22.7 ± 1.2
Tensile (yield), MPa	22.2 ± 2.7	17.9 ± 1.3	14.8 ± 0.6
Elongation (break), %	277.0 ± 60.8	259 ± 16.9	213.0 ± 155.9
Elongation (yield), %	4.2 ± 1.8	3.4 ± 0.5	1.9 ± 0.8

Elastic modulus, MPa	892.3 ± 59.3	726.7 ± 6.0	1109.3 ± 66.0
Thickness, µm	39	48	43
Width, cm	13.0	6.0	8.0

3.2.5. 6th trial

In this trial, three formulations with varying ratios of PHBV (Tianan Enmat Y100P) and PBAT (Ecoworld Jinghui Zhaolong) were tested. Similar to the fourth and fifth trials, the formulations included low (L), medium (M), and high (H) ratios of PHBV. During the compounding process, temperatures were set between 130 °C and 150 °C. The process was stable, with only minor issues occurring during the pelletizing (**Figure 16, left**). Compounds produced were characterized in the same way as PHBV/PBSA and PHBV/PBS formulations, with results presented in **Table 14** and **Figure 17**.

As in the recent trials, the film extrusion temperatures for the formulations containing a low amount of PHBV were typically around 135 °C. However, for formulations with a higher percentage of PHBV, the extrusion temperature was adjusted and increased by 20 °C. The material with a high ratio of PHBV proved unsuitable for blow extrusion due to its stickiness and tackiness. In contrast, the extrusion process for the material with a low percentage of PHBV proceeded without any issues (**Figure 16, right**). All produced films were evaluated for their mechanical properties and the results are shown in **Table 15**.

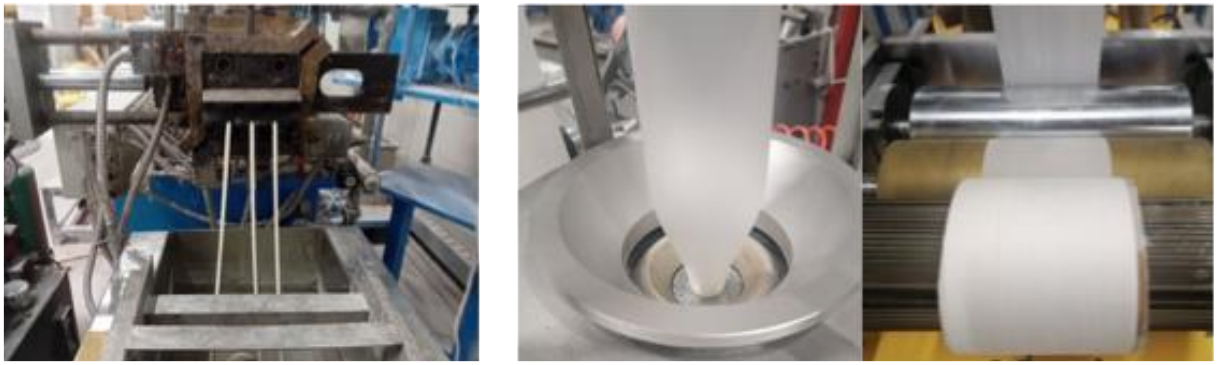

Figure 16. Compounding process (left) and film (blow) extrusion (right) of PHBV/PBAT formulations – 6th trial

Table 14. Characterization of PHBV/PBAT compounds – 6th trial

Formulation	Tm (°C)	MFR (g/10 min)	MFR (g/10 min)	Density, ($g.cm^{-3}$)	Moisture content

		(160 °C - 2.16 kg)	(190 °C - 2.16 kg)		(%)
PHBV(L)/PBAT	120,2/168,0	1.0	11.3	1.241	0.380
PHBV(M)/PBAT	120,8/167,0	0.3	14.4	1.214	0.395
PHBV(H)/PBAT	118,5/168,0	No flow	24.1	1.200	0.408

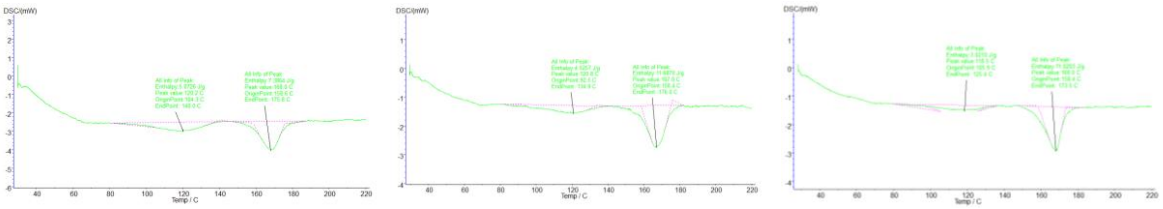

Figure 17. DSC thermograms of PHBV(L)/PBAT (left), PHBV(M)/PBAT (middle), PHBV/PBAT (right)

Table 15. Mechanical properties of PHBV/PBAT films – 6th trial

	PHBV(L)/PBAT	PHBV(M)/PBAT	PHBV(H)/PBAT
Tensile (break), MPa	25.5 ± 1.1	17.5 ± 0.9	17.8 ± 1.2
Tensile (yield), MPa	9.8 ± 0.7	7.6 ± 1.2	10.3 ± 2.4
Elongation (break), %	475.0 ± 4.4	458.7 ± 18.7	494.3 ± 29.9
Elongation (yield), %	11.3 ± 0.8	7.0 ± 1.7	1.8 ± 0.6
Elastic modulus, MPa	280.0 ± 16.5	370.0 ± 33.2	1154.3 ± 9.5
Thickness, µm	33	45	84
Width, cm	9.0	10.0	8.0

3.2.6. 7th trial

Based on the results from the fourth, fifth, and sixth trials, the three best formulations with low (L) PHBV content were selected for the scaling-up phase, where the tests with the chosen formulations were repeated using commercially available materials.

During the compounding step for all three formulations, PHBV(L)/PBSA, PHBV(L)/PBS, and PHBV(L)/PBAT, the same processing parameters were used, consistent with previous trials. To prevent thermal degradation, the extrusion temperature was kept between 130 °C and 150 °C. The processing remained stable for all formulations (**Figure 18**). However, there were issues with pelletizing the PHBV(L)/PBAT formulation, which required additional material shredding. After compounding, all three materials were characterized as described previously, and the results of this characterization are presented in **Table 15** and **Figure 19**.

Figure 18. Compounding process – 7th trial

Table 16. Characterization of compounds – 7th trial

Formulation	Tm (°C)	MFR (g/10 min) (160 °C - 2.16 kg)	MFR (g/10 min) (190 °C - 2.16 kg)	Density, ($g.cm^{-3}$)	Moisture content (%)
PHBV(L)/PBSA	90.6/169.3	0.9	13.9	1.315	0.155
PHBV(L)/PBS	117.3/169.3	0.8	12.4	1.220	0.124
PHBV(L)/PBAT	120.0/168.8	1.1	10.0	1.210	0.148

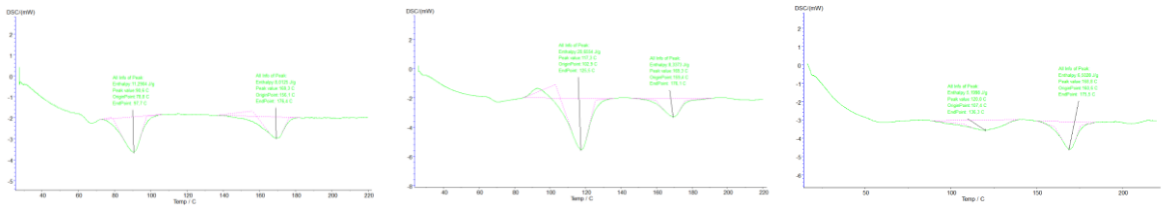

Figure 19. DSC thermograms of PHBV(L)/PBSA (left), PHBV(M)/PBS (middle), PHBV/PBAT (right)

Characterized materials were extruded into films using a blow extruder. During the film extrusion of PHBV(L)/PBSA, the initial temperatures were set between 135 °C and 150 °C. However, due to the unstable bubble and the slight stickiness typical of PHBV, the temperatures were then reduced to a range of 130 °C to 140 °C, which made the process easier to manage. It was not possible to produce films with a thickness of less than 30 µm.

For the extrusion of PHBV(L)/PBS into films, the initial temperatures were also set between 130 °C and 140 °C. Due to the deflation of the bubble, the processing temperatures were increased by 10 °C. Again, it was not feasible to produce thinner films (below 30 µm).

During the film extrusion of PHBV(L)/PBAT, the temperature profile was set between 130 °C and 135 °C. Due to uneven feeding, the bubble was unstable and deflated. As a result, material was added in small amounts and pushed manually.

All produced films were characterized according to the previously mentioned standard ASTM D882, and the results are presented in **Table 17**.

Table 17. Mechanical properties of produced films – 7th trial

	PHBV(L)/PBSA			PHBV(M)/PBS			PHBV(H)/PBAT			
Tensile (break), MPa	20.8 ± 0.8	20.8 ± 1.6	22.1 ± 0.8	35.5 ± 0.2	38.0 ± 4.9	34.5 ± 4.3	30.6 ± 3.3	30.2 ± 1.9	28.4 ± 2.4	28.9 ± 4.0
Tensile (yield), MPa	11.4 ± 2.7	9.4 ± 0.8	15.3 ± 0.7	16.1 ± 0.1	17.2 ± 2.1	15.8 ± 1.9	14.3 ± 2.3	13.8 ± 0.7	13.0 ± 1.2	13.2 ± 1.8
Elongation (break), %	553.2 ± 28.5	423.4 ± 47.1	667.0 ± 55.4	321.6 ± 5.9	499.7 ± 53.4	435.3 ± 51.8	307.3 ± 48.0	403.6 ± 38.6	492.0 ± 33.4	541.6 ± 64.1
Elongation (yield), %	2.6 ± 0.1	2.5 ± 0.4	2.7 ± 0.2	2.8 ± 0.2	2.7 ± 0.2	2.4 ± 0.3	2.0 ± 0.3	2.3 ± 0.0	2.5 ± 0.3	2.4 ± 0.2
Elastic modulus, MPa	253.6 ± 17.2	255.4 ± 38.3	342.7 ± 47.0	527.8 ± 24.5	567.6 ± 78.6	623.1 ± 48.4	219.3 ± 21.8	189.3 ± 25.1	148.0 ± 29.2	153.7 ± 5.0
Thickness, µm	38	34	42	18	33	29	14	19	29	42
Width, cm	10.4	10.0	9.7	9.8	10.0	12.2	9.8	10.0	10.0	9.4

3.2.7. 8th trial

In July 2025,an 8th test was conducted using project materials. One kilogram of PHBV was supplied by UNIVR, along with PHBV from Paques Biomaterials (PBM) (**Figure 20**).

Figure 20. PHBV from Paques Biomaterials (left) and PHBV from UNIVR (right)

Both types of PHBV underwent characterization according to relevant standards prior to testing. The results of this characterization are presented in **Table 18**. Density measurements could not be performed due to the powder form of both types of PHBV. The measurement of the MFR at 190 °C for

PBM was not conducted, as extremely high MFR values had already been observed at 160 °C. Due to a high moisture content of 5.846 %, the PHBV from UNIVR was dried in hot air dryer at 60 °C. However, even after two days of drying, the moisture content didn't decrease below 3 %. PHBV UNIVR had very unpleasant odour, while PHBV PBM had to be milled before processing and had spongy texture.

Table 18. Characterization of PHBV UNIVR and PHBV PBM

	Tm (°C)	MFR (g/10 min) (160 °C - 2.16 kg)	MFR (g/10 min) (190 °C - 2.16 kg)	Density, ($g.cm^{-3}$)	Moisture content (%)
PHBV (Tianan Enmat Y100P)	174.3	No flow	19.9	1.183	0.191
PHBV UNIVR	164.5	No flow	No flow	x	5.846 (3.114)
PHBV Paques Biomaterials	160.5	>70	x	x	0.846

After characterization, the compounding process was conducted on twin screw extruder, where the project PHBV UNIVR and PHBV PBM, along with commercial PHBV was blended with PBAT, PBSA, and MI3.

Compounding of PBAT/PHBV. During the compounding of PBAT with commercial PHBV (Tianan Enmat Y100P), no issues were encountered. However, when compounding PBAT with PHBV PBM, the PHBV PBM melted in the feeder and was unable to pass through the screw (**Figure 21**). Attempts to lower the temperatures did not resolve the issue, so the solution was to manually feed the material directly onto the screw. During the extrusion of PBAT/PHBV UNIVR, milder processing conditions were applied, and no problems were observed.

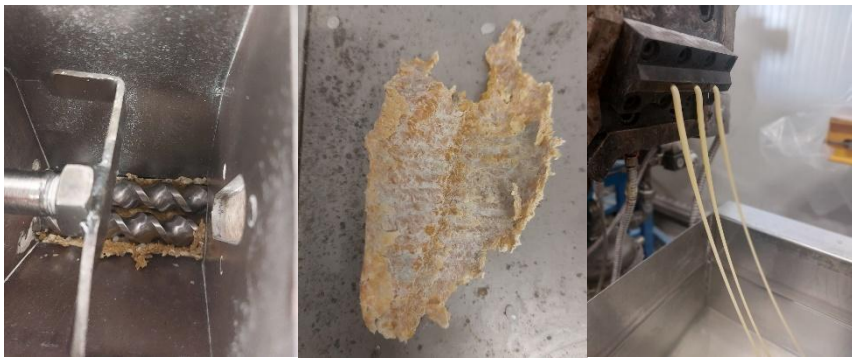

Figure 21. Compounding of PBAT/PHBV PBM – 8th trial

Compounding of PBSA/PHBV. During the compounding of PBSA with commercial PHBV, the process remained stable. Similarly to the processing PBAT/PHBV formulations manual feeding directly onto the

screw was necessary while compounding PBSA with PHBV PBM. In contrast, for the extrusion of PBSA/PHBV UNIVR, milder conditions needed to be applied, however, the process ran smoothly overall (**Figure 22**).

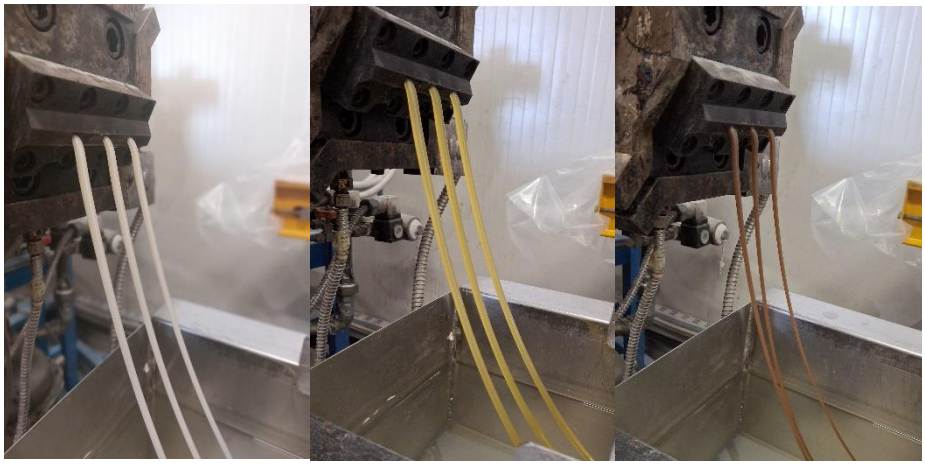

Figure 22. Compounding of PBSA/PHBV Tianan Enmat Y100P (left), PBSA/PHBV PBM (middle), and PBSA/PHBV UNIVR (right) – 8th trial

Compounding of MI3/PHBV. The compounding of MI3 with commercial PHBV and PHBV PBM was stable. However, when MI3/PHBV UNIVR formulation was added, the pressure increased rapidly, leading to distorted and runny strands (**Figure 23**). To stabilize the process, it was necessary to significantly reduce the screw speed.

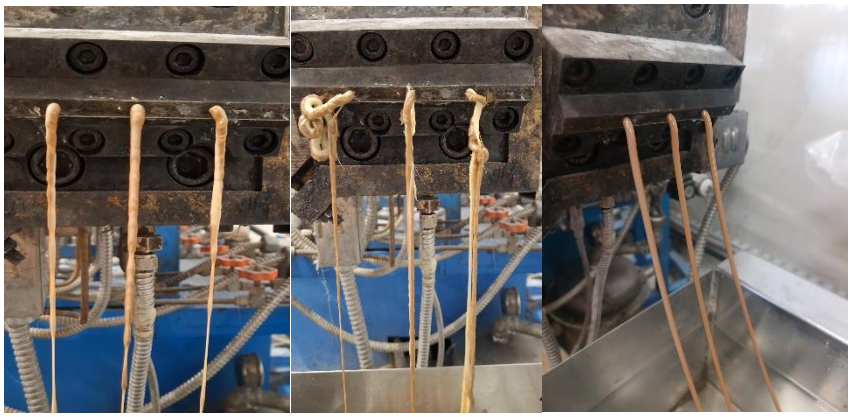

Figure 23. Compounding of MI3/PHBV UNIVR – 8th trial

All produced materials were characterized according to standards (**Table 19**) before further processing into films. After characterizing the formulations, each was extruded into films on the blow extruder.

Table 19. Characterization of compounds – 8th trial

Formulation	Tm, °C	MFR, g/10 min (160 °C/2.16 kg)	MFR, g/10 min (190 °C/2.16 kg)	density, gcm^{-3}	moisture, %
PHBV Enmat Y1005/PBSA	91.8/168.1	3.8	8.1	1.208	0.178
PHBV UNIVR/PBSA	92.7	32.6	>100	1.214	0.424
PHBV Paques biomaterials /PBSA	91.3	3.4	6.8	1.204	0.214
PHBV Enmat Y1005/PBAT	122.3/168.3	2.5	8.0	1.211	0.230
PHBV UNIVR/PBAT	118.9	9.1	25.3	1.226	0.296
PHBV Paques biomaterials /PBAT	118.2	4.0	8.8	1.186	0.249
PHBV Enmat Y1005/MI3	115.2/168.7	1.9	6.6	1.258	0.285
PHBV UNIVR/MI3	116.3	4.3	10.2	1.248	0.765
PHBV Paques biomaterials /MI3	114.9	3.3	6.8	1.253	0.336

Blow extrusion of PBAT/PHBV. During the film extrusion of the PBAT/PHBV based formulations, stability was observed with all three types of PHBV (**Figure 24**). Films made from commercial PHBV exhibited some stickiness, while those produced with PHBV PBM were even stickier, causing them to adhere to one another and difficult to separate. The PBAT/PHBV UNIVR films showed a grainy texture, which can be attributed to the low purity levels in the PHBV used.

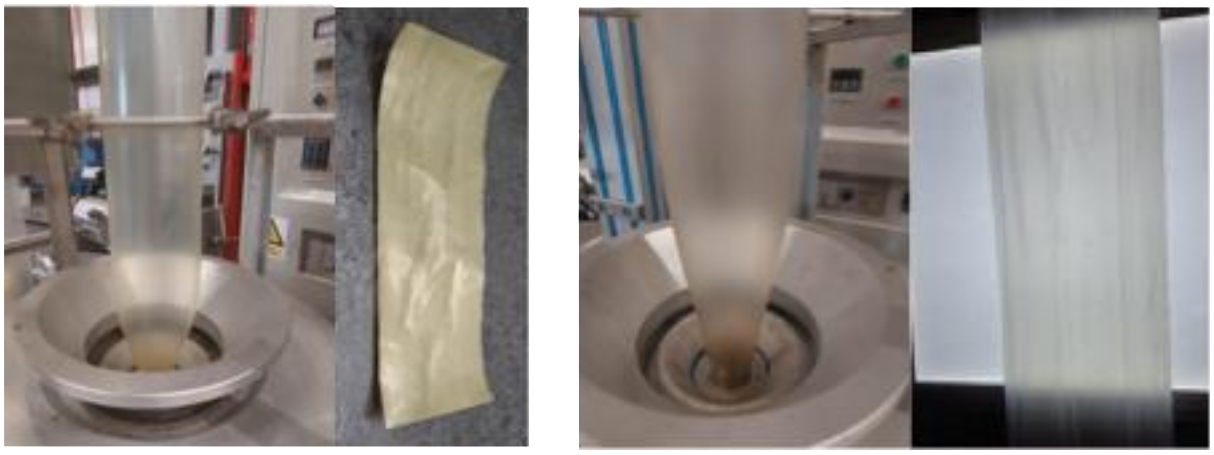

Figure 24. Film (blow) extrusion of PBAT/PHBV PBM material (left) and PBAT/PHBV UNIVR (right) – 8th trial

Blow extrusion of PBSA/PHBV. During the film extrusion of PBSA/PHBV PBM, maintaining process stability proved to be challenging. The bubble formed during the process was unstable, leading to the appearance of wrinkles (**Figure 25**). This issue was consistent with the processing of the PBSA/PHBV formulation, where commercial PHBV was used. Furthermore, during the extrusion of PBSA/PHBV UNIVR into films, the bubble deflated very quickly. This behaviour was anticipated based on the high MFR of that particular formulation. Despite applying several temperature profiles, it wasn't possible to successfully extrude the films.

Figure 25. Film (blow) extrusion of PBSA/PHBV UNIVR material (top) and PBSA/PHBV PBM (bottom) – 8th trial

Blow extrusion of MI3/PHBV. The film extrusion process for MI3/PHBV using commercial PHBV was stable (**Figure 26**). However, when the material was replaced with MI3/PHBV PBM, the bubble became unstable. Multiple temperature profiles were necessary to achieve a stable process similar to that of the commercial PHBV. On the other hand, the film extrusion of MI3/PHBV UNIVR proceeded smoothly, although the films exhibited a grainy texture due to the low purity of the PHBV. Film rolls are presented in **Figure 27**.

Figure 26. Blow extrusion of MI3/PHBV Tianan Enmat Y100P (left), MI3/PHBV PBM (middle), and MI3/PHBV UNIVR (right) – 8th trial

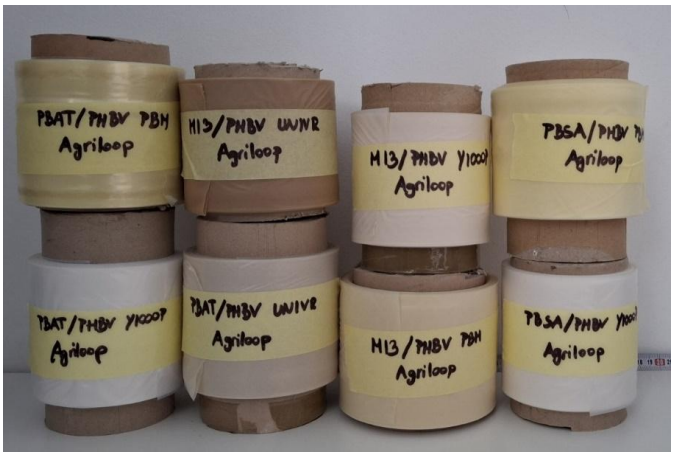

Figure 27. Film rolls of materials prodced within the 8th trial

The produced films were characterized in the same manner as in previous trials, and the results are presented in **Table 20**. All the formulations with commercially available PHBV along with PBSA/PHBV PBM and MI3/PHBV PBM exhibit good performance and therefore they are good candidates for further scale up trials. Despite of the low purity of PHBV UNIVR, formulations with PHBV UNIVR have shown satisfactory results but they won't be considered for next scale up trials.

Table 20. Mechanical properties of produced films – 8th trial

	Tensile (break) (MPa)	Tensile (yield) (MPa)	Elongation (break) (%)	Elongation (yield) (%)	Elastic modulus (MPa)	Thickness (µm)	Width (cm)
PHBV Enmat Y1005/PBSA	28.2 ± 1.9	14.7 ± 2.1	663.8 ± 46.3	10.0 ± 0.0	183.2 ± 12.5	38	10.2
PHBV UNIVR/PBSA	/						
PHBV Paques biomaterials /PBSA	31.1 ± 0.2	14.2 ± 0.4	740.3 ± 85.6	6.0 ± 2.0	164.0 ± 7.4	39	10.0
PHBV Enmat Y1005/PBAT	35.0 ± 1.7	15.8 ± 0.8	670.4 ± 21.2	9.3 ± 1.2	73.7 ± 3.9	42	10.3
PHBV UNIVR/PBAT	25.5 ± 1.0	11.5 ± 0.4	741.6 ± 13.0	14.0 ± 3.5	57.1 ± 2.8	45	10.3
PHBV Paques biomaterials /PBAT	34.6 ± 3.9	17.6 ± 4.9	786.8 ± 69.8	16.0 ± 0.0	76.4 ± 5.5	91*	10.3
PHBV Enmat Y1005/MI3	21.5 ± 0.5	11.8 ± 3.5	793.7 ± 6.4	8.0 ± 0.0	105.3 ± 8.6	42	10.5
PHBV UNIVR/MI3	19.8 ± 1.2	10.5 ± 0.4	718.6 ± 13.3	4.0 ± 0.4	73.2 ± 3.4	40	9.5

PHBV Paques biomaterials /MI3	17.1 ± 0.8	7.7 ± 0.4	568.4 ± 9.3	1.1 ± 0.1	72.3 ± 4.5	41	10.1

3.2.8. Conclusion and perspectives

Each trial highlighted that the PHBV content strongly influences both processability and film quality: **lower PHBV percentages facilitate processing**, whereas **higher percentages hinder processability and degrade mechanical properties**. The purity of PHA was not questioned until the final trial (no. 8), which revealed significant issues: PHBV from Paques was irregular in shape and unsuitable for industrial processing, while PHBV from UNIVR had a purity of only about 60%. For instance, using UNIVR PHBV at ~60% purity, we formulated three blends but limited PHBV content to 10–20%. Increasing it to 20–40% would have made the blend unprocessable and the results unattainable.

The results of the last trial will serve for the further scale up and the **production of mulching films that will be evaluated for their field performance in close-to-real conditions during the last year of the Agriloop project**.

3.3. Cutin/PHBV blends (UNIBO)

3.3.1. Introduction

The incorporation of natural polyesters such as cutin into biopolymeric matrices represents an emerging strategy to improve the performance and sustainability of bio-based plastics. **Cutin**, a highly cross-linked plant-derived polyester, is known for its hydrophobicity, structural complexity, and potential as a renewable additive for polymer composites. On the other hand, **poly(3-hydroxybutyrate-co-3-hydroxyvalerate)** (PHBV) is a biodegradable and biocompatible polymer whose mechanical and thermal properties can be tuned by varying the 3-hydroxyvalerate (HV) content. This section explores the preparation, characterization, and mechanical behavior of blends composed of PHBV and cutin extracted from tomato pomace, aiming to evaluate their thermal and mechanical properties, and structure–property relationships. The study also investigates the **potential of cutin as a plasticizing or reinforcing agent in PHBV matrices** to design bio-based materials suitable for sustainable packaging and agricultural applications.

3.3.2. Materials and methods

3.3.2.1. Materials

PHI003, a commercial PHBV with 1.5 mol% of HV, was purchased from Natureplast. PHBV Paques, with 29.9 mol% of HV was purchased from Paques Biomaterials; the sample was produced by the PHA2USE consortium in the Caleyda® demo production plant. INRAE cutin was extracted from tomato pomace by INRAE Centre Pays De La Loire (Nantes, France); TomaPaint cutin was provided by TomaPaint (Parma, PR, Italy).

Cutin samples were dried in an oven for 24 hours at 60 °C under vacuum to remove the absorbed water. Afterwards, cutin was either cut into 1 mm^2 pellets when mixed in the Brabender mixer or milled into a fine powder when processed into a twin-screw extruder. It was kept in a desiccator to avoid the formation of humidity until melt processing. The water content was monitored using an Ohaus moisture analyzer.

3.3.2.2. Blending technique

For the use of the twin-screw extruder, cutin in the form of powder and PHI003 was initially dry mixed in the corrected relative amounts and then the mixture was added continuously to the Process 11-Twin Screw extruder supplied by Thermo Fisher Scientific. A sheet-die head was mounted to the extruder to obtain films 3 cm wide and 30 mm thick. The temperature profile was the following: 140 °C (feeder) – 180 °C – 175 °C (die). The rotational speed of the screws was set at 100 rpm. The films were then shaped into strip specimens of 1 cm width x 10 cm length for the subsequent mechanical testing.

The blends of PHBV Paques and cutin were obtained using a batch mixing strategy. PHBV and cutin were first mixed in the PL-2000 Plasti-Corder Brabender mixer chamber and for 4.5 minutes at 50 rpm, at a temperature of 150 °C. Then, the blends were milled using a MultiDrive MI 250 T mill. The so-obtained powder with a 0.4 mm granulometry was used to obtain films via compression molding, using

a Carver Laboratory Press Model C at 150°C and 10 000 pounds. The films were then shaped into strip specimens of 10 mm wide x 150 mm long for the subsequent mechanical testing.

3.3.2.3. Nuclear Magnetic Resonance (NMR)

Nuclear Magnetic Resonance spectroscopy is one of the main techniques to collect information on the structure of molecules. In the present work, ^{1}H NMR technique was employed to verify the chemical structure of PHBV samples. The NMR techniques used were. PHBV samples were dissolved in chloroform (NMR grade) and 1, 1, 1, 3, 3, 3 - hexafluoro – 2 – propanol if needed.

3.3.2.4. Thermal characterization

Studies on thermal stability of the samples were performed via Thermogravimetric Analysis (TGA) using a Perkin Elmer (Waltham, MA, USA) TGA4000 apparatus under nitrogen atmosphere (gas flow: 40 mL/min). The test implied to heat the sample (10-15 mg) at 10°C.min^{-1} from 30 °C up to 800 °C. The result obtained was a curve showing the weight loss percentage as a function of temperature. The temperature of maximum weight loss (T_{max}) was calculated as the minimum value of the thermogram derivative, while $T_{5\%}$ was determined as the temperature corresponding to the 5% of mass loss.

To evaluate the thermal behavior, including transition temperatures and enthalpy changes, Differential Scanning Calorimetry (DSC) was performed using a Perkin Elmer DSC 4000 (Waltham, MA, USA). Samples of 5-10 mg were encapsulated in aluminum pans and placed inside the instrument together with the reference (empty aluminum pan). The furnace was purged constantly with dry nitrogen gas at 20 ml/min. Data was analyzed with the software PYRIS. The program used for PHBV samples is reported herein:

- 1st heating scan: −50 °C to 200 °C for PHI003, 190 °C for PHBV Paques at 20 °C.min^{-1}
- Isotherm of 2 min at 200°C/190°C
- Cooling from 200/190 °C to -50°C at 10 °C.min^{-1}
- Isotherm of 2 min at -50 °C
- 2nd heating scan: −50 °C to 200/190 °C at 10 °C.min^{-1}

The program used on the cutin samples is reported herein:

- 1st heating scan: −70 °C to 190 °C at 20 °C.min^{-1}
- Isotherm of 2 min at 190°C
- Cooling from 190 °C to -70°C at 10 °C.min^{-1}
- Isotherm of 2 min at -70°C
- 2nd heating scan: −70 °C to 190 °C at 10 °C min^{-1}

3.3.2.5. Mechanical characterization

The tensile properties of the blends were evaluated as strip specimens 10 mm wide, 0.30 mm thick and 150 mm long with two parallel gauge marks, 50 mm apart, on the central portion of the specimen. The instrument used for the testing was an Instron 5966 dynamometer (Turin, Italy) equipped with a 10 kN load cell (test speed 5 mm min^{-1}, room temperature 25 ± 1 °C).

3.3.3. Results and discussion

3.3.3.1. Preparation and characterization of cutin

The two samples of cutin, TomaPaint and INRAE, were characterized for their initial water content, using the Ohaus moisture analyzer. TomaPaint cutin had a 42% w/w water content; INRAE only 10% w/w. To remove the water content, the samples were dried as described in the experimental section. Removal of water is essential for the following preparation of blends to avoid hydrolytic degradation processes. The samples were analyzed for their thermal stability and degradation behavior. **Figure 28** shows the result of the thermogravimetric analysis for the samples, evaluated both before and after being dried.

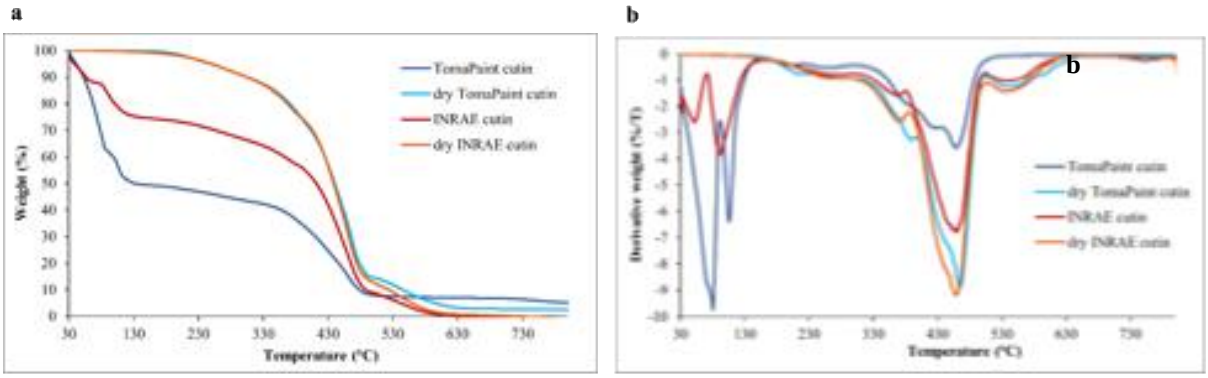

Figure 28. (a) TGA and (b) DTGA of cutin samples before and after drying.

The TGA curves (**Figure 28a**) indicate that both INRAE and TomaPaint cutin samples exhibit an initial weight loss between 30 °C and 130 °C, corresponding to the evaporation of physically absorbed and bound water. The temperatures at which the maximum rate of weight loss occurs during this stage (T_{max}) are summarized in **Table 21**. The derivative thermogravimetric (DTGA) curves (**Figure 28b**) highlight distinct peaks associated with these processes. For wet TomaPaint cutin, two peaks are observed at 52 °C and 90 °C, both attributed to water loss. In contrast, the wet INRAE cutin displays less pronounced peaks at 80 °C and 106 °C, suggesting a lower water content or stronger water–matrix interactions. The corresponding value obtained by Ohaus moisture analyser is slightly lower, 10% w/w. At higher temperatures, all samples show a significant mass loss in the range of approximately 360 °C to 550 °C, with a complex profile in the TGA curves. This degradation stage is likely associated with dehydration and decarboxylation of hydroxyacids, as well as fragmentation of aliphatic chains from fatty acids, oligomers, or polymeric structures. The most intense DTG peak appears at around 460 °C, which likely corresponds to the main thermal decomposition of the cutin network, involving the breakdown of its aliphatic backbone.

These observations are consistent with the results reported by (Cifarelli et al. 2016), who also described a gradual, multi-step degradation process for cutin, beginning around 400°C and showing three main DTG peaks at approximately 400 °C, 450 °C, and 490 °C. Such thermal behavior is characteristic of complex, heterogeneous, biomass-derived materials (Liang and McDonald 2014).

Table 21. Temperatures at which 5% of weight loss ($T_{5\%}$) and the maximum weight loss (T_{max}) occur for cutin samples.

Sample	$T_{5\%}$ (°C)	T_{max} (°C)
TomaPaint cutin (40% water)	41	52, 90, 460
Dried TomaPaint cutin	248	460
INRAE cutin (10% water)	39	80, 106, 460
Dried INRAE cutin	250	460

Both cutins were also evaluated for their thermal properties via Differential Scanning Calorimetry. The DSC thermograms of INRAE and TomaPaint cutin (**Figure 29**) display similar overall thermal behavior, showing characteristic endothermic and exothermic transitions associated with the physical and structural properties of cutin.

The cooling curves show no significant exothermic crystallization peaks, suggesting that the cutin structure remains largely amorphous after the first heating cycle. Likewise, the second heating scans display nearly flat baselines, with only slight fluctuations, indicating that no clear melting or glass transition events occur within the measured temperature range. This behavior supports the idea that cutin is a highly cross-linked, irregular and complex polyester network with limited molecular mobility and poor crystallinity, typical of natural plant polyesters. Both cutins display a glass transition temperature at around -20 °C, consistent with results found in literature (Benítez et al. 2022).

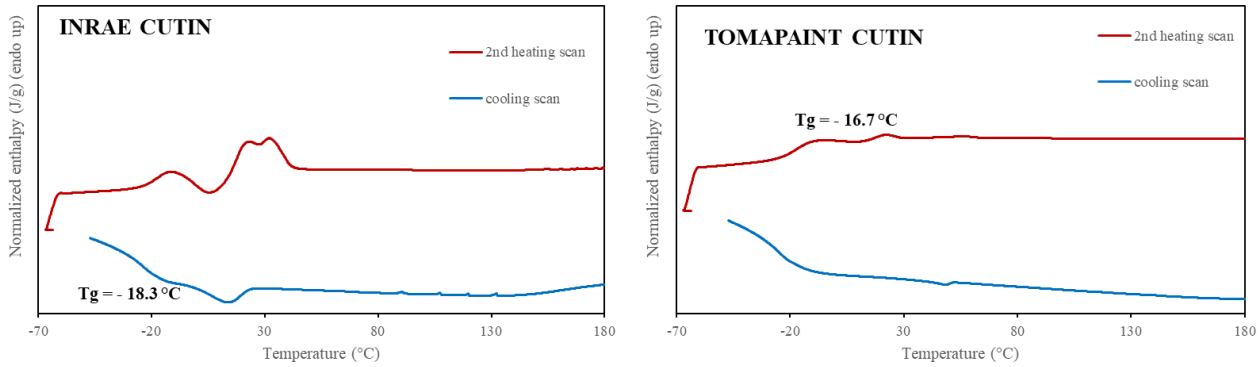

Figure 29. DSC curves of INRAE and TomaPaint cutin.

3.3.3.2. Chemical characterization of PHBV samples (NMR)

Figure 30 shows the ^{1}H NMR spectra of PHI003, where the observed peaks are assigned to the correspondent 3-hydroxybutyrate (HB) and 3-hydroxyvalerate units. The peak for the methine of HB is clearly visible, whereas the one of HV is difficult to be detected. An analogous situation is present in the peak for the methyl protons. To obtain a quantified value, the molar percentage of HV in each sample can be determined from the spectra by calculating normalized integral of relevant peaks for both HB and HV units. In this case, the measurement was carried out by using the values from the two protons of the methyl groups (pink and green dots in **Figure 30**), positioned around 0.9 and 1.5 ppm. Results revealed that PHI003 has a molar content of 1.5% of HV units.

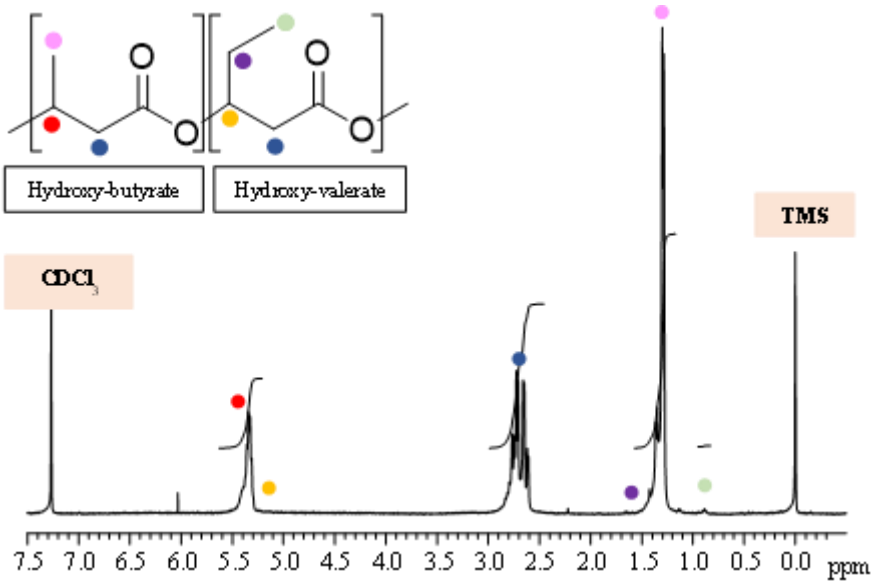

Figure 30. ^{1}H NMR spectra of PHI003.

3.3.3.3. Thermal characterization of PHBV samples.

The thermal behavior of the PHBV samples was evaluated via Differential Scanning Calorimetry (DSC). The DSC scans of PHI003 and PHBV Paques are displayed in **Figure 31**.

In the first heating scan, PHI003 sample is characterized by a fairly narrow melting peak, that indicates a good crystal perfection. The T_m of PHI003 is 171 °C, close to that of PHB (i.e., 175 °C) since the percentage of HV is extremely low (i.e., 1.5%, as determined via ^{1}H NMR). The enthalpy of melting (ΔH_m) gives information on the crystallinity of a polymer, since it indicates the heat required to melt the crystalline regions and transform them into a liquid state. The more the crystalline regions are, the more is the heat required to disrupt them (Kong and Hay 2003). PHI003 has a value of ΔH_m equal to 76 J/g that can be considered a high value. PHBV Paques, on the other hand, display a very complicated profile during the 1st heating scan (**Figure 31b**). This is due to the fact that the Caleyda® sample is a

blend of PHBV with different HV content. For this reason, the sample has 3 melting temperature peaks, relative to possibly three copolymers at different HV content present in the blend.

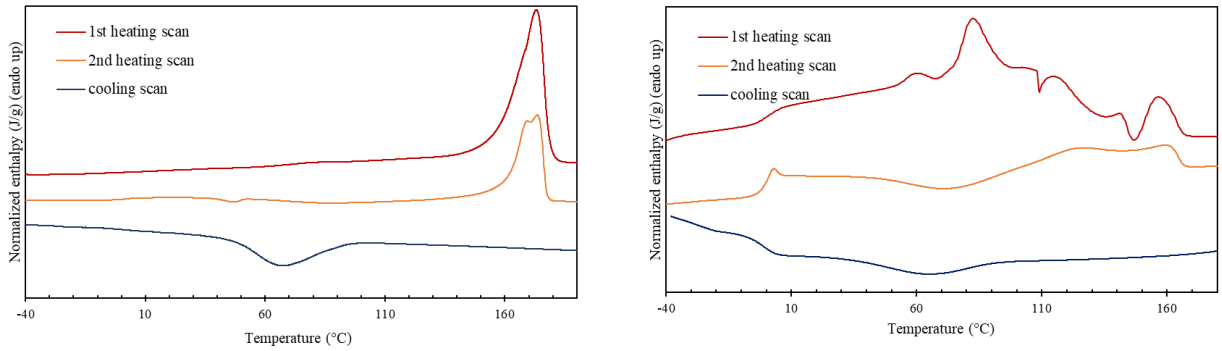

Figure 31. DSC scan of PHI003 (a) and PHBV Paques (b).

During the first heating scan, the melting peaks occur at 83, 116 and 157 °C. In this case, the enthalpy of melting of each peak is considerably lower than that of PHI003, signifying that the material has a lower crystallinity degree.

From **Table 22**, it is evident that PHI003 sample displays a crystallization process during the cooling scan. Accordingly, **Figure 31** shows an exothermic peak in the cooling step for the PHI003 sample. This behavior means that the copolymer containing a low amount of HV units is able to regularly pack and form crystals. This is proper for polymers with high crystallization rate and able to achieve a high crystallinity level. PHBV Paques also shows a crystallization process during the cooling step, although showing a very wide peak. The enthalpy of crystallization of this sample is lower than that of PHI003, further supporting the lower crystallinity of this material.

Table 22. DSC results of the PHBV samples.

	1st heating scan		Cooling scan		2nd heating scan					
Sample	**T_m (°C)**	**ΔH_m (J/g)**	**T_c (°C)**	**ΔH_c (J/g)**	**T_g (°C)**	**ΔH_{Cp} (J/g)**	**T_{cc} (°C)**	**ΔH_{cc} (J/g)**	**T_m (°C)**	**ΔH_m (J/g)**
PHI003	171	76	63	31	5	0,3	49	10	171	78
PHBV Paques	83; 116; 157	7; 9; 5	65	15	-1	0,4	-	-	-	-

In the second heating scan, an endothermic shift of the baseline is evident. Glass transition temperature (Tg) is an important parameter to understand how the polymer will behave at room temperature. The increase in HV content should lower the Tg, making the polymer more flexible at lower temperatures. Indeed, PHI003 displays a Tg of 5 °C whereas PHBV Paques has a Tg of -1 °C, confirming that a higher HV content corresponds to a greater fraction of more mobile units along the macromolecular chain. After Tg, the PHI003 sample is able to crystallize and melt, as observed in the first scan, whereas PHBV Paques shows a a very complex DSC profile, not easily understandable. In any case, the difficulty of the copolymer at high HV content to rearrange in a crystalline phase is confirmed.

Further DSC studies are in progress in order to better understand the thermal behavior of the PHBV samples.

3.3.3.4. Preparation of the blends

PHI003 was blended with both INRAE and TomaPaint cutin in the weight ratio 95:5, 90:10, 80:20. PHBV Paques was employed in blends with INRAE cutin in the weight ratio 95:5, 90:10, 80:20. The preparation of the blends followed the procedure reported in the experimental section. **Figure 32** displays the so-obtained materials. It is notable that the colour of the materials shifts towards darker tones as the amount of cutin increases.

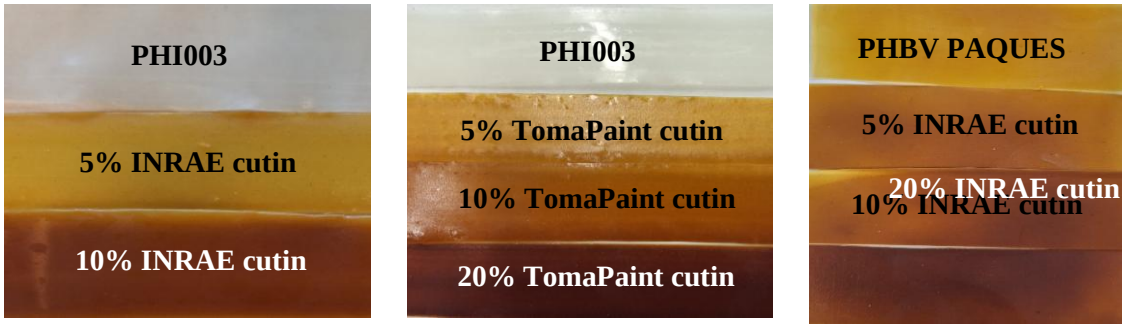

Figure 32. PHBV-cutin films prepared at the twin-screw extruder (PHI003) and by compression moulding (PHBV Paques).

3.3.3.5. Thermal characterization of the blends

The blends were also characterized in terms of their thermal behavior. The second DSC heating scan of the blends between PHI003 and the two cutin samples are displayed in **Figure 33**. The exothermal and endothermal peaks can be attributed to the crystalline phase of PHB. By considering the melting process, that always occurs at about 160°C, it is possible to observe that the endothermic peaks are complex, often double. This behavior suggests the presence of melting-recrystallization and re-melting processes, typical of polyesters. Therefore, it is difficult to use the melting enthalpy data to determine a degree of crystallinity. In any case, the profiles of the curves suggest that cutin has the effect of decreasing the crystallization rate of PHBV. In fact, by increasing the cutin content PHBV decreases its ability to crystallize during the cooling scan. Indeed, for the sample containing 10% of cutin, an exothermal peak appears during the second heating scan. In addition, there is the presence of a glass transition whose temperature tends to decrease with the increment of cutin amount. Therefore, cutin appears to act as a plasticizer, reducing crystallinity and lowering the Tg.

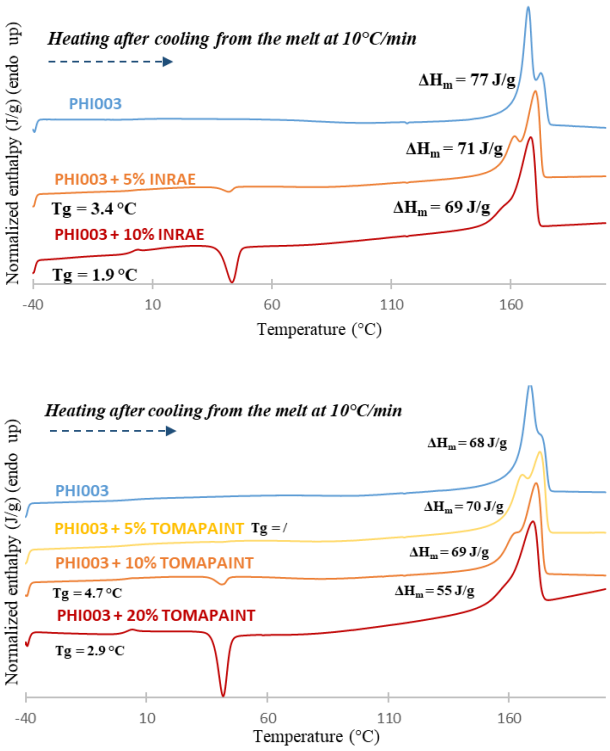

Figure 33. DSC profiles during the second heating step of PHI003-cutin blends.

The blends between PHBV Paques (**Figure 34**) and INRAE cutin display different profiles during the second heating scan. With the presence of cutin, the PHBV DSC curve is again very complex. The PHBV sample is not able to crystallize during cooling scan (data not shown), therefore no melting peak can be observed during the heating scan.

Similarly to the blends with PHI003, Tg decreases at the increasing of cutin content. This might also suggest that cutin may act as a plasticizer. In the range between –50 - 20 °C, there is the presence of two endothermic peaks that increase in intensity as the cutin content increases. These peaks could be attributed to the presence of cutin, as observed in Figure 3.3.4.2. Therefore, an incomplete miscibility and poor interaction between PHBV and cutin can be present: the peaks indicate phase-separated cutin domains that are dispersed in the PHBV. This statement is also reinforced by the fact that cutin itself shows endothermic peaks in that temperature range (**Figure 29**). Furthermore, the blends with the highest amount of cutin (i.e., B – PHBV Paques + 20% INRAE) show a flex at around 20°C, correspondent to the Tg of cutin (blue circle in **Figure 34**).

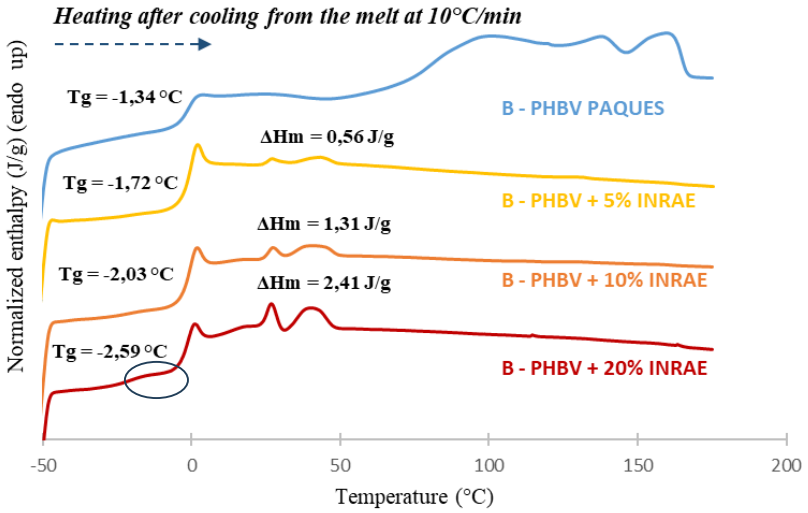

Figure 34. DSC profiles during the second heating step of PHBV Paques-INRAE cutin blends. Blue circle represents the Tg of cutin.

3.3.3.6. Mechanical properties of the blends

The blends were characterized also in terms of mechanical properties. Regarding the PHI003-cutin blends, the elastic modulus is similar for all the blends and the reference (**Table 23**). Stress at break tends to decrease with the increase in cutin content (**Figure 35a**). The elongation at break is very low but increases with increasing cutin content (**Figure 35b**). Cutin is thought to reduce the weak interactions among the chains and therefore enhance the mobility of the amorphous regions, leading to reduced brittleness and promoting ductility. As previously suggested, cutin might act as a plasticizer, softening the rigid PHI003 matrix and leading to a material that is more processable and with mechanical properties that are more optimal for packaging and agricultural applications. PHBV Paques alone already shows good flexibility and ductility in respect to PHI003.

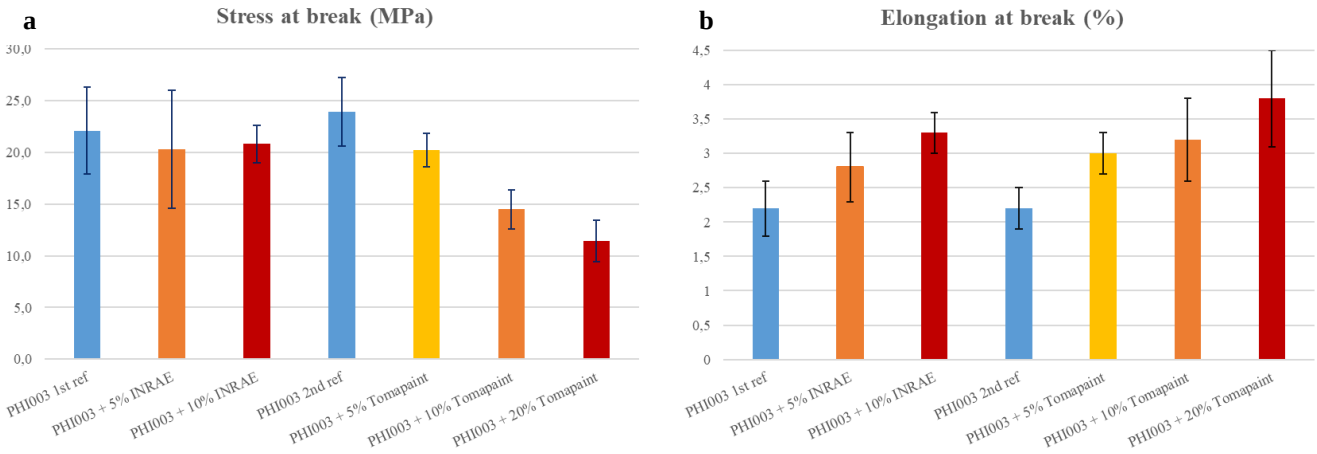

Figure 35. Results of the tensile properties of PHI003-cutin films: (a) stress at break and (b) elongation at break (%).

Concerning the blends containing PHBV Paques, all the three mechanical parameters decrease by increasing the cutin content (**Figure 36**). So, cutin does not have the same effects in the blends with PHI003 and PHBV Paques. When cutin is incorporated it does not integrate well within the amorphous phase due to poor interfacial compatibility, as already suggested from the DSC results. It introduces discontinuities and weak interfaces, reducing stress transfer efficiency. Both modulus and strength decrease because the cutin domains act as mechanical defects. The strain at break also decreases because these defects promote premature fracture instead of energy dissipation. Here, cutin acts as a rigid, poorly compatible filler, weakening the overall mechanical integrity.

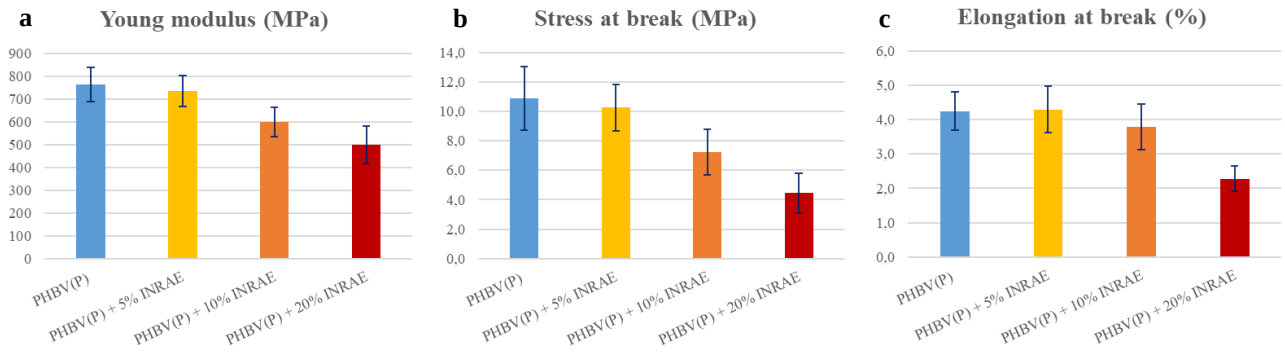

Figure 36. Results of the tensile properties of PHBV Paques-INRAE cutin films: (a) Young modulus (MPa), (b) stress at break and (c) strain at break.

Cutin might still be used in blends to obtain materials with antimicrobial and barrier properties. A lower loading of cutin (5-10 wt%) could be added to obtain a material that still has acceptable mechanical properties. The use of bio-based compatibilizers or plasticizers in addition to cutin could be evaluated to increase interfacial compatibility and obtain improved mechanical performances. All data are summarized in the table below (**Table 23**).

Table 23. Tensile test results for PHI003 and PHBV Paques blends with cutin. (E= extruded, B= prepared using the Brabender mixer)

SAMPLE	Young Modulus [MPa]		Stress at break [MPa]		Elongation at break [%]	
E - PHI003	1685	± 633	22,1	± 4,2	2,2	± 0,4
E + 5%INRAE	1535	± 531	20,3	± 5,7	2,8	± 0,5
E + 10%INRAE	1519	± 394	20,8	± 1,8	3,3	± 0,3
E - PHI003	1410	± 415	23,9	± 3,3	2,2	± 0,3
E + 5%Tomapaint	1045	± 343	21,0	± 1,9	3,1	± 0,3
E + 10%Tomapaint	1453	± 153	14,5	± 1,9	3,2	± 0,6
E + 20%Tomapaint	1048	± 98	11,4	± 2,0	3,8	± 0,7
B - PHBV PAQUES	765	± 75	10,9	± 2,2	4,3	± 0,6
B + 5%INRAE	735	± 68	10,3	± 1,6	4,3	± 0,7
B + 10%INRAE	600	± 64	7,2	± 1,6	3,8	± 0,7
B + 20% INRAE	500	± 82	4,4	± 1,4	2,3	± 0,4

3.3.4. Conclusion

The results demonstrate that cutin influences both the thermal and mechanical behavior of PHBV blends, with effects depending on the HV content of the polymer matrix. For PHI003 (low HV content), the addition of cutin decreased crystallinity and glass transition temperature, indicating a plasticizing effect that improved ductility while slightly reducing tensile strength. Conversely, for PHBV Paques (high HV content), the incorporation of cutin led to phase separation and poorer interfacial compatibility, resulting in reduced mechanical performance. Thermal analyses confirmed incomplete miscibility, especially at higher cutin loading, where phase-separated domains were evident. Overall, the study suggests that **small amounts of cutin (≤10 wt%) can beneficially modify PHBV properties, enhancing flexibility and potentially imparting barrier or antimicrobial functionalities**. Further optimization through compatibilizers or tailored processing could expand the applicability of PHBV–cutin blends in sustainable bioplastic formulations.

3.4. Cutin-based materials with antimicrobial properties (ITQB)

3.4.1. Introduction

Tomato pomace is an agro-industrial waste from the tomato processing industry, composed of peels, seeds and stems of tomatoes (Benítez et al. 2018; Ouatmani et al. 2022). This waste has already been used to produce animal feeding, compost and bioenergy, reaching technology readiness levels (TRL) between 7 to 9[1]. Despite these applications, tomato pomace has the potential for more valorization processes if cascading principles were implemented, since its rich in a wide variety of biomolecules (e.g. lipids, proteins, polysaccharides) (Yaashikaa et al. 2022; Almeida et al. 2024; Benítez et al. 2018; Al-Wandawi et al. 1985). Recently, we demonstrated that tomato pomace and tomato peels constitute the main source of cutin, a plant polyester that has been shown to be a valuable component of bio-based materials (article in submission). Cutin oligomeric mixtures (COMs) have also been proven to have bactericidal activity against Escherichia coli (E. coli) and Staphylococcus aureus (S. aureus) (Escórcio et al. 2022).

Carboxymethylcellulose (CMC) is water-soluble cellulose synthesized by its reaction with alkali and chloroacetic acid (Yang and Zhu 2007). CMC can be used as a polymer matrix to blend with cutin hydrolysates since it contains both free hydroxyl and free acid groups that can act as linkers through esterification (e.g. polycondensation) and create a functional material. Various studies using CMC as a polymer matrix for antimicrobial applications either on nanomaterials, hydrogels and films were already reported (Lee et al. 2006; Capanema et al. 2018; Siqueira et al. 2014; Elmehbad et al. 2024).

The aim of this work is **to develop at lab scale materials based on CMC and COMs and to study their antimicrobial properties**. The materials were prepared by casting using 3 different concentrations of COMs (10%, 20% and 30% w/w) and CMC as blank. We further evaluated their antimicrobial and anti-biofouling capacity, by exposing the films against E. coli and S. aureus. Other properties such as water swelling and hydrophobicity were also accessed.

3.4.2. Production of cutin/carboxymethycellulose films

Cutin oligomeric mixtures (COM^{1P}) were generated by the alkali hydrolysis of cutin extracted from tomato peels (see WP2, deliverable 2.1). Then the COMs were dissolved in acetone and blended with carboxymethylcellulose (CMC) (sigma-aldrich) solubilized in acidic water, in three different concentrations 10%, 20% and 30% w/w (**Figure 37**).

The blended solutions were transferred to Teflon molds (40.7 cm^3) and placed overnight at room temperature (20-25 °C). Afterwards the materials were heated in an oven at 40 °C for 16h followed by another heating of 16h at 150 °C. The materials were washed with 70% ethanol to remove non-bonded components and then dried at 40 °C overnight. The materials were stored at room temperature.

The materials are not homogeneous, so it is possible to see structures of the oligomeric mixtures that weren't dissolved in acetone (**Figure 37**). The drying process after the hydrolysis favors the formation of crystalized structures that are hard to solubilize.

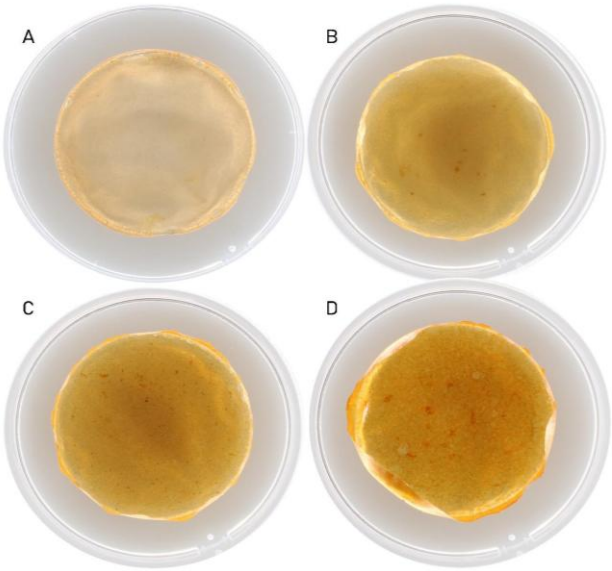

Figure 37. Materials produced with CMC and COMs at different concentrations. A- CMC; B- 10% COM; C- 20% COM; D- 30% COM.

Table 24 shows the amount of lost mass in the ethanol washing step as well as the materials thickness (mm). The results show that when the COMs concentration increases there's less compounds washed by ethanol therefore indicating that esterification is occurring.

Table 24. Quantification of ethanol washed mass and COM^{1P}-based films thickness.

	Washed mass (mg)/film	Thickness (mm)
CMC	~9.6 mg	0.066 ± 0.001
10%	~26.1 mg	0.087 ± 0.009
20%	~15.6 mg	0.080 ± 0.011
30%	~13.7 mg	0.056 ± 0.011

To confirm these results, we analyzed the materials in ATR-FTIR (**Figure 38**). The spectra were recorded in transmission mode in the range 4000-600 cm^{-1} with 4 cm^{-1} resolution and accumulating 128 scans analysed by OPUS software. The spectra show an amplification of the region around 1730 cm^{-1} that corresponds to ester C=O band. All the concentrations show the presence of esterification, however, the presence of this band doesn't discriminate if the esterification is within the COMs or between COMs and CMC or both hypotheses.

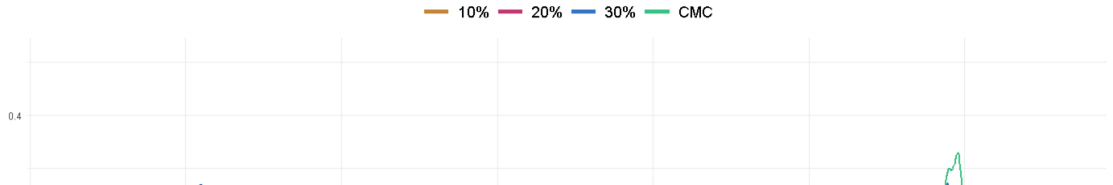

Figure 38. ATR-FTIR spectra of the materials.

3.4.3. Water resistance of cutin/carboxymethycellulose films

The capacity of the materials to swell and absorb water was analyzed. The initial weight of the materials with dimensions of 0.5 × 2 cm (1 cm^2) was noted. The samples were fully immersed in 6 mL of bidistilled water; after 120 min the samples were removed from the water and patted dry and the weight was noted again. The test was performed in triplicates at room temperature. The following formula (Equation 2) was used to calculate the percentage swelling:

$$\% \text{ Swelling} = \frac{\text{Film weight after swelling} - \text{Initial weight of the film}}{\text{Initial weight of the film}} \text{x} 100 \quad \text{(Equation 2)}$$

Table 25. Water uptake (%) of the COM^{1P}-based materials.

	% Swelling
CMC	70.4 ± 3.9
10%	44.6 ± 3.3
20%	34.7 ± 0.3
30%	23.7 ± 2.5

The swelling results indicate that the progressive incorporation of COM^{1P} significantly decreases the material's ability to retain water—by more than threefold compared to the CMC control. This reduction in water uptake upon addition of cutin hydrolysates has been previously reported and is attributed to their lipidic nature (Tedeschi, Benitez, et al. 2018; Mroczkowska et al. 2024). Although this behavior depends on the duration of the swelling protocol, the procedure is well established in the literature: for instance, Mroczkowska et al. (2024) applied a 2-hour swelling test to bioplastics

containing cutin monomers, while (Shanmathy et al. 2021) monitored samples at different time points and observed that starch-based bioplastics reached a swelling plateau after only 5 minutes.

3.4.4. Antimicrobial properties

The antimicrobial activity of the materials was tested (**Figure 39**). S. aureus NCTC8325 and E. coli TOP 10 cells (5×10^5 cells·mL^{-1}) in Mueller–Hinton broth (MHB) media were exposed for 24h to 7.9 mm^2 of the films at 37 °C under orbital agitation (100 rpm). After 24 h, the antimicrobial effect was evaluated through colony-forming units (CFU).

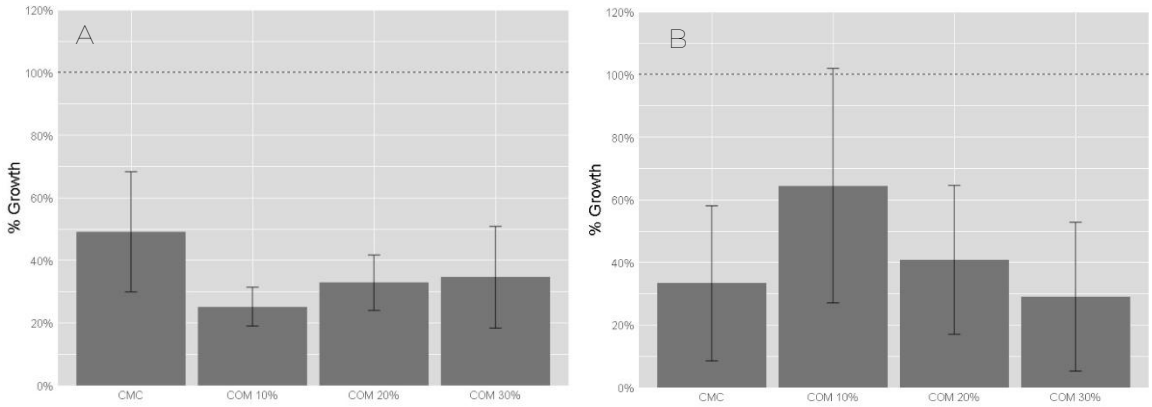

Figure 39. Antimicrobial activity of cellulosic films miwed with COM^{1P} against S. aureus (A) and E. coli (B).

Interestingly, even if not statistically significant, the activity for both S. aureus and E. coli is similar in all the COM^{1P} concentrations and CMC blank. For S. aureus the bacterial growth is reduced, 85%, 75%, 68% and 66% for CMC, 10%, 20% and 30%, respectively. For E. coli the bacterial growth is reduced, 67%, 46%, 60% and 72% for CMC and the progressive addition of COM^{1P}.

Despite not having a clear impact on the antimicrobial activity, the addition of the COM^{1P} mixture improves some properties of the materials such as less water uptake and increased hydrophobicity. These results support a previous study that observed that materials made with glycerol and hydroxy-fatty acids from tomato cutin were not capable of killing bacteria (Marc et al. 2021). One hypothesis that derives from these results is that esterification blocks either hydroxyl or acid groups that are required to provide activity to these oligomeric mixtures while reducing their mobility. This hypothesis is supported by (Zheng et al. 2005), who demonstrated that esterification (methyl esters) inhibited the antimicrobial activity of long-chain unsaturated fatty acids against S. aureus.

The materials were also tested to observe the impact of COM^{1P} on bacterial adhesion (Figure 40) since the CMC materials do not adhere to cells. The results qualitatively indicate that the degree of adherence of S. aureus to the materials is positively correlated with the content of COM^{1P}, while effectively preventing E. coli adhesion. Marc et al. (2021) observed a similar trend in co-polyesters from cutin hydroxy-fatty acids, with a higher number of S. aureus cells adherent, while the E. coli cells adhesion was low.

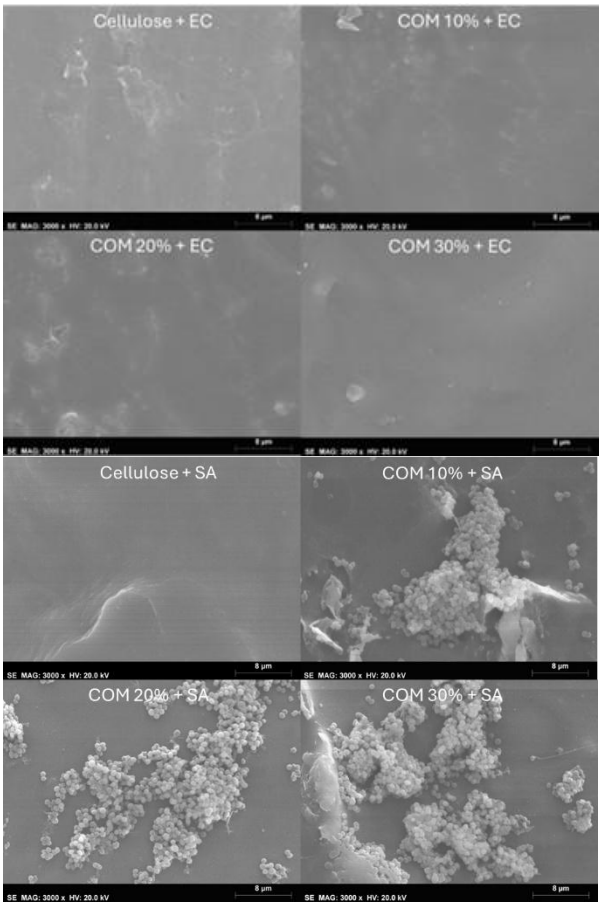

Figure 40. SEM micrographs of bacterial adhesion (EC: E. coli; SA: S. aureus) against the materials.

3.4.5. Conclusion and perspectives

Overall, the results showed that **material prototypes composed of CMC and COMS were antimicrobial and inhibited up to 75% of S. aureus cells and 71% of E. coli, showing a broad-spectrum activity**. Despite the unclear impact of the COMs on the antimicrobial activity, their addition improved the overall hydrophobicity and reduced the water uptake up to 3 times. Additionally, the materials exhibited anti-biofouling against E. coli cells. Future analysis would be needed to evaluate the mechanical and thermal properties of the biopolymer films, including their biodegradability.

3.5. Cutin-coated papers with improved surface hydrophobicity (INRAE-Nantes)

3.5.1. Introduction

Cellulose-based materials are widely used in various industrial applications such as paper manufacturing, food packaging, and drug delivery in nanomedicine. Cellulose is the most abundant terrestrial plant polymer, mainly provided by wood processing, and the corresponding derived materials are generally valued for their biocompatibility, biodegradability, and recyclability to be safe for human health and to meet the environmental constraints of replacing petroleum-based materials and limiting deforestation in a climate change issue. However, the hydrophilic nature of cellulose limits applications where water resistance can be critical. Due to its potential for sustainable material innovation, cellulose hydrophobization has garnered significant attention from the scientific community including physical modifications of cellulose (Rodríguez-Fabià et al. 2022a), polymer grafting (Rodríguez-Fabià et al. 2022c) or chemical multi-steps modifications often using silane derivatives or halogenated molecules including per- and polyfluoroalkyl substrates (Cunha and Gandini 2010; Rodríguez-Fabià et al. 2022b; Shahid et al. 2022).

Synthetic polymers coatings based on silicones (Guan et al. 2020; Ogihara et al. 2012), per- and polyfluoroalkyl substances (Kissa 2001; Paul et al. 2009; Wang et al. 2013), paraffins (Wewei Zhang et al. 2014; Zhao et al. 2018), PHBV (Pieters and Mekonnen 2024), or fatty acids acyl chloride (Pignères et al. 2024; Stinga 2008) have been developed. More recently, the development of bio-based alternative coatings (Asim et al. 2021; Basak et al. 2024; Hubbe and Pruszynski 2020; Martins et al. 2024; Rastogi and Samyn 2015). Within this perspective, several biopolymers have been used including polysaccharides (Khwaldia 2013; Kim et al. 2023; Matsui et al. 2004), proteins (Khwaldia 2010; Rhim et al. 2006), and lipids (Weiwei Zhang et al. 2014; Hu et al. 2009; Huang et al. 2023; Le and Nguyen 2020; Li et al. 2023; Liu et al. 2019; Parvathy and Sahoo 2021; Si et al. 2016; Wennman et al. 2023; Yadav et al. 2014; Majoudi et al. 2025). These bio-based alternatives remain however less effective and more expensive than their fossil-based equivalents. In addition, biomolecules can be mixed with other polymers or fillers to improve their hydrophobic properties (Hood et al. 2021; Liu et al. 2019).

Despite significant efforts to develop stable, and environmentally friendly methods for modifying the surface properties of cellulose, the hydrophobization of cellulose materials is still a challenge. Indeed, these hydrophobization must reach the best compromise between environmental sustainability, hydrophobicity, stability, and impact on the mechanical properties of the modified cellulosic material.

To overcome such bottlenecks new mimicry strategies using bio-sourced molecules could be based on our increasing knowledge of the relationships between molecular interactions of natural polymer composites and the formation of the architecture of natural hydrophobic assemblies (Yaraghi and Kisailus 2018). Indeed, biomimicry is becoming a relevant strategy for the design of new polysaccharide composites (Teeri et al. 2007). Plant secondary cell walls located at the surface of aerial plant organs, i.e. cuticle layers are naturally water-repellent which could inspire bio-based hydrophobic materials (Koch and Barthlott 2009). The plant cuticle is a complex composite composed of a polyester of hydroxy fatty acids, i.e., cutin together with waxes, polysaccharides and phenolics (Heredia-Guerrero et al. 2014; Jeffree 2006; Reynoud et al. 2021). More specifically, interactions between cutin and cellulose in the cuticle have been observed by immunolabelling labelling and Raman imaging (Philippe

et al. 2020; Reynoud et al. 2021). This peculiar assembly confers unique hydrophobic and mechanical properties to the cuticle and plays a crucial role in the growth and development of plant organs and in the interactions between the plant and its environment (e.g. resistance to biotic and abiotic stress) (Yeats and Rose 2013). It protects internal tissues from dehydration (Riederer and Schreiber 2001). Recently, several studies have exploited these structural properties to develop cutin-like coatings for food cans (Benítez et al. 2020), hydrophobic films for packaging applications (Manrich et al. 2017; Singha et al. 2021; Tedeschi, Benítez, et al. 2018) or design of shape-memory hydrophobic biopolymers and elastomers (Marc et al. 2021; 2024). These technological advances have also benefited from the biorefinery processes which isolate large quantities of hydroxy fatty acids from agro-wastes from the fruit industry at the industrial level (Ninčević Grassino et al. 2020; Radić et al. 2024).

In this context, we investigated a fully bio-based approach for the hydrophobization of cellulosic material, using a non-catalytic process that mimics cellulose/cutin interactions and provides insights into sustainable alternatives for hydrophobization of cellulose. We focus on (1) developing a simple coating technique for hydrophobic modification of cellulosic material (paper and fabric) with hydroxy-fatty acid extracted from fruit pomace; (2) characterizing the hydrophobic and mechanical properties of the coated substrates. The chemical and morphological structure of the coated substrates were also analyzed by spectroscopy (FTIR), while the barrier properties of the substrates were evaluated by water vapor and oxygen permeability measurements. This approach could lead to the development of a fully bio-sourced and recyclable hydrophobic cellulosic material for food packaging, providing a sustainable solution for the valorization of agro-waste.

3.5.2. Materials and methods

3.5.2.1. Materials

Coating method. The cutin monomers were produced from French industrial tomato pomaces characterized in WP2 (Milestone 8). The paper substrate being porous, the modification process with an ethanolic hydroxy fatty acid solution can be roughly described as a coating process, but it necessarily involves at least a partial impregnation of the substrate. The sample preparation consists of 3 steps: 1) dry and weighed commercial filter paper sheets were put in contact with the coating solution, either by dipping or by spraying at a distance of 10 cm using a pump sprayer to reach a coating weight of about 10 $g.m^{-2}$). The resulting coated papers were dried at room temperature to evaporate ethanol. 3) Samples were then placed at 150 °C for 24h.

3.5.2.2. Barrier and mechanical properties

The surface properties of the coated papers and cotton fabrics were evaluated using a drop tensiometer (Tracker™, Teclis Scientific, Longessaigne, France). According to the standard test method ASTM D724-99, static contact angle measurements were done on 5 µL droplets of MilliQ water, ethylene glycol and formamide, 5 and 60s after their formation on the surface of the substrate. Measurements were realized at 25°C on 10 different points of the substrate. The water vapor permeability (WVP) of uncoated and coated papers was determined gravimetrically according to an adapted ASTM E96 standard test method. The tensil tests for mechanical properties were conducted as previously described (Marc et al. 2024). the O2 permeability was conducted at IATE according to the experimental setup described in Marc et al. (2021).

3.5.3. Results and discussion

3.5.3.1. Chemical structure and morphology of the cutin-coated papers.

The whole spectral signature of pristine paper and modified paper were compared by FTIR spectroscopy (**Figure 41**) and show a strong chemical association between hydroxylated fatty acids and cellulose. FTIR spectra of the paper highlights typical cellulose fingerprint including absorption bands at 1428, 1367, 1334, 1027 and 896 cm^{-1} corresponding to stretching and bending vibrations of -CH2 and -CH, -OH and C-O bonds in cellulose (55,56) and 1640 cm^{-1}, assigned to OH bending vibration of sorbed water on cellulose (Hospodarova et al. 2018; Polovka et al. 2006) and 1640 cm^{-1}, assigned to OH bending vibration of sorbed water on cellulose (Polovka et al. 2006; Célino et al. 2014). The modified paper showed characteristic peaks. In particular increased signal at 2923 cm^{-1} and 2850 cm^{-1} is associated to the aliphatic C-H stretching bands of the hydroxy fatty acids from tomato cutin. Interestingly, modified paper spectra also highlighted carbonyl bands at 1728 cm^{-1} and 1711 cm^{-1} (**Figures 41B and 41D)** both assigned to esterified carbonyl, the later corresponding to esterified carbonyls involved in hydrogen bonds (H-bonds) (Chaudhari and Singhal 2015; Heredia-Guerrero et al. 2014; Marc et al. 2021). This indicated that all the cutin monomers deposit are no more under the carboxylic acid (1703 cm^{-1}) form but rather esterified (**Figure 41-F**).

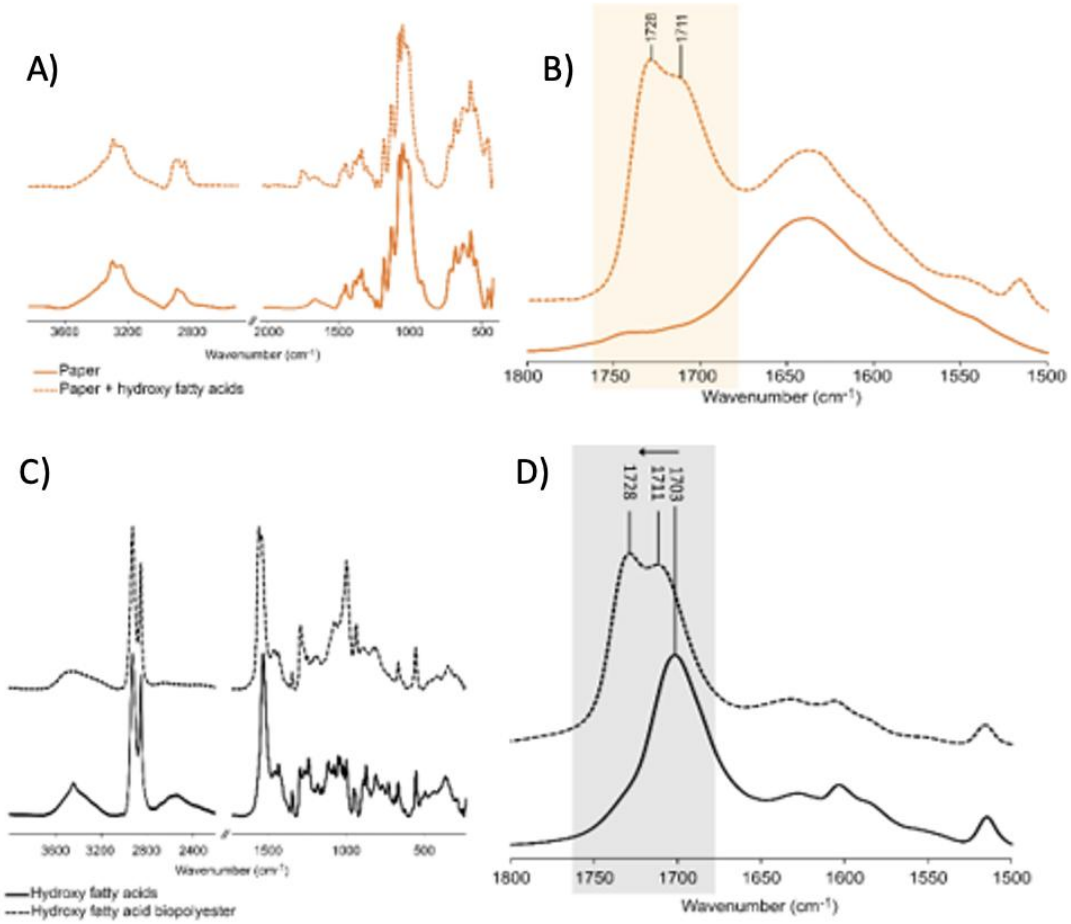

Figure 41. Fourier transform infrared (FTIR) spectra of paper (A, B) and hydroxy fatty acids (C, D) from 400 to 4000 cm^{-1}. control and modified substrates are represented by continuous lines and dash lines, respectively. The region of interest between 1500 and 1800 cm^{-1} is zoomed on (B) and (D).

3.5.3.2. Barrier properties of the cutin-coated papers

Hydrophobic properties. According to the hydrophilic properties of the untreated cellulosic material, the water contact angle on the pristine paper showed the smallest initial θ_C value (50° measured within 5 s of droplet deposition), which decreased rapidly due to penetration of the water droplet into the paper sheet. Conversely, the coated surfaces show hydrophobic properties with high initial θ_C values at 120 °. Conversely, the coated surfaces show hydrophobic properties with high initial θ_C values at 120 °. These values are comparable to the value obtained with silane formulations on paper (Perdoch et al. 2025) or obtained with chlorinated fatty acid derivatives. Moreover, these initial θ_c values are higher than those reported for other coating of cellulose with fully biobased substrates such as alginate and soy protein (Rhim et al. 2006), chitosan/zein (Kansal, Hamdani, Ping, Sirinakbumrung, et al. 2020); starch/zein blend (Kansal, Hamdani, Ping, and Rabnawaz 2020), fatty acids (Almasi et al. 2015; Lee et al. 2011; Peydecastaing et al. 2006), or plant triglycerides (Dankovich and Hsieh 2007).

Water vapor permeability. Despite hydrophobic character of the coated papers, pristine and cutin-grafted papers showed comparable water vapor permeability whatever the coating process (spaying or dipping), with WVP values ranging from to $8.9 \cdot 10^{-12} \pm 4 \cdot 10^{-13}$ mol·m·m^{-2}·s^{-1}·Pa^{-1} to $1.2 \cdot 10^{-11} \pm 7 \cdot 10^{-13}$ mol·m·m^{-2}·s^{-1}·Pa^{-1}. Overall, the water vapor barrier properties of the coated samples are in the range of the ones reported for other cellulosic materials coated with esterified lignin (Hult et al. 2013; Singh et al. 2022), chitosan/zein (Kansal, Hamdani, Ping, Sirinakbumrung, et al. 2020), or stearic acid (Huang et al. 2023).

Oxygen permeability. All paper samples showed similar PO2, whatever the coating the coating process, with PO2 values ranging from to 6.6·10-12 ± 1.1·10-12 mol·m·m-2·s-1·Pa-1 to 7.5·10-12 ± 0.4·10-12 mol·m·m-2·s-1·Pa-1. According to these value, the cutin-grafted papers seems quite permeable to O2 compare to other packaging materials such as poly(3-hydroxybutyrate-co-3-hydroxyvalerate) − 10-17 mol·m·m-2·s-1·Pa-1 − (Ambrosio-Martin et al. 2016; Crétois et al. 2014), polylactic acid – 10^{-16} - 10^{-14} mol·m·m^{-2}·s^{-1}·Pa^{-1} – (Lehermeier et al. 2001; Mahmoodi et al. 2019; Palai et al. 2019) or low-density polyethylene – 1 - $2 \cdot 10^{-15}$ mol·m·m^{-2}·s^{-1}·Pa^{-1} – (Durmuş et al. 2007; Matar et al. 2018; Motedayen et al. 2019); and cutin-derived co-polyesters – 0.7 – $1.4 \cdot 10^{-14}$ mol·m·m^{-2}·s^{-1}·Pa^{-1} – (Marc et al. 2021). Conversely, a decrease in barrier properties of a tomato cutin/sodium alginate composite film with tomato cutin amount has been reported (Tedeschi, Benítez, et al. 2018). Other studies showed significant improvement of water vapor barrier properties of papers coated with stearic acid (Huang et al. 2023), palmitic acid-chitosan emulsion (Bordenave et al. 2010) or paraffin (Khwaldia 2010), due to filling of pores of the cellulose with the coating agent.

Oxygen permeability of a material depends on the nature of the polymer used for the coating, the coating weight but also the number of coating layers (Pignères et al. 2024; Afra et al. 2016; Christophliemk et al. 2023; dos Santos et al. 2022; Kunam et al. 2024; Lavoine et al. 2014). It had been shown that a minimum coating weight is required to cover cellulose fibers with a homogeneous layer and consequently improve barrier properties (Aulin et al. 2010; Kjellgren et al. 2006; Shen et al. 2021). Thus, it would be interesting to modify the coating process by increasing the coating weight above 25g.m^{-2} or increasing the number of coating layers.

To better apprehend the structure of the coated samples, a series resistance model was used to predict theoretical PO_2 values of all coated papers (Equation 3):

$$\frac{l_{\text{coated paper}}}{PO_{2\ \text{coated paper}}} = \frac{l_{\text{uncoated paper}}}{PO_{2\ \text{uncoated paper}}} + \frac{l_{\text{coating layer}}}{PO_{2\ \text{coating layer}}} \qquad \text{(Equation 3)}$$

where l is the thickness (in m) and PO_2 is the oxygen permeability (in mol·m·m^{-2}·s^{-1}·Pa^{-1}) of the material.

This model relies on the hypothesis of a homogeneous dense coating layer with hydroxy fatty acids embedded within the cellulose fiber matrix. According to this hypothesis, experimental results obtained for OP were around 1000 times lower than values calculated from Equation 3. This result does not seem to support the hypothesis of a canonical composite material but rather porous materials.

3.5.1.3. Mechanical properties of the cutin-coated papers

Cellulose hydrophobization can have significant effects on the mechanical properties of the papers produced from it, and this is something that should be considered when choosing a production method. Some studies reported a decrease in rigidity induced by coating, due to a lack of adhesion between the hydrophilic cellulosic matrix and the hydrophobic coating agent (Balasubramaniam et al. 2020; Huang et al. 2023; Matsui et al. 2004; Rhim et al. 2006; Tedeschi et al. 2018). Actually, contrasting effect have been reported depending on the hydrophobization method used. Therefore, tensile tests were conducted on pristine and cutin-like-coated materials.

Our present data show that coating with hydroxy fatty acids induced improved mechanical properties of paper whatever the deposition process (**Table 26**). This increase in modulus may suggest that hydroxy fatty acids, by wrapping fibers individually strengthen the cellulose fibers network. A similar trend was observed for cellulose coated with other biosourced molecules including chitosan/starch and zein (Kansal, Hamdani, Ping, Sirinakbumrung, et al. 2020; Kansal, Hamdani, Ping, and Rabnawaz 2020), sodium caseinate (Khwaldia 2010), HPMC (Khwaldia 2013), chitosan nanowhiskers (Kim et al. 2023), oleic acid (Li et al. 2023) or esterified lignin and cellulose acetate (Singh et al. 2022).

Table 26. Mechanical properties of cutin-coated papers

Sample	Coating process	AGOH (g/m²)	σ_R (MPa)	ε_R (%)	E (MPa)
pristine paper	-	0	12.1 ± 0.9	4.1 ± 0.4	503.3 ± 41.6
	spraying	11	26.4 ± 0.2	8.2 ± 0.3	639.2 ± 40.6
	dipping	11	24.2 ± 0.8	6.4 ± 1.7	679.2 ± 111.4

3.5.3. Conclusion

The cutin-monomer-based coated papers highlighted **improved surface hydrophobicity and mechanical properties, with no significant change of oxygen and water vapour permeability**. These results indicate that cutin-like grafted papers could be suitable for packaging fresh, respiring products such as fruits and vegetables.

3.6. Cutin-coated PHBV films (UNIBO/INRAE-Montpellier)

3.6.1. Introduction

Surface modification of biopolymers through natural coatings represents a promising approach to enhance their functionality while maintaining full biodegradability. In this context, cutin, a hydrophobic polyester naturally forming the protective cuticle of plants, was investigated as a bio-based coating material for PHBV films. The goal of this work was to improve the surface hydrophobicity, and durability of PHBV films through the **deposition of cutin layers** obtained from tomato pomace extracts. Furthermore, cutin was applied to impart to the material antimicrobial and barrier properties. Two types of cutin (INRAE and TomaPaint) were applied using ethanol-based coating solutions, with additional surface pre-treatments (corona discharge) and curing steps to promote adhesion and crosslinking. The study focused on **understanding the influence of surface pre-treatments on cutin coating uniformity, adhesion, and surface wettability**, assessed through visual inspection and contact angle measurements.

3.6.2. Materials and methods

3.6.2.1. Materials

PHI003, a commercial PHBV with 1.5 mol% of HV, was purchased from Natureplast; PHBV 16%HV was produced and furnished by Sapienza University of Rome. INRAE cutin was extracted from tomato pomace by INRAE Centre Pays De La Loire (Nantes, France); TomaPaint cutin was provided by TomaPaint (Parma, PR, Italy).

3.6.2.2. Preparation of PHBV films

The technique used to obtain films of PHBV was compression molding, by which the material is pressed between two halves of a heated mold and transformed into a molded part after cooling. The samples used were the PHBV purchased from NaturePlast (PHI003) and the PHBV produced by Sapienza University of Rome. This technique was performed by using a Carver Laboratory Press Model C. The operating temperature for PHI003 was 180 °C; for PHBV 16%HV it was 150°C. After having positioned the PHBV powder in the press, the temperature had to stabilize again at the respective operating temperature. Then, the pressure is raised to 10 000 pounds. The polymer was kept under pressure for 1 minute and then cooled inside the press using cooling water.

3.6.2.3. Coating of PHBV films with cutin

To coat PHBV films with cutin, solutions of cutin were prepared. Cutin was solubilized in ethanol, obtaining a final concentration of 600 mg/ml (60%). Two different solutions were obtained: one using the cutin from TomaPaint, the other with cutin from INRAE. The solutions were kept in agitation at room temperature to fully solubilize cutin. Then, cutin solution was deposited on the PHBV films (both from Sapienza and NaturePlast) using a ZAA2300 Automatic film applicator from Zehntner (Switzerland). The wire bar applicator produces a wet film thickness of 20.57 µm. In some samples, prior to coating, the PHBV films underwent corona discharge pretreatment to improve surface compatibility with the cutin-based coating. After coating, in some samples a curing step was performed

to promote hardening and adhesion of the coating layer. It was carried out in an oven at 60°C under vacuum.

3.6.2.4. Water Contact Angle

The hydrophilicity/hydrophobicity of polymeric films was studied through evaluation of the contact angle. The measurement was performed using a Kruss DSA-30 instrument (Hamburg, Germany) comprised by a camera and syringe placed perpendicularly to a mobile table. The samples were placed on the mobile table and the syringe was charged with deionized water. A drop was deposited on the film by placing it in contact with the polymeric surface using the syringe needle. Side profiles of deionized water drops was recorded for image analysis. In order to evaluate the reproducibility of the results, images of 4-6 different drops placed in different areas for each film were acquired. The final value of contact angle was reported as the average value ± standard deviation.

3.6.3. Results and discussion

3.6.3.1. Coating of PHBV films

The coating procedure applied to PHBV films is detailed in the Experimental Section. The method relies on the use of cutin oligomers dissolved in an organic solvent. Solubility tests were first conducted to identify the most suitable solvent for cutin dissolution. Ethanol was selected as the optimal option, and both TomaPaint and INRAE cutin extracts were used to prepare solutions at a concentration of 60% w/w in ethanol. These solutions were subsequently applied to PHBV films produced by compression molding from the commercial grade PHI003 (NaturePlast).

As mentioned in the experimental section, corona pretreatment and curing were performed. Corona treatment is a surface modification process commonly used to increase the surface tension and polarity of polymeric substrates. It enhances wettability and promotes adhesion of subsequent layers. The process involves generating a visible electrical discharge from a linear array of electrodes operating at low voltage and high frequency. The discharge partially ionizes the surrounding atmosphere, forming reactive species such as free radicals, ions, and electrons (O'Hare et al. 2002). These species interact with the polymer surface, introducing new polar functional groups (e.g., hydroxyl, carboxyl, carbonyl, and amide groups) through oxidation reactions. The increased surface polarity and reactivity improve the compatibility of the PHBV surface with hydrophilic coatings such as cutin (Ozdemir et al. 1999).

Curing, performed after the coating step, induces chemical reactions leading to the hardening of the coating and the formation of a continuous, stable layer (Gold et al. 2025). This process involves cross-linking between cutin monomers and oligomers, and potentially between the coating and the PHBV substrate, thus enhancing the interfacial adhesion. Curing was carried out under vacuum at 60 °C for 24 hours, allowing both the progression of cross-linking reactions and the removal of the solvent (ethanol).

As shown in **Figure 42**, the PHI003 films treated with corona discharge and coated with TomaPaint or INRAE cutin solutions appeared homogeneous immediately after deposition. Corona pretreatment did not alter the visual appearance of the coating. However, after curing, the coated films exhibited a

glossier surface, indicating the formation of a more compact and cross-linked layer. In contrast, non-cured samples showed poor adhesion, as the cutin layer could be easily scratched off, regardless of the corona treatment. This behavior confirms that curing promotes cross-linking within the coating and improves interfacial bonding with the PHBV substrate, resulting in enhanced coating integrity and durability.

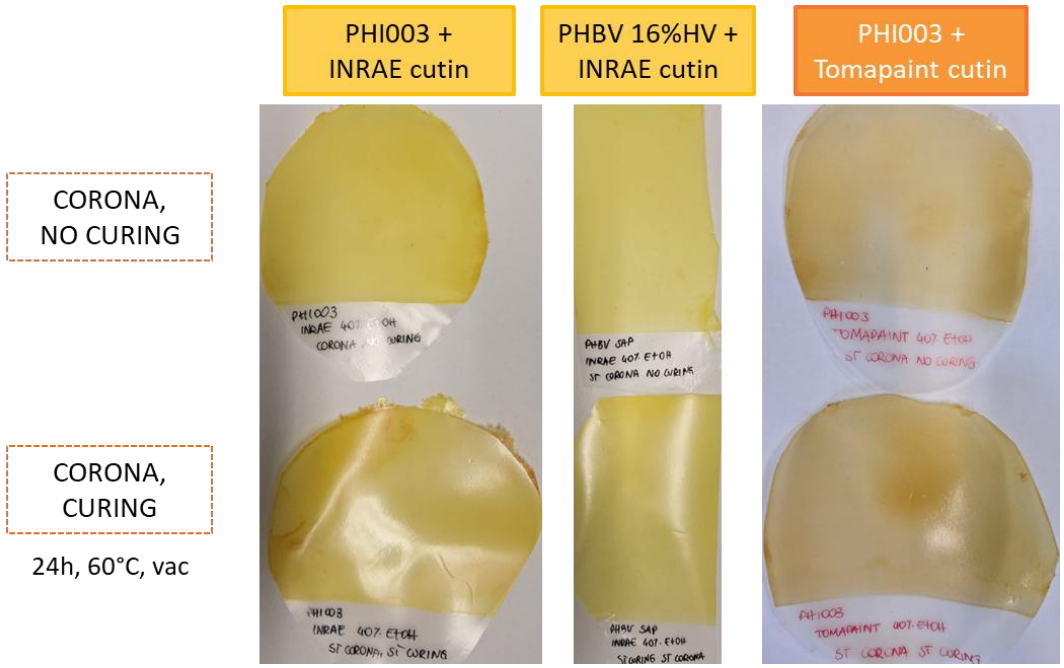

Figure 42. PHI003 films and PHBV 16% HV coated with INRAE and TomaPaint cutin.

As a conclusion, the success of the coating process seems to be strongly connected to the treatment of curing at high temperature.

3.6.3.1. Water contact angle

To evaluate the effects of the coating of cutin by corona treatment and curing steps on the final properties of the new materials, the water contact angle was measured for all PHI003 samples coated with cutin, where none, one, or both processes were applied. This measurement provided insights into the material's hydrophilicity and, consequently, the interaction between the coated films and the liquid (i.e., water).

The contact angle measurements presented in **Figure 43** reveal that when curing is performed (**Figure 43 c - g**), the hydrophobicity level increases, possibly due to the crosslinking between the terminal polar groups of cutin oligomers and monomers. Corona treatment tends to cause a decrement of the contact angle, when curing is performed (**Figure 43 d, g**). This might be caused by the creation of new polar groups that increase hydrophilicity. Some of the polar groups can interact with the polymer surface, creating new bonds and increasing affinity.

Surfaces coated both with INRAE and TomaPaint cutin exhibit hydrophobic behavior, characterized by contact angles exceeding 90°. For INRAE cutin, the average contact angle is approximately 103°, while TomaPaint cutin shows a slightly lower value of about 100°, indicating comparable surface properties

between the two materials. The high contact angles confirm that both cutins are composed of long-chain aliphatic polyesters with low surface energy, which effectively repel water. This hydrophobicity is consistent with the natural function of cutin as a protective barrier in plant cuticles, minimizing water permeability. In conclusion, curing treatment is confirmed to definitely affect the hydrophobicity of the films by increasing it, leading to the creation of a homogeneous and durable layer of coating.

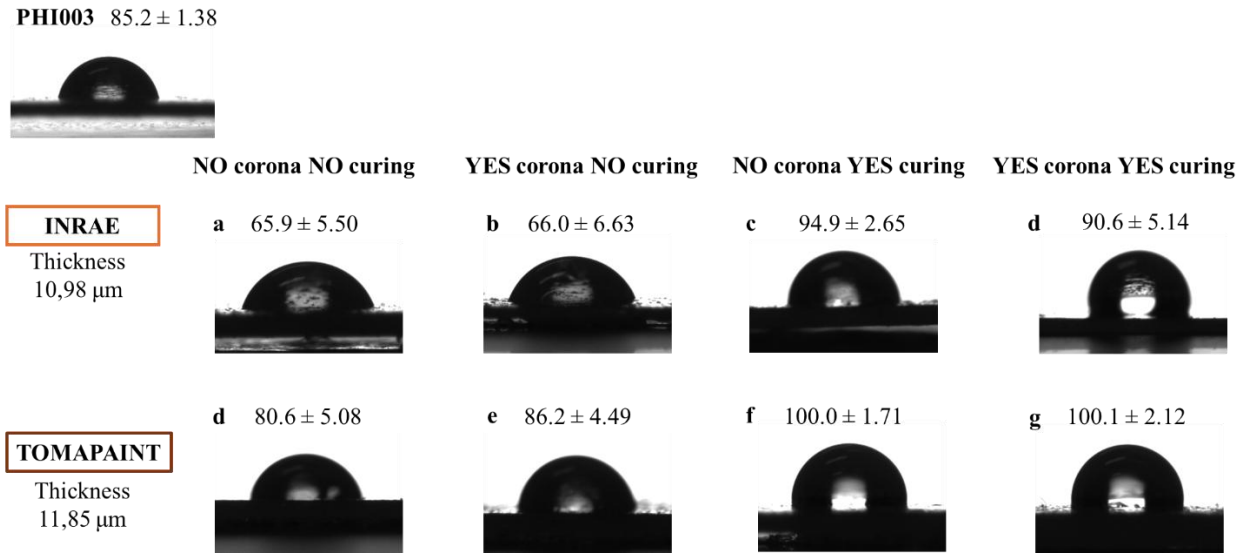

Figure 43. Water contact angle results for PHI003 films coated with cutin.

3.6.4. Conclusion

The coating of PHBV films with cutin successfully enhanced surface hydrophobicity and coating stability, particularly when a curing step was included after deposition. Curing promoted cross-linking among cutin components and improved adhesion to the PHBV substrate, resulting in a compact, glossy, and durable coating layer. Corona pretreatment increased surface polarity and wettability, thereby favoring interfacial bonding, although it slightly reduced hydrophobicity when combined with curing. Water contact angle measurements confirmed the formation of hydrophobic surfaces, with values above 100°, consistent with the natural barrier role of cutin. These findings demonstrate the effectiveness of using plant-derived polyesters as functional coatings for biopolymers, opening perspectives for developing fully bio-based materials with tailored surface properties for packaging and agricultural applications.

3.7. PHBV/lignocellulosic fillers biocomposites for rigid applications (UM)

3.7.1. Introduction

The development of biocomposites through the integration of lignocellulosic fillers derived from agricultural residues into bio-based and biodegradable polymer matrices is gaining increasing attention as a sustainable alternative to conventional plastics, while also valorizing underutilized biomass. Among the most promising biopolymers, **poly(3-hydroxybutyrate-co-3-hydroxyvalerate) (PHBV)** stands out as a bacterial polyester that is biodegradable in all environments and can be synthesized from a wide range of carbon-rich residues (Meereboer et al. 2020; Paloyan et al. 2025).

Incorporating low-cost lignocellulosic fillers obtained via dry fractionation of residues such as vine shoots (David et al. 2021), olive pomace (Lammi et al. 2018), wheat straw (Berthet et al. 2016; 2017; Berthet, Angellier-Coussy, Chea, et al. 2015), green waste from urban parks and gardens (Viretto et al. 2021), pistachio shells (Altun et al. 2023), and coffee grounds (Janowski et al. 2025) offers a means to reduce both the cost and environmental footprint of PHBV-based materials, while tailoring their properties (David et al. 2021). However, the increase of the filler content is known to negatively impact the processability of PHBV-based materials and increase the brittleness of the materials (Ahankari et al. 2011; Avella and Errico 2000; Baiardo et al. 2004; David et al. 2021; Dufresne et al. 2003; Gallardo-Cervantes et al. 2021; Ludueña et al. 2012; Mathel et al. 2025; Mazur et al. 2022; Viretto et al. 2021; Singh and Mohanty 2007; Berthet, Angellier-Coussy, Chea, et al. 2015). This is mainly ascribed to a lack of interfacial adhesion between the hydrophobic matrix and hydrophilic fibers, but also, in the case of PHBV, to the thermal degradation of the polymer matrix itself during the thermomechanical process. Berthet et al. (2015) further demonstrated that reducing the median apparent diameter of wheat straw fillers from 469 to 17 mm improved their dispersion within the PHBV matrix and enables higher filler loadings. Therefore, **the design of PHBV-based biocomposites requires a careful balance between filler content, particle size, and the preservation of mechanical performance**.

Numerous studies have revealed the presence of **contaminants** such as heavy metals, pesticides, microplastics and mycotoxins in agricultural residues (Omeje et al. 2021; Oswald et al. 2024). Their up-cycling as fillers in composite materials raises important questions regarding the fate and potential ecotoxicological risks of these substances throughout the transformation processes. These processes include pre-treatments (e.g., washing, peeling, soaking), thermal treatments (e.g., drying, roasting, autoclaving), mechanical treatments (e.g., grinding), and thermomechanical treatments (e.g., melt extrusion, injection moulding). Several studies have investigated the behavior of pesticides during food processing involving fruits and vegetables, focusing either on the entire transformation chain or on specific steps (Xiao et al. 2025; Terfe et al. 2023). To evaluate the effectiveness of decontamination at each stage, researchers use the processing factor, which compares pesticide levels before and after treatment, based on maximum residue limits (MRLs) established by the FAO/WHO and the EU. These investigations have shown that pesticides can be partially or fully eliminated through various mechanisms such as oxidation, hydrolysis, and temperature effects (Subramani et al. 2022; Amvrazi 2011; Xiao et al. 2025). Among the different methods, thermal treatments have proven to be particularly effective in reducing pesticide residues (Bajwa and Sandhu 2014; Pandiselvam et al. 2022;

Kariyanna et al. 2024; Popescu (Stegarus) et al. 2024; Zhang et al. 2022; Phopin et al. 2022; Islam et al. 2022; Słowik-Borowiec and Szpyrka 2020). **The development of biocomposites overlooks the potential presence of hazardous substances in raw materials.** However, growing regularity attention at the European level, such as the Safe and Sustainable by Design (SSbD) framework, has made the consideration of such contaminants increasingly critical for the safe use and application of final products (European Commission 2022).

Among the various agricultural residues, **peanut shells** are of particular interest due to their significant global availability, with an estimated annual production of around 50 million tons (USDA 2025). The shells, which account for approximately 21-29% of the total peanut weight, contain 22-35% lignin, 34-43% cellulose, and 7-29% hemicellulose, making them a candidates for use as natural fillers in composites (McNeill et al. 2024). Peanut shells-based composites have already been developed using various polymer matrices: calcium alginate (Perez-Ameneiro et al. 2015), bio-based high-density polyethylene (Garcia-Garcia et al. 2016), polylactic acid (Yamoum and Magaraphan 2017), recycled polypropylene (Zaaba et al. 2014; Fasihah Zaaba et al. 2018) and polylactic acid with thermoplastics corn starch (Zaaba and Ismail 2020). However, peanut's cultivation involves the use of various pesticides (herbicides, fungicides, nematicides and insecticides) (Blair and Lamb 2025), which can remain in the final products after harvesting and processing (Cui et al. 2022; Duan et al. 2022).

In closed interaction with WP1, this study aims at including for the first-time safety criteria for the development of biocomposites whose fillers are derived from agricultural residues. For that purpose, raw peanut shells were voluntarily spiked with five pesticides (azoxystrobin, ametoctradin, thiamethoxam, carbofuran and malathion) selected for their diverse physicochemical properties (polarity and molecular weight), serving as molecular models. To investigate the mechanisms and efficiency of decontamination, samples were collected at each step of the transformation process to quantify residual pesticide content. Regarding the production of biocomposites, two particle sizes were obtained through dry grinding of the peanut shells. Biocomposites with varying filler contents were then produced using a thermomechanical treatment, consisting of twin-screw extrusion to produce the compounds, followed by injection-molding to shape the final items. These items were subsequently characterized in term of mechanical and thermal properties to determine potential applications.

In the present deliverable 4.1., only the results regarding the performance of biocomposites are presented. The results dealing with the decontamination are presented in deliverable 1.8.

3.7.2. Materials and methods

3.7.2.1. Materials

Poly-(3-hydroxybutyrate-co-3-hydroxyvalerate) (PHBV) in a form of pellets was purchased from NaturePlast (France) under the commercial name of PHI002. It has a true density of 1.23 g.cm^{-3} and a melting temperature of 175°C. Raw peanut shells (PS) were provided by Shandong Jinsheng Grain & Oil Group (China).

3.7.2.2. Production of PHBV/PS biocomposites

Dry fractionation of PS. PS particles were dried overnight at 60 °C and then sequentially ground using cutting, impact, and ball milling techniques to produce two filler fractions, referred to as PS-F and PS-UF (**Figure 44**). Cutting was performed with a SM300 (Retsch) mill at 3000 rpm using a 2 mm sieve, followed by impact milling with a UPZ 100 (Hosokawa-Alpine) at 18,000 rpm, with a feed rate of 1.5 kg·h^{-1} and a 0.3 mm sieve. Half of the batch was further processed by ball milling (FEMAG) at 300 rpm, using 250 g of peanut husk powder and 7 kg of 6 mm stainless steel balls. This was followed by a final impact milling step (UPZ 100, Hosokawa-Alpine) at 18,000 rpm with a 0.2 mm sieve.

Production of PHBV/PS compounds. Composite compounds were produced using a co-rotating twin screw extruder (Eurolab 16 Thermo Scientific, length to ratio of 40) (**Figure 45**). The polymer pellets and the PS powders were dried overnight at 60 °C before extrusion. The PS particles and the PHBV pellets were introduced by using two volumetric. The total flow rate was 1.0 kg.h^{-1} and the screw speed was 300 rpm. The profile temperature from the feeding to the die varied from 140 to 160 °C (140-160-160-160-170-170-175-170-160), biocomposites were produced with a room temperature of 27 ± 0.5 °C and a relative humidity of 35 ± 0.5 %. A filament die of 3 mm was used to produce a continue filament. In this conditions, the average residence time was 1.75 min (PhD thesis of Grégoire David).

This filament was introduced to a pelletizer (AM11/003431 Thermo Scientific) to obtain pellets. Filler contents of up to 15 wt% and 20 wt% were respectively achieved for PS-F and PS-UF. Above these contents, decohesion occurred in the extruded rod.

The true filler content determination by calcination at 900 °C during 1 hour in muffle furnace, using **Equation 4**:

$$w_f = \frac{R_c - R_m}{R_f - R_m} * 100 \quad \textbf{(Equation 4)}$$

with w_f the filler content, R_c the residue fo the composite, R_m the residue of the neat PHBV matrix, and R_f the residue of the PS powder.

Production of dog-bone specimens by injection molding. The extruded compounds were dried at 60°C overnight prior to injection molding process. Tensile test specimens (ISO 527-2-1BA) were produced using a MiniJet Pro injection molding machine (Thermo Scientific). The injection molding parameters were set as follows: cylinder temperature at 185°C, mold temperature at 70°C, injection pressure of 400 bar for 20 seconds, followed by a holding pressure of 100 bar for 10 seconds. Specimens were stored over silicagel during 14 days before further characterization.

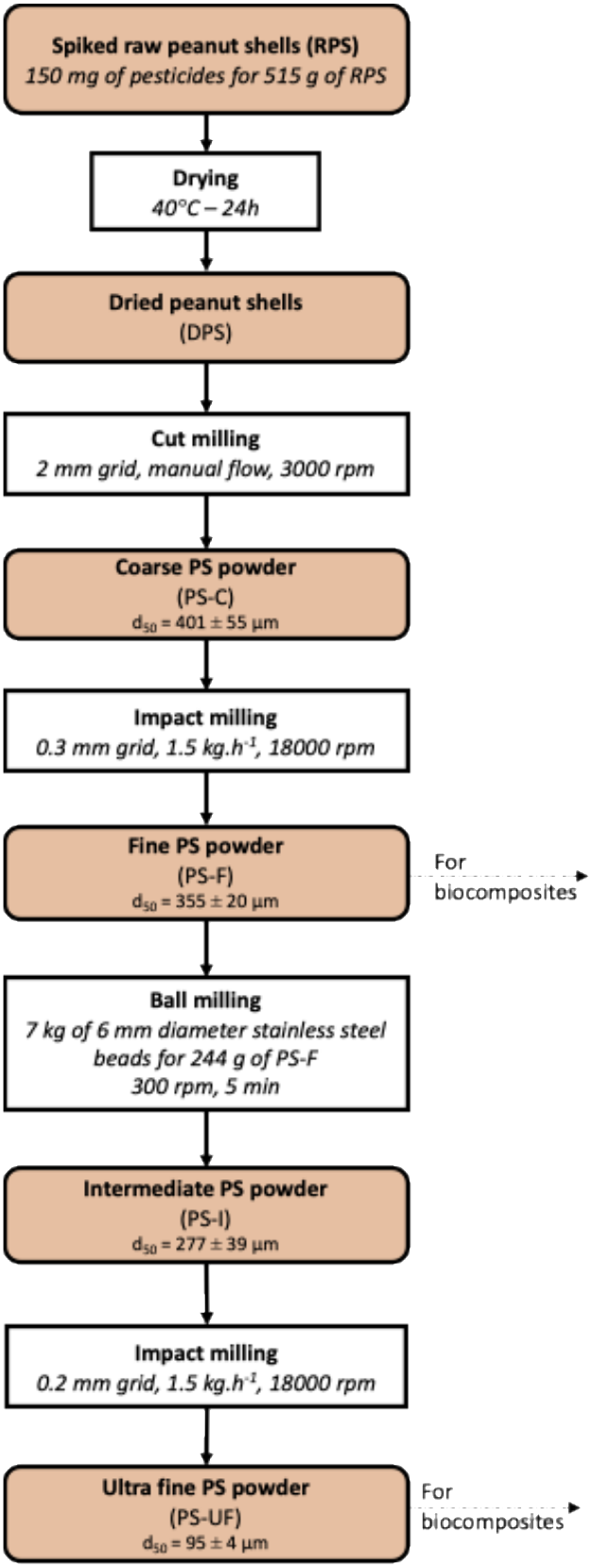

Figure 44. Dry fractionation of peanut shells using successive grinding steps. Square shapes show the processes step and brown square shape show the products.

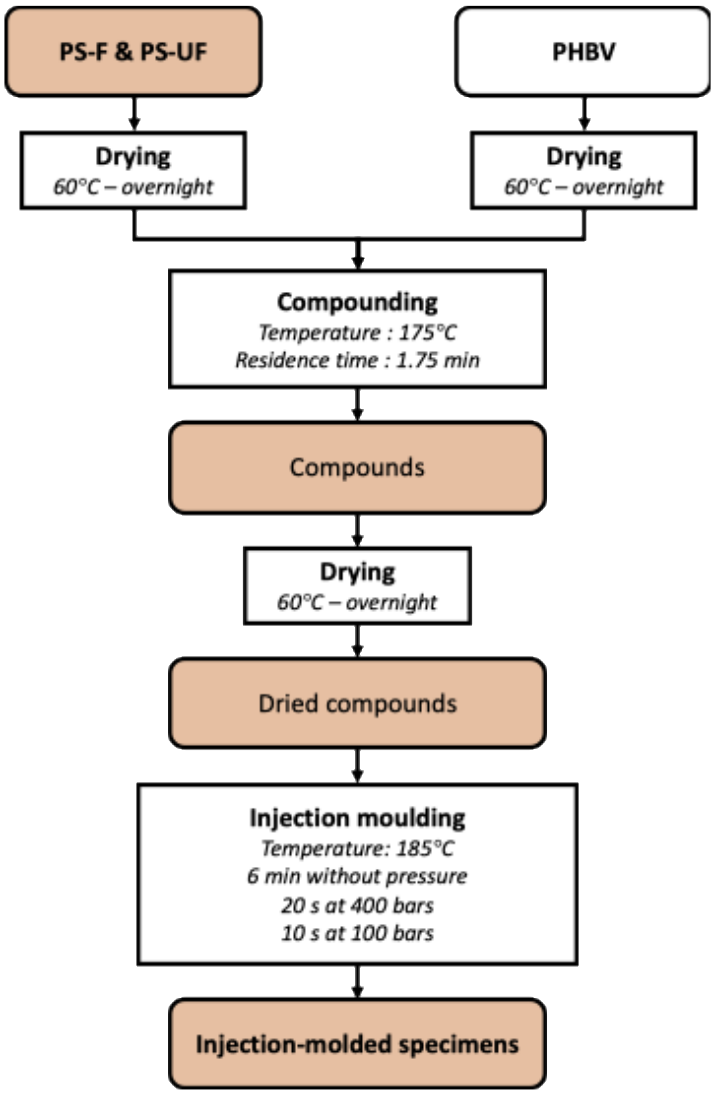

Figure 45. Itinerary of production of PHBV/PS biocomposites

3.7.2.3. Characterization of PS fillers and PS-based biocomposites

Laser granulometry analysis. The volume size distribution of PS powders was determined using a laser diffraction granulometer (LS13 320 XR, Beckman Coulter) equipped with a dry powder dispersion module. The powders were dispersed by aspiration and analyzed as they passed through a laser beam. From the resulting volume distribution data, the apparent particle diameters (d_{10}, d_{50}, d_{90}) and the span value were calculated.

Pycnometry. The true density of PS powder was measured using a gas pycnometer (ULTRAPYC 1200e, Quantachrome). Approximately 10 mm^3 of powder was placed into the analysis chamber, and nitrogen gas at 40 kPa was used as the displacement medium. Measurements were performed in triplicate.

Scanning electron microscopy (SEM). PS particles and fractured surfaces of biocomposites were examined using a scanning electron microscope (SEM, Phenom ProX, Phenom World) equipped with a backscattered electron detector (BSD) and operated at an accelerating voltage of 10 kV. Prior to imaging, samples were coated with a 4 nm layer of palladium using a sputter coater (Quorum SC7620).

SEM analysis of PS particles provided information on surface morphology, roughness, and aspect ratio. The fracture surfaces of the biocomposites were observed in order to identify the mechanisms involved in the fracture process.

Color analysis. Color attributes of PS powders from International Commission on Illumination (L*, a*, and b*) were measured with a Minolta chromatometer (CR-410, Konica Minolta Sensing Inc., Osaka, Japan). Measurements were done in triplicate.

Contact angle measurements. PS powders have been dried at 60°C overnight then pressed to form tablets (6000 mm^3) using a hydraulic press (Perkin-Elmer) at a pressure of 150 MPa during 30s. Contact angle measurements were performed using a goniometer instrument (Digidrop, GBX, France) at room temperature equipped with a CCD camera (23 frame.s^{-1}). The dispersive (γ_S^d) and polar (γ_S^p) components of the solid surface tension were evaluated by applying the Owens–Wendt (Owens and Wendt 1969). For that purpose, four solvents (distilled water, ethylene glycol, formamide and diiodomethane) were used in triplicate with a 3 µL drop volume and the "contour" mode. Their respective surface tension components were taken from the literature and are listed in **Table 27** (Montaño-Leyva et al. 2013). In order to calculate the work of adhesion (W_{12}) between the wheat gluten-based matrix (γ_1) and the wheat straw fibers (γ_2), the following harmonic-mean equation was used:

$$W_{12} = \frac{4\gamma_1^d\gamma_2^d}{\gamma_1^d+\gamma_2^d} + \frac{4\gamma_1^p\gamma_2^p}{\gamma_1^p+\gamma_2^p} \quad \textbf{(Equation 5)}$$

Then, the interfacial tension (γ_{12}) was calculated using equation 5:

$$\gamma_{12} = \gamma_1 + \gamma_2 - W_{12} \quad \textbf{(Equation 6)}$$

Table 27. Surface tension components (γ_L^d, the dispersive component, γ_L^p, the polar component, and, γ_L, the total surface tension) of the reference liquids (Montaño-Leyva et al. 2013).

Liquids	γ_L^d (mJ.m^{-2})	γ_L^p (mJ.m^{-2})	γ_L (mJ.m^{-2})
Water	21.8	51.0	72.8
Formamide	39.0	19.0	58.0
Diiodomethane	50.8	0.0	50.8
Ethylene glycol	29.0	19.0	48.0

Thermogravimetric analysis (TGA). The thermal stability of PS powders and corresponding composites was evaluated by TGA (TGA2, Mettler Toledo), carried out by heating about 10 mg of samples from room temperature up to 900°C, at a heating rate of 10°C min^{-1} under either air or nitrogen (flow rate of 50mL.min^{-1}). The thermal degradation temperature, Tdeg, was measured from the maximum value of weight loss derivative.

Dynamic scanning calorimetry analysis (DSC). Differential scanning calorimetry was used to measure the melting (T_m) and crystallization (T_c) temperatures of materials, as well as their crystallinity (X_c). Measurements were done with a thermo-modulated calorimeter (DSC25, TA Instruments, New Castle, USA). Around 5 mg of sample were placed in hermetic aluminum pans (Zero Aluminium Hermetic pan, TA Instruments New Castle, USA).

The melting behavior of the compounds was initially investigated to determine the appropriate temperature for injection molding. For this purpose, samples were subjected to a thermal scan from −50 °C to 200 °C at a heating rate of 10 °C·min^{-1}.

Then, the thermal behavior of extruded compounds was studied by applying a heating / cooling / heating cycle at 10 °C.min^{-1}. Samples were first heated from -50 to 185 °C, then maintained at 185 °C during 30 seconds, cooled down to -50 °C and maintained at -50 °C during 2 min, before being heated again up to 185 °C.

Finally, the thermal behaviour and properties of final injected-molded specimens have been studied applying heating/cooling/heating cycles at 10 °C.min^{-1}. Sample were first heat -50 to 200 °C then maintained at 200 °C during 1 min. Cooled down to -50 °C and maintained at this temperature during 2 min, before heating up again to 200 °C.

Overall crystallinity was determined from melting enthalpy (measured during both the first and the second heating ramps) using **Equation 7**.

$$X_c = \frac{\Delta H_m}{\Delta H_m^0 * (1 - \frac{\%wtfiller}{100})} * 100 \quad \textbf{(Equation 7)}$$

where ΔH_m is the melting enthalpy in J.g-1, ΔH_m^0 is the melting enthalpy of 100% crystalline PHBV. A value of 146 J.g^{-1} was considered (Barham et al. 1984a).

Tensile tests. Mechanical properties (Young's modulus, nominal stress at break and nominal strain at break) of injection molded sampled were determined using tensile tester (INSTRON 68SC-5) using a 2 kN captor. Before analysis, sample have been stabilized during two weeks into a desiccator under vacuum at room temperature. Conditions of analysis followed the norm ISO 527-2:2025 (International Organization for Standardization 2025).

3.7.3. Results and discussion

3.7.3.1. Color of PS powders

The PS powders exhibit a grey-orange hue, with similar colour parameters for both particle sizes (L* ≈ 64, a* ≈ 4, b* ≈ 20), as shown in **Table 27** and **Figure 46**. A slight increase in b* indicates a more yellow tone.

Table 28. Colorimetry parameters of PS-F and PS-UF

	L*	a*	b*
PS-F	64.5 ± 0.3	3.4 ± 0.1	18.3 ± 0.2

PS-UF	63.8 ± 0.7	3.9 ± 0.1	20.8 ± 0.2

3.7.3.2. PS particle size, shape and density

The median particle sizes (d_{50}) of PS powders were about 355 µm for PS-F and 95 µm for PS-UF, respectively, confirming the efficiency of the grinding protocol in producing fine and ultra-fine fractions.

Both particle populations displayed significant **heterogeneity**, as evidenced by the volume-based size distribution curves obtained via laser granulometry (**Figure 46**) and the SEM micrographs (**Figure 47**). This pronounced polydispersity originates from the intrinsic structure of raw peanut shells, which consist of various histological tissues and anatomical regions. Similar observations have been reported for other lignocellulosic materials such as wheat straw, where successive grinding steps yield particles with diverse characteristics in terms of size, shape, density, and surface morphology (Montaño-Leyva et al., 2012).

The polydispersity was particularly pronounced in the PS-UF sample, as indicated by a higher span value (2.4 compared to 1.8 for PS-F) and a sharper multimodal size distribution curve, revealing at least six distinct particle populations within a single sample. This polydiversity may be due to the **presence of constituents that are recalcitrant to dry grinding**, resulting in an unevenly effect of disintegration upon different histological tissues. Notably, achieving the ultra-fine fraction proved especially challenging. While only three grinding steps (cutting, impact milling, and ball milling) are sufficient to obtain ultra-fine powders from wheat straw, a fourth step—additional impact milling—was required for peanut shells to reach an apparent median diameter below 100 µm (**Figure 44**). Worth to note that it was not possible to achieve a d_{50} below 20 µm, a threshold that is readily attainable with wheat straw (Montaño-Leyva et al. 2013).

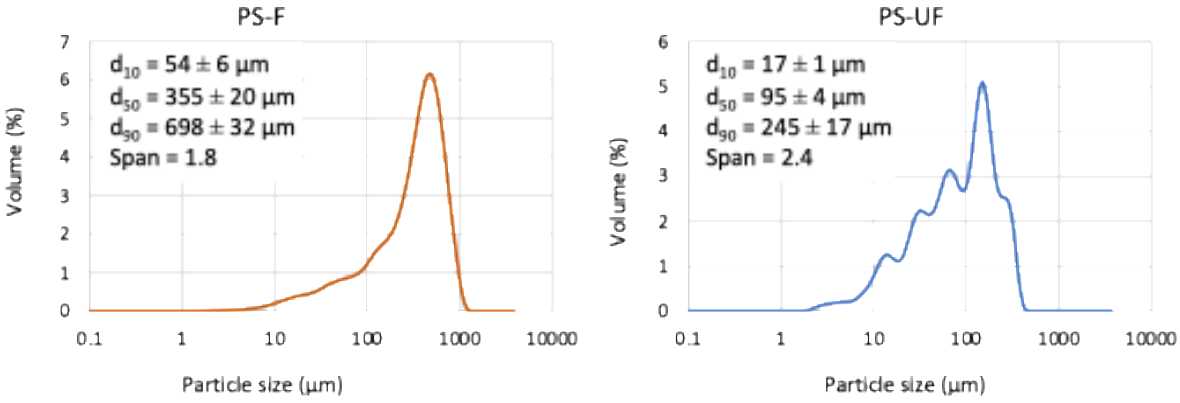

Figure 46. Volume size distributions obtained by laser granulometry for PS-F and PS-UF.

Regarding the shape of particles: The two PS fractions encompass a **broad spectrum of particle morphologies**, generally characterized by low aspect ratios (Figure 47). Hence the use of the term "particles" rather than "fibers." SEM observations revealed significant surface roughness, which may

promote mechanical interlocking with the PHBV matrix and enhance interfacial adhesion in biocomposites.

The **true density** of particles was measured for both PS-F and PS-UF, yielding values of 1.429 ± 0.002 g·cm^{-3} and 1.465 ± 0.003 g·cm^{-3}, respectively. The slightly higher density observed for the finer particles (PS-UF) is consistent with a reduction in intrinsic closed porosity, which typically occurs during particle size reduction.

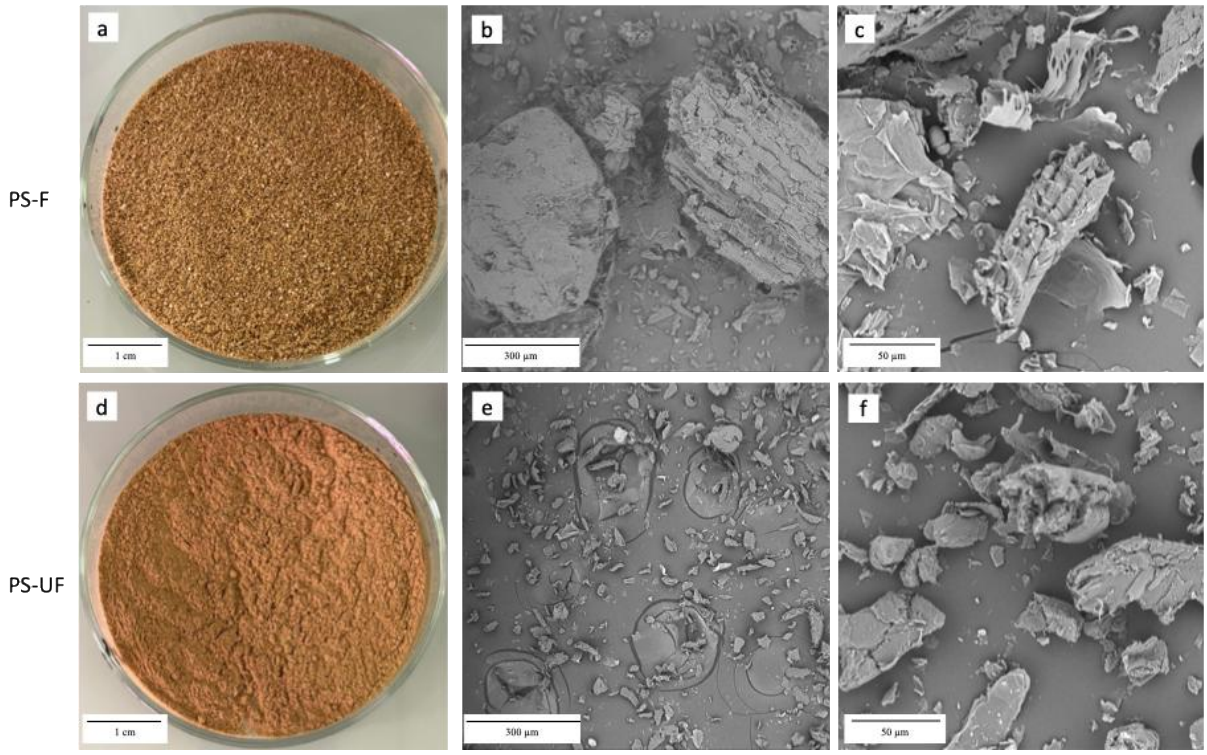

Figure 47. Pictures (a,b) and SEM micrographs (b,c,e,f) of PS-F (a,b,c) and PS-UF (d,e,f) powders

3.7.3.3. Particle surface energy

PS-F and PS-UF exhibited similar surface free energy values, around 55 mJ·m^{-2} (**Table 29**), which are in the range of values reported in the literature for lignocellulosic fillers, ranging between 30 and 60 mJ·m^{-2}(Berthet, Angellier-Coussy, Machado, et al. 2015). Overall, the surface energy of PS was approximately evenly distributed between polar and dispersive components, as expected from an OH-rich surface. However, a closer examination reveals that, despite similar total values, the relative contributions of the polar and dispersive components differ between the two fractions. Grinding results in a slightly more hydrophilic fraction, characterized by a decrease in the dispersive component (from 28.4 to 25.1 mJ·m^{-2}) and an increase in the polar component (from 26.4 to 31 mJ·m^{-2}). This shift is expected to result in reduced affinity with hydrophobic polymer matrices such as PHBV (polar component of 6.2 mJ·m^{-2} and dispersive component of 42.8 mJ·m^{-2}).

The work of adhesion between the PHBV matrix and PS fillers was calculated using data reported in the literature for PHI002 processed in similar conditions (David 2019). Low interfacial tension values combined with high work of adhesion values are indicative of good compatibility between the constituents. PS-F showed slightly greater affinity for PHBV compared to PS-UF, although the

differences were minor and further replicates would be necessary to confirm this trend. Worth to note that the predicted work of adhesion between PHBV and PS is higher than the one reported for wheat straw fillers (50 mJ.m^{-2}) or torrefied wheat straw fillers (68 mJ.m^{-2}).

Table 29. Contact angle values (°) of liquids of reference on PHBV and PS fillers, polar (γ_S^p) and dispersive (γ_S^d) components of the solid surface energy (γ_S), and predicted work of adhesion (W_{12}) and interfacial tension (γ_{12}) between PS fillers and PHBV.

	Contact anle (°)				Solid surface tension (mJ.m^{-2})			W_{12} (mJ.m^{-2})	γ_{12} (mJ.m^{-2})
	Water	Ethylene glycol	Formamide	Dioodomethane	γ_S^p	γ_S^d	γ_S		
PHBV*	68	45	39	20	6.2	42.8	48.9	n.c.	n.c.
PS-F	33.6	37.9	39.1	37.1	26.4	28.4	54.8	88.4	15.4
PS-UF	28.8	36.7	40.3	44.8	31	25.1	56.1	84.0	21.1

*from (David 2019)

3.7.3.4. Thermal behavior of biocomposites

The melting and non-isothermal crystallization behavior of injection molded biocomposites and the corresponding neat matrix were analyzed by DSC by applying heating-cooling-heating cycles (**Figures 48A, B and C**). The maximum temperature selected in this cycle (185°C) corresponded to the temperature applied during the injection process.

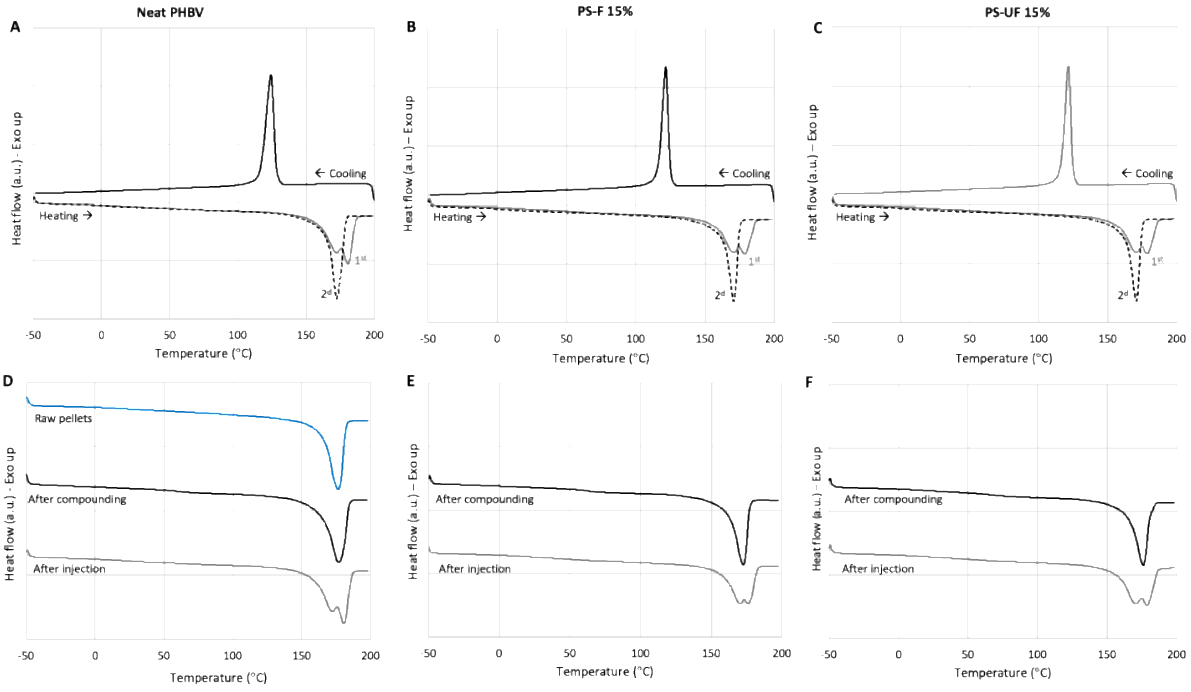

Figure 48. DSC thermograms of (A,B,C) heating-cooling-heating cycles for injection molded specimens, and of (D,E,F) the first heating of samples after the compounding and the injection molding steps, for (A,D) the neat matrix, and composites containing 15wt% of either (B,E) PS-F fillers or (C,F) PS-UF fillers.

All injection-molded specimens display similar thermal behavior. During the first heating ramp, a bimodal melting peak was detected: the first (Tm_1) around 172 °C and the second (Tm_2) near 180 °C. This dual melting phenomenon is evident in both the pure PHBV matrix and its composite formulations, demonstrating that it does not result specifically from the incorporation of PS fillers. Worth to note that following the compounding step, a single melting peak was observed within the same temperature range (**Figures 48D, E, and F**), indicating the formation of two distinct crystalline populations during the cooling phase of the injection molding process. During the cooling ramp, a well-defined crystallization peak is observed. In the second heating ramp, i.e. after thermal history erase, no cold crystallization was detected, confirming complete crystallization of the polymer during cooling. This is due to the presence of boron nitride (used a nucleating agent) in the commercial PHBV grade used. The second heating scan displays a single melting peak centered at approximately 172 °C, indicating the exclusive presence of less-ordered crystals. This peak is associated with a higher melting enthalpy compared to the first heating ramp, reflecting an increase in crystallinity (**Table 30**). Thermal degradation is presumed to occur throughout the successive thermomechanical processing steps, as evidenced by a slight decrease of about 2°C in the melting temperature across all samples (data not shown).

Table 30. Thermal characteristics measured by DSC analysis on injection-molded specimens during heating-cooling-heating cycles

Injection-molded specimens	1st heating ramp				Cooling ramp		2nd heating ramp		
	Tm1 (°C)	Tm2 (°C)	Xc (%)	ΔHm ($J.g^{-1}$)	Tc (°C)	ΔHc ($J.g^{-1}$)	Tm (°C)	Xc (%)	ΔHm ($J.g^{-1}$)
PHBV	172.5 ± 0,5	179.7 ± 1.2	63 ± 2	92 ± 3	124.5 ± 0.3	89 ± 1	172.4 ± 0.1	68 ± 1	100 ± 1
PS-F 5wt%	172.0 ± 0.4	179.5 ± 1.3	60 ± 2	83 ± 3	123.9 ± 0.9	81 ± 2	171.9 ± 0.6	66 ± 2	91 ± 3
PS-F 10wt%	172.2 ± 1.8	176.9 ± 2.3	58 ± 2	77 ± 3	122.6 ± 1.4	73 ± 3	170.8 ± 1.3	63 ± 2	83 ± 2
PS-F 15wt%	170.4 ± 0.2	178.7 ± 2.5	58 ± 4	72 ± 5	121.9 ± 1.2	68 ± 3	171.3 ± 1.5	62 ± 3	77 ± 4
PS-UF 5wt%	171.9 ± 0.1	181.2 ± 0.7	62 ± 2	86 ± 3	123.7 ± 0.2	84 ± 3	171.8 ± 0.5	68 ± 1	94 ± 1
PS-UF 10wt%	172.2 ± 0.2	178.9 ± 0.8	63 ± 2	83 ± 3	122,6 ± 0.3	78 ± 2	171.5 ± 0.2	67 ± 1	88 ± 2
PS-UF 15wt%	171.3 ± 0.4	178.3 ± 0.8	63 ± 2	77 ± 2	121.4 ± 0.1	73 ± 1	170.5 ± 0.3	66 ± 2	82 ± 2
PS-UF 20wt%	170.3 ± 0.5	176.0 ± 1.5	62 ± 2	72 ± 2	122,5 ± 0.4	70 ± 2	172.4 ± 0.1	68 ± 1	79 ± 1

Given the standard deviation values, no significant effect of PS particle size nor content was observed on the melting temperatures (**Figure 49, Table 30**). This is in agreement with previous results of PHBV

materials reinforced with lignocellulosic fillers (Munch et al. 2022). In terms of crystallization behavior, the incorporation of increasing content of PS fillers up to 15 wt% led to a slight decrease in the crystallization temperature of the polymer matrix, by up to 3 °C. This trend was accompanied by a modest reduction in crystallinity for the PS-F-based formulations. These observations globally suggest that the incorporation of PS fillers slightly hinders the crystallization process, acting as anti-nucleating agents. The more pronounced effect observed with PS-F may be attributed to its better affinity with the polymer matrix, as shown from the prediction of the work of adhesion, which could restrict chain mobility and thus impede crystallization. It is worth noting, however, that the overall impact remains minimal and is likely masked by the presence of boron nitride in the formulation.

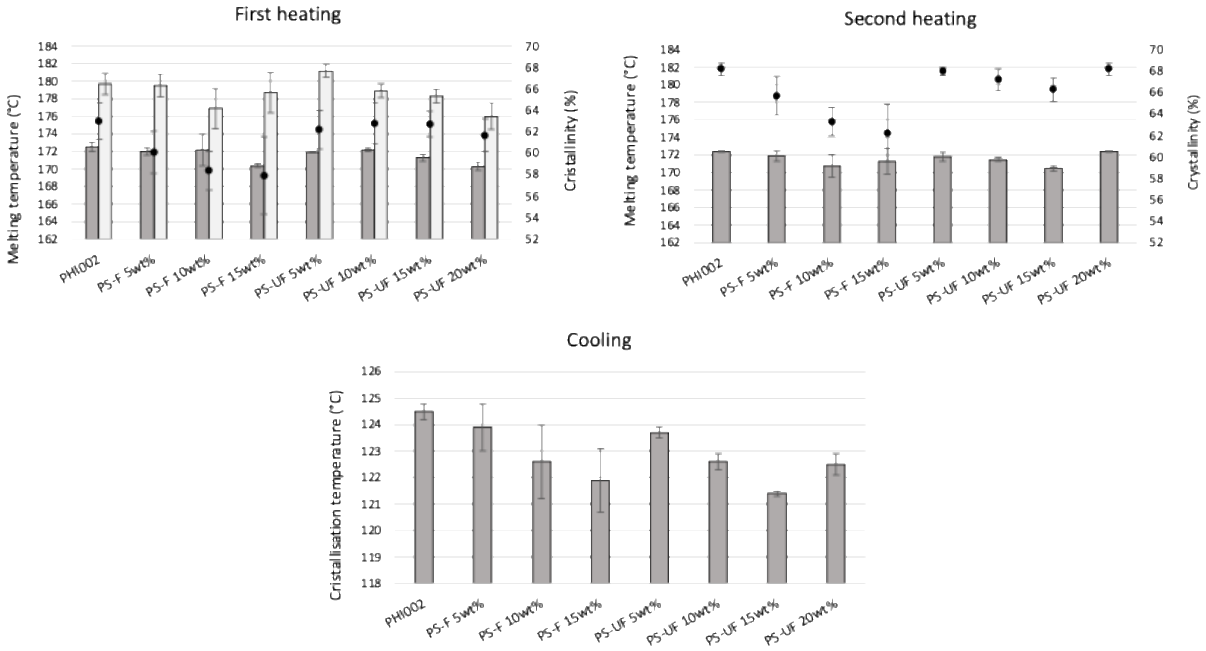

Figure 49. Melting (Tm1, in dark grey, Tm2, in light grey) and crystallization (Tc) temperatures, and crystallinity (black dots) measured by DSC analysis on injection-molded specimens during heating-cooling-heating cycles.

3.7.3.5. Mechanical performance of biocomposites

Typical stress–strain curves revealed a stiff and brittle behavior for all PHBV-based materials, including the neat matrix (**Figure 50**). For the neat matrix, a Young's modulus of 2.2 GPa, a tensile strength of 58.8 MPa, and a strain at break of 4.4% were recorded. These values are consistent with those reported by (Viretto et al. 2021), who used the same PHBV grade and processing method.

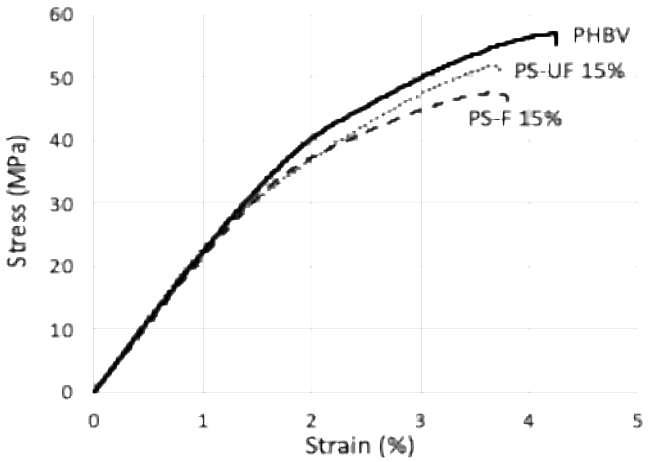

Figure 50. Typical curves of the stress vs. strain for the neat PHBV and PHBV-based composites filled with 15 wt% of PS-F and PS-UF (injection-molded specimens).

Regardless of the PS filler size, the incorporation of PS particles increased the brittleness of the materials, as evidenced by a slight but significant decrease in both strain and stress at break (**Figure 51, Table 31**). Up to a filler content of 15 wt%, no noticeable effect of filler content was observed. The use of PS-UF seems to better preserve the mechanical strength, with no positive effect on the strain at break. For a filler content of 20 wt%, which was only achievable to the PS-UF fraction, a significant 30% decrease of the strain at break was reported. Meantime, Young's modulus was not significantly impacted up to 15 wt% of filler for both fillers. It was slightly increased when adding 20 wt% of PS-UF.

Table 31. Tensile properties of PHBV/PS injection-molded specimens.

	Young's Modulus (GPa)	Stress at break (MPa)	Strain at break (%)
PHBV	2.2 ± 0	58.8 ± 2.2	4.4 ± 0.4
PS-F 5 wt%	2.1 ± 0.1	50.6 ± 2.7	3.9 ± 0.3
PS-F 10 wt%	2.1 ± 0	49.2 ± 2.1	3.9 ± 0.3
PS-F 15 wt%	2.2 ± 0	49.3 ± 2.8	3.8 ± 0.3
PS-UF 5 wt%	2.2 ± 0	56.3 ± 1.8	4 ± 0.2
PS-UF 10 wt%	2.3 ± 0	53.9 ± 0.9	3.9 ± 0.1
PS-UF 15 wt%	2.2 ± 0.1	49.1 ± 6.5	3.8 ± 0.3
PS-UF 20 wt%	2.5 ± 0	48.3 ± 5.9	3 ± 0.5

As reported by Munch et al. (2022) in a data paper gathering almost 100 formulations of PHBV-based lignocellulosic composites, the mechanical performance of PHBV-based composites is significantly affected by the type and content of lignocellulosic fillers. At a filler content of 15 wt%, the average ratios between the propreties of the composite and that of the neat matrix are 0.80 for the stress at break and 0.69 for the strain at break (pool of data including the following biomasses : olive pomace stone-rich, olive pomace pulp-rich, leaves, grass, branches, rice husk, hemp core, wood flour). We can thus consider that ultimate properties of PS-based biocomposites are here rather well preserved. Such

good preservation of mechanical properties was also observed for wood flour and ground branches (Viretto et al. 2021).

As largely described in the literature, the decrease in ultimate tensile properties induced by the presence of lignocellulosic fibres could be mainly ascribed to a lack of adhesion and/or adherence between the hydrophobic matrix and lignocellulosic fibers. In the case of PS-based composites, the rather good preservation of mechanical properties was ascribed to an efficient interfacial adhesion and/or adherence. On one hand, the adhesion is a purely physico-chemical phenomenon that is governed by the surface free energy and roughness of fibres, as well as the surface tension of the polymer matrix (Le Moigne et al. 2018). On the other hand, adherence refers to the interfacial strength developed between the fibres and the matrix within the consolidated composite when subjected to mechanical stress (Le Moigne et al. 2018). Consequently, additional factors such as fibre/matrix chemical interactions, mechanical interlocking, and transcrystallinity also come into play.

The filler surface free energy the filler is directly related to its biochemical composition and location of components. The stress at break is known to increase exponentially with the cellulose content in the filler and inversely proportionally with the lignin content (Berthet et al. 2016). Wood flour: lignin content of 20.3% and cellulose content of 37% / ground branches: lignin content of 23.5% and cellulose content of 30% (Munch et al. 2022).

Interfacial adhesion is also influenced by the physical properties of the surface. Increased surface roughness enhances mechanical interlocking. PS-F and PS-UF exhibit significant surface roughness (**Figure 47**), which can promote adhesion through mechanical interlocking mechanisms (Amiandamhen et al. 2020; Le Moigne et al. 2018; Mohammed et al. 2022).

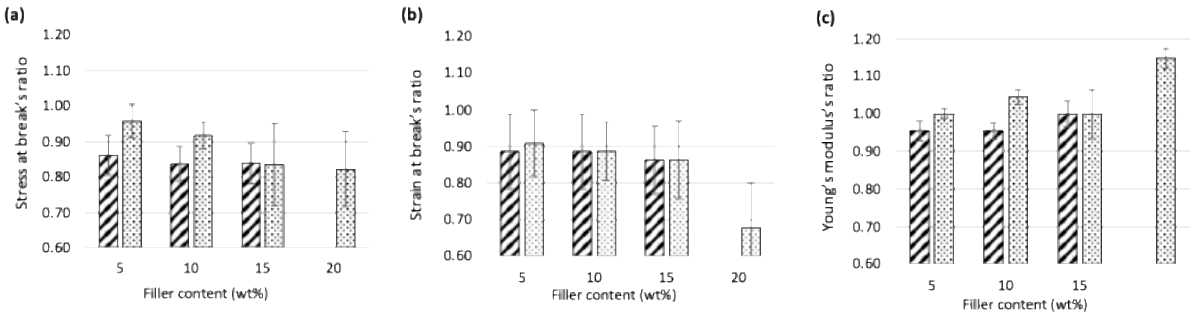

Figure 51. Mechanical properties of injected specimen remated to those of the neat matrix: (a) stress at break, (b), strain at break, and (c) Young's modulus.

The interfacial adhesion was qualitatively assessed by SEM observation of the cross-section of specimens after mechanical testing (**Figure 52**). The qualitative indicators included the occurrence of failure surfaces, particle pull-outs, interfacial gaps around fillers, debonding, and the degree of filler wetting by the polymer. As previously reported for PHBV/wheat straw fibers composites (Berthet et al. 2016), poor interfacial adhesion was inferred from the presence of interfacial voids and numerous fiber pull-outs. In the present study, composites containing 15 wt% PS particles exhibited good wetting by the polymer, with no visible interfacial gaps—similar to observations made by Viretto et al. (2021)

for wood flour. Nonetheless, a few pulled-out particles were observed, particularly in the PS-F sample.

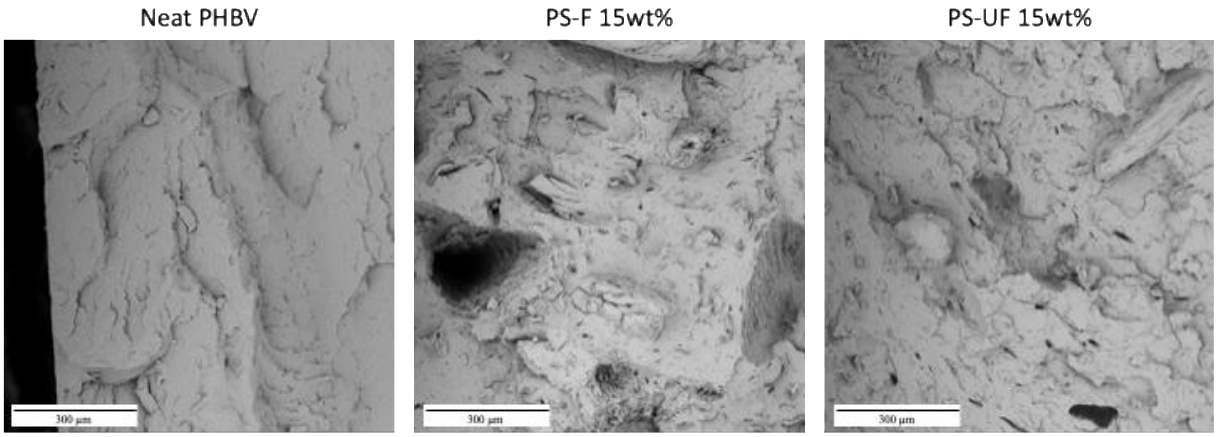

Figure 52. SEM observation of cross-section of injection-molded specimens after mechanical testing.

3.5.4. Conclusion

This study demonstrates the **feasibility of developing PHBV-based biocomposites incorporating peanut shell (PS)** fillers obtained through dry fractionation. Two fractions were produced, a fine fraction (PS-F), with a d_{50} of 355 mm, and an ultra-fine fraction (PS-UF), with a d_{50} of 95 mm. Up to respectively 15 and 20 wt% were incorporated by melt extrusion without any processability issue. Rigid items were shaped by injection molding.

Despite the inherent brittleness of PHBV, the incorporation of PS fillers did not significantly compromise the mechanical performance, with Young's modulus remaining stable and only moderate reductions observed in tensile strength and elongation at break. These results suggest a relatively good interfacial adhesion and/or adherence between the PS fillers and the PHBV matrix, likely promoted by the surface roughness and biochemical composition of the fillers. SEM observations confirmed the absence of interfacial gaps and the presence of good polymer wetting, especially for PS-UF-based composites.

In strong interaction with WP1, a **critical analysis will be conducted to evaluate the trade-offs between safety, processability, and performance** for PHBV-based biocomposites, leading to recommendations based on these criteria and the intended uses of the final materials.

5 kg of PHBV/PS-F compounds (with 15 wt% of PS-F) were sent to CAVI (France) for the production of clips for vineyards, and further testing in close-to-real conditions (task 4.2.).

4. Extraction of plant molecules at pilot scale

4.1. Extraction of cutin from tomato peels (TOMA)

At the Tomapaint facility (**Figure 53a**), the bioresin cutin is extracted from the cuticle of the tomato peels using an optimized, standardized, and patented method ("Process For The Extraction Of Cutin From Tomato Processing Waste" EP 4116352). The process is eco-friendly, since no organic solvents are used unlike other methods reported in the literature (Pecorini et al. 2025). The tomato by-products, collected during the tomato season, are stored under anaerobic conditions. Tomato pomace contains peels and seeds in roughly equal amounts of dry matter.

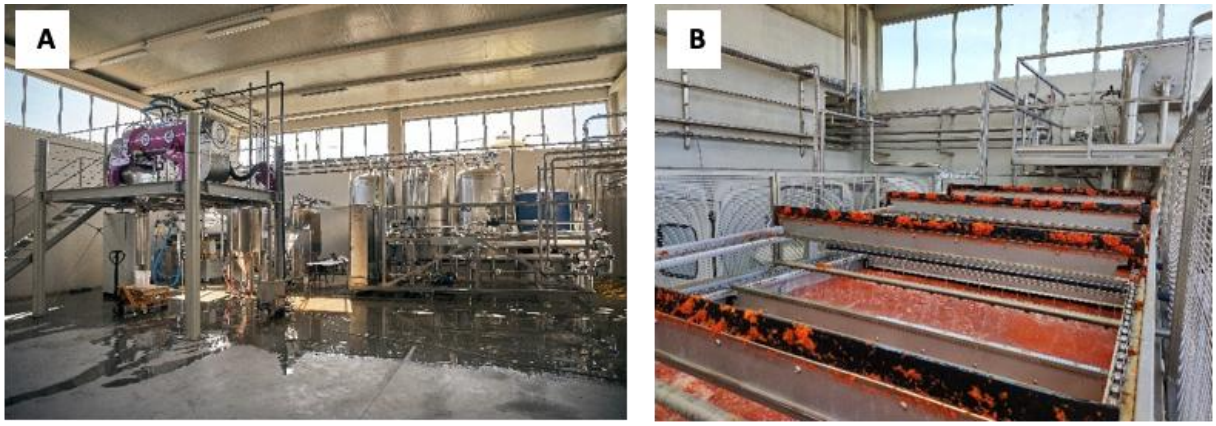

Figure 53. (a) Plant for cutin extraction and (b) flotation system.

The first step of the extraction process consists in the separation of peels and seeds by flotation (**Figure 53b**). The efficiency of this step is evaluated by the amount of seeds that residues in the floated peels. During the Agriloop project the efficiency of the separation was improved modifying some parameters of the floatation tank, mainly flow rate and water hardness. The results obtained are reported in **Table 32**.

Table 32. Amount of seeds in floated peels.

Flotation conditions	Seeds in floated peels, % (w/w)
Standard	3.75±1.27
News	1.14±0.70

Pomace, seeds and peels are then dried in a dryer developed in the Agriloop project (**Figure 54**). It works using renewable energy; the heat comes from the Biogas plant near the extraction plant. The capacity is 20kg/day of wet by-products.

Figure 54. Dryer system.

The average moisture content of the by-products is reported in the **Table 33** with the efficiency of the equipment.

Table 33. Efficiency of the drying system.

	Pomace	Seeds	Peels
Wet (kg)	40	40	110
Dried (kg)	4	4	8
Umidity wet %, Thermobalance 110°C	71.7	72.1	76.4
Umidity dried %, Thermobalance 110°C	3.3	5.2	4.2

The floatation steps is followed by heat treatment of the peels at high temperature in an alkaline NaOH solution (**Figure 55a**). Then the separation of liquid alkaline phase from exhausted peels by means of an horizontal centrifuge is carried out. Finally, the cutin is precipitated by acidification, using an inorganic acid, and separated by centrifugation (**Figure 55b**). The resulting cutin, brown in colour, is a paste with a solid content higher than 60% (**Figure 56**).

Figure 55. Dryer system.

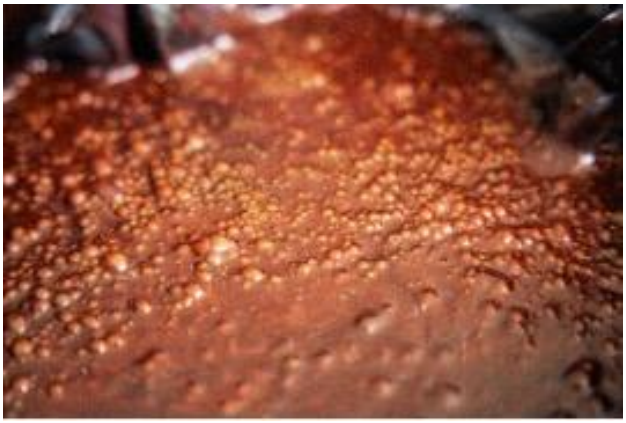

Figure 56. Cutin from the Tomapaint process.

The standard yield of the process is about 13% (w/w) calculated on the wet peels. In order to increase the process yield, an integration of the plant line has been realized in the first 10 months of 2025, allowing the recovery of some cutin usually lost in the streams. In the new part of the plant line were added two tanks, one as a buffer and the second one for cutin decantation (**Figure 57**) with two objectives:

- to increase the yield from 13%w/w up to 30%w/w
- to reduce the organic contamination of the streams

Figure 57. Integrated system to increase process yield.

From February to August 2025 10 batches of cutin were produced, 25kg/batch. Results of the analysis carried out on the cutin samples are shown in **Table 34**.

Table 34. Cutin analysis.

Batch Code	pH (20°C)	Humidity % (Thermobalance,110°C)
T01	4.6	29.3 ± 2.6
T02	4.5	28.8 ± 4.6
T03	4.5	32.2 ± 2.6
T04	4.4	29.4 ± 2.9
T07	4.5	32.1 ± 2.0
T10	4.6	30.1 ± 2.8
T12	4.4.	29.9 ± 2.4
T13	4.5	30.9 ± 1.8
T21	4.6	32.8 ± 3.3.
T25	4.5	32.5 ± 1.0

In **Table 35**, a standard chemical composition of cutin is reported. The results are referred to the Batch coded T13. Summarizing 1700kg of wet pomace were used to obtain 870kg of wet peels, 800kg of wet seeds and 250kg of cutin. Based on the results obtained, 25kg of cutin for each of the batches n.T01, T13 and T25 have been stored in the fridge and are available for the following steps and analysis.

Table 35. Cutin chemical composition.

Constituent	Content (g/100g)	Method
Proteins	2.68	Istisan 96/34 page 13
Fats	1.73	Istisan 96/34 page 41
Fibres	6.50	AOAC 985.29
Ash	0.95	Istisan 96/34 page 77
Sugars	0.19	P-PRO-ALI-32
Cutin	87.95	By difference

4.2. Extraction of polyphenols from green apple juice (SDIC)

4.2.1. Introduction

To further advance the collaborative R&D efforts on **high-efficiency apple polyphenol extraction technology**, a pilot experiment was carried out at the Rushan R&D Center. Building on the existing polyphenol extraction process for green apple juice developed at Beijing University of Chemical Technology. The experiment aimed to efficiently recover apple polyphenols from the resin eluent generated during the concentrated apple juice production process.

4.2.2. Pilot Experiment on polyphenol extraction from green apple juice

Polyphenols were extracted from the eluent of the resin of concentrated green apple juice on the production line. Three pilot experiments were carried out in August 2025, with the following pilot experiment process (**Figure 58**).

(I) Resin process. I.1. Resin pretreatment. The decolorization resin was sequentially pre-treated with dilute hydrochloric acid and sodium hydroxide, then rinsed with deionized water to a neutral pH. **I.2. Raw materials.** The prepared concentrated green apple juice was properly diluted and used as the sample feedstock. **I.3. Sample injection.** The diluted green apple juice was fed into the resin, with the flow rate controlled according to the sample injection conditions. **I.4. Resin washing with water.** After sample injection, the resin was rinsed with deionized water. **I.5. Alkali elution.** The resin was desorbed with NaOH solution, and the eluent was adjusted to acidic condition to obtain the subsequent membrane feed solution.

(II) Membrane process. The eluate was concentrated via membrane filtration until the soluble solids content exceeded 15 °Brix. The concentrated solution was taken for spray drying.

(III) Spray drying. The final concentrated solution was subjected to spray drying, and finally, a powder was obtained after spray drying, with a brownish-yellow color.

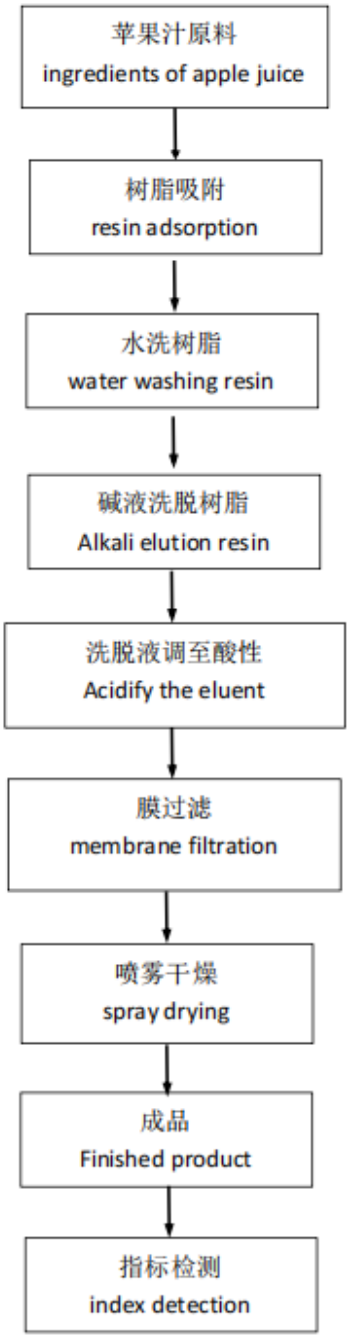

Figure 58. Extraction process of polyphenols from the waste of the mature apple juice.

4.2.3. Results

The results were highly promising, with polyphenol purity exceeding 75%, and reaching up to 81% in the third pilot experiment (**Table 36**). A total of 14.1 kg of polyphenol-rich powder was obtained across the three pilot-scale trials (**Figure 59**).

Table 36. Physicochemical data of spray-dried powders from the three pilot experiments.

Serial Number	Polyphenol Purity (%)	Ash Content (%)	Moisture Content (%MC)	Mass (kg)
1	75	3.1	2.02	5
2	76	2.2	2.1	3.6
3	81	1.7	3.8	5.5

Figure 59. Samples from the polyphenol-rich powders recovered from the three pilot experiments.

4.2.4. Conclusion and perspective

In addition to green apple juice, a pilot experiment for extracting polyphenols from the eluent of the resin in mature apple juice is currently underway. **The aim is to achieve polyphenol extraction from the waste of the mature apple juice production line.**

4.3. Extraction of proanthocyanidins from peanut's red skin (SJCOF)

4.3.1. Introduction

The company mainly studies the **extraction of proanthocyanidins from peanut red skins.** The main process flow is as follows: pretreatment of peanut red skin raw materials → solution extraction → heating → vacuum concentration → filtrate → secondary extraction - degreasing of secondary extraction liquid → concentration tank → secondary vacuum concentration → concentrated liquid → vacuum drying → proanthocyanidin extract from peanut red skins (**Figure 60**).

Figure 60. From peanut red skins to proanthocyanidin extract.

4.3.2. Results and discussion

Effects of different solid-liquid ratios, raw material crushing particle sizes, extraction time and extraction temperature on the extraction rate of proanthocyanidins were analyzed. The response surface was optimized toto maximize the extraction rate and determine the optimal process parameters. The response surface analysis (RSM) was used to optimize the extraction process of proanthocyanidins from peanut red skins, and the optimal process conditions were determined as follows: the raw materials were crushed and passed through a 60-mesh sieve, the ratio of material to liquid was 1:20, the extraction time was 2 hours, and the extraction temperature was 57 °C. Under these conditions, the extraction rate of proanthocyanidins can reach 11.25%.

The purity of proanthocyanidins is optimized to the greatest extent by changing the concentration of analytical ethanol, concentration temperature and volume of elution liquid. Orthogonal experiments were designed to optimize the purification technology and determine the optimal process parameters. The purification technology of peanut red skin proanthocyanidins was optimized by orthogonal design, and the optimal process conditions were determined: ethanol elution concentration of 70%, concentration temperature of 75 °C, elution volume of 3BV (bed volume, hat it is approximately 6 to 8 cubic meters per column). Under these conditions, the purity of proanthocyanidins can reach 99.9%.

The project has extended the deep processing industrial chain of peanuts, with an annual output of 180 tons (**Figure 61**). The purity of the prepared products can reach up to 99.9%. The extracted proanthocyanidins have a low degree of polymerization, high antioxidant activity, good water solubility, and can better exert their biological activity. Raw material pretreatment, flocculation and impurity removal, and resin adsorption can effectively remove harmful substances such as heavy metals and aflatoxins, improving product quality and safety.

Figure 61. Equipments used for the extraction of proanthocyanidins from peanut red skins and examples of commercial products.

4.3.3. Conclusion

By controlling the process parameters and procedures of each step, the goal of obtaining a controllable purity of proanthocyanidin products can be achieved. The obtained products have different specifications, and can be developed for use in fields such as health care products, food, medicine and cosmetics. The extraction conditions are mild, the process operation is simple, it is highly efficient and low-energy consumption, achieving full utilization of raw materials and complete recycling and reuse of solvents. There is no discharge of production wastes, making it a typical green production process.

5. Production of microbial proteins at pilot scale for feed applications

5.1. Production of MP from grey starch (AVECOM, UGENT)

5.1.1. Introduction

Organic wastes originating from food industries have enormous potential as low-cost carbon sources for microorganisms to produce valuable products, such as microbial protein (MP) (Piercy et al. 2024). However, not all carbon sources are readily available for microbial conversion and might therefore require additional preprocessing steps prior to fermentation. The polysaccharide starch is a good example for such a carbon source, it consists of long chains of glucose molecules which are entangled as linear and branched chains. Due to the complexity and large size of the molecule it cannot be transported into the cell directly, therefore a pretreatment step, breaking down starch into fermentable sugars (mono- and disaccharides), is required. Among other methods, this can be done through enzymatic hydrolysis using purified enzymes or through fermentation with mixed microbiomes where enzymes are secreted by the microorganisms (Nygaard et al. 2025). A thoughtful selection of adequate strains for MP production is required to ensure a safe and high-quality product, which can be produced fast (high growth rates) and efficient (good yields). Especially, the amino acid composition is an important criterion to ensure that the final product has a balanced amino acid profile and contains essential amino acids (Rasool et al. 2023).

Many routes to produce MP, using different waste streams and different process setups, have been demonstrated and are currently being explored. However, MP is still not commonly recognised as animal feed by the market (Rasool et al. 2023). Thus, **designing and demonstrating efficient and sustainable processes at a larger scale is essential to promote a more widespread acceptance and use of microbial protein from waste sources**. Here, the conversion of grey starch (GS) (a side stream from the potato industry) to microbial protein for feed applications will be explored at pilot scale in order to demonstrate the potential of a circular waste-to-feed economy.

5.1.2. Description of the production process

The microbial protein production process from grey starch involves three critical steps to ensure the production of high-quality microbial protein: pretreatment, MP production, and de-watering (**Figure 62**).

Pretreatment. A pretreatment step is required to solubilize the organic compounds present in grey starch (expressed as volatile solids (VS) or as chemical oxygen demand (COD)), making them bioavailable for MP production. A pretreatment by fermentation (biological anaerobic acidification) was evaluated by UGENT (Deliverable 3.1). Moreover, a pretreatment by enzymatic hydrolysis was investigated by AVECOM (to be reported in Deliverable 3.2). Grey starches from local potato processing companies with varying properties were subjected to enzymatic treatment and evaluated based on the solubilization efficiency (Deliverable 3.2). Enzymatic hydrolysis was more successful than anaerobic acidification, yielding up to 88% COD solubilization of which 75% was in the form of glucose. Thus, enzymatic hydrolysis will be used as the pretreatment step for the pilot scale production of MP.

MP production. UGENT performed well-plate tests using a synthetic medium containing glucose. Since the strain C. necator H16, originally used in experiments with fermented GS, was not able to grow on this medium, the strain C. necator H1 G^{+}3 (DSM 545) was purchased. Well-plate tests confirmed that C. necator H1 G^{+}3 was able to grow in the synthetic medium supplemented with glucose and in follow up tests on the hydrolised grey starch as well. Preliminary fed batch reactor tests with C. necator H1 G^{+}3 (DSM 545) resulted in biomass concentration of 9 to 12 g/L with protein content of 50-66%.

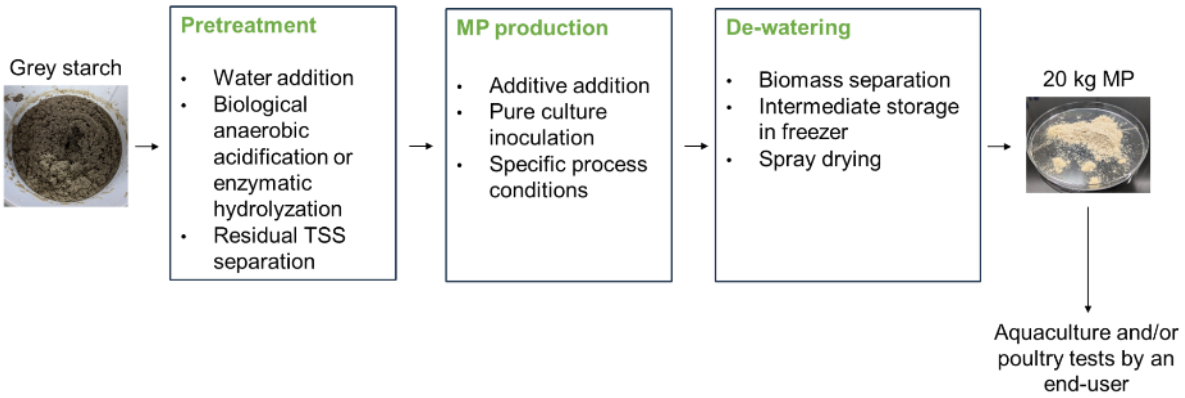

Figure 62. Critical steps involved in MP production.

Based on previous experience, AVECOM has set up a preliminary scheme for the pilot-scale production of microbial protein (**Figure 63**). During pretreatment, grey starch will be diluted and treated by enzymatic hydrolysis and then centrifuged. Subsequently, the supernatant will be diluted - if necessary - and additives will be added (NH_4Cl and K_2HPO_4) to reach a N/COD ratio of 4% w/v and a P/COD ratio of 0.8% w/v. For the influent, a COD concentration between 20 and 30 g/L will be targeted. C. necator cultivated under sterile conditions will be used as inoculum (5% v/v). The MP reactor will be operated under non-sterile conditions in continuous mode. To obtain a protein-rich biomass, the HRT will be decreased from 10 to 2.5-3 days within the first two weeks.

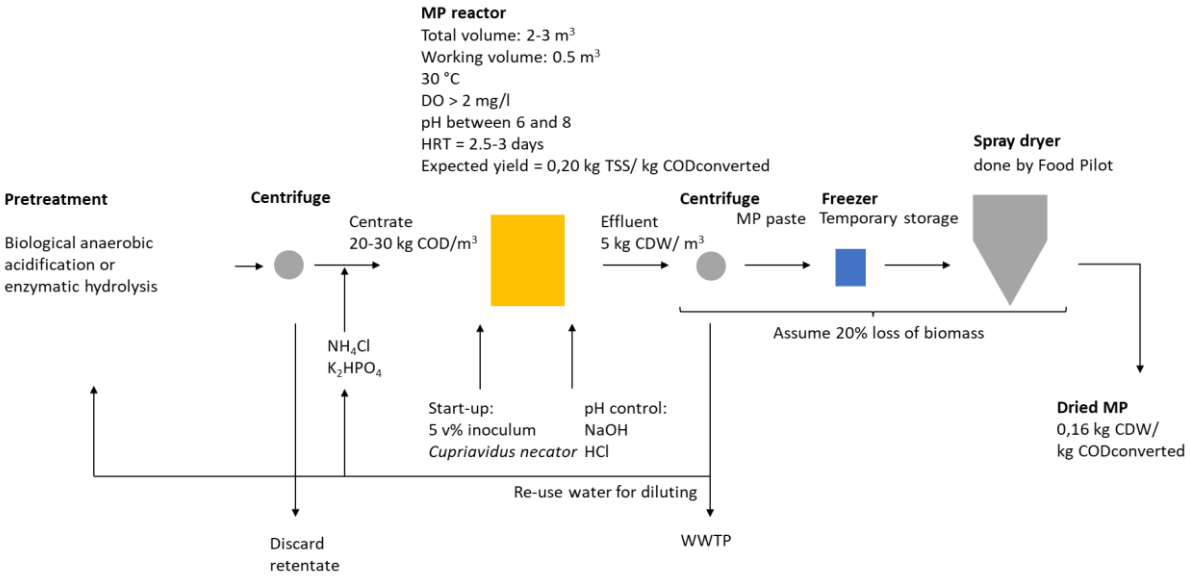

Figure 63. Preliminary overview of the set-up for the pilot-scale production of microbial protein.

5.1.3. Characterization of microbial proteins

Data from previous tests with Cupriavidus necator, courtesy of Dr Sakarika (Kerckhof et al. 2021), were utilized to inform our expectations on protein characteristics. While the exact concentrations of amino acids may vary depending on the substrate used as reported by Lee et al., (2006) and Sakarika et al., (2020), we anticipate that the amino acid composition will be similar to that observed in prior analyses (**Figure 64**) (Lee et al. 2006; Sakarika et al. 2020). This assumption is based on the consistent performance of Cupriavidus necator in similar conditions and substrates. C. necator protein content on formate was 52 $\%_{CDW}$, while it was 46 $\%_{CDW}$ on acetate (Sakarika et al. 2020).

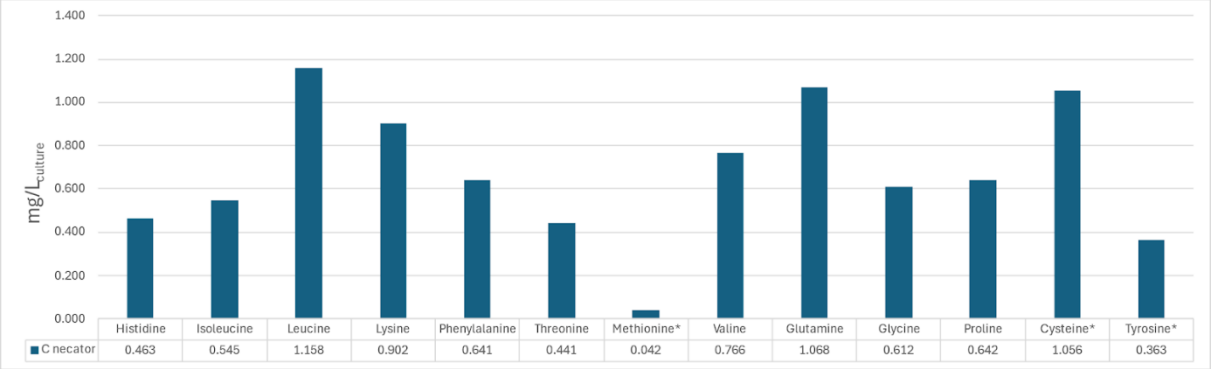

Figure 64. Amino acid composition (DSMZ medium 81; 46% H_2, 12% CO_2, 30% O_2, and 12% CH_4 in headspace) (adapted from (Kerckhof et al. 2021)).
***partially destroyed during acid hydrolysis**

5.1.4. Conclusion and perspectives

Initial trials showed that enzymatic hydrolysis was the best pretreatment method to solubilize the majority of the starch as fermentable sugars. UGENT is currently optimising a Fed-Batch strategy for the fermentation with C. necator and following this the process will be scaled to pilot scale at AVECOM to provide sufficient microbial protein for subsequent feed trials.

5.2. Production of yeast proteins from distiller's grains (HZAU, SCRG)

5.2.1. Introduction

The annual output of distiller's grains in China exceeds 10 million tons. In recent years, driven by national policies, the application of distiller's grains in the feed and fertilizer industries has achieved preliminary progress. However, the efficiency and value of the recycling and utilization of these resources still remain at a relatively low level. **Runge Biology is committed to the high-value utilization of distiller's grains and promotes the effective circulation of agricultural waste**.

5.2.2. Description of the process

The process for preparing yeast protein is illustrated in **Figure 65**. Fresh distiller's grains are first selected, and rice husk components are removed through drying, crushing, and screening. A diluted acid solution is then added for high-temperature sterilization, following a feed-to-water ratio of 1:7. This is followed by a 48-hour liquid enzymatic hydrolysis using glucanases and amylases. Yeast, proteases, and urea are subsequently inoculated to initiate liquid fermentation. Finally, the fermented mixture is spray-dried to obtain the finished yeast protein product.

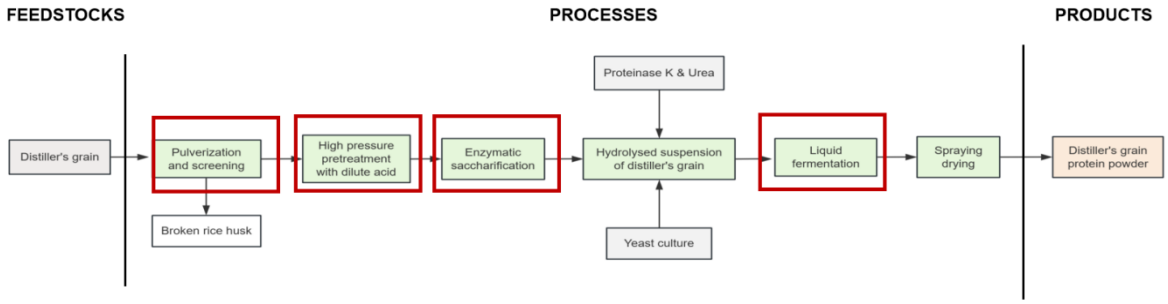

Figure 65. Preparation process of yeast proteins from distiller's grains.

5.2.3. Yeast protein composition

The first image on **Figure 66** is sourced from project partner HZAU. By subtracting the raw material protein, inoculated yeast protein, and residual urea protein from the total protein of the product, an additional 8.25 kg of yeast protein was obtained. The data in **Figure 67** comes from the enterprise's SCRG pilot test, which finally added 4.841 kg of protein. After analysis, the data is significantly low, mainly because of the loss of spray drying link. This situation is expected to be alleviated when the test system is scaled up.

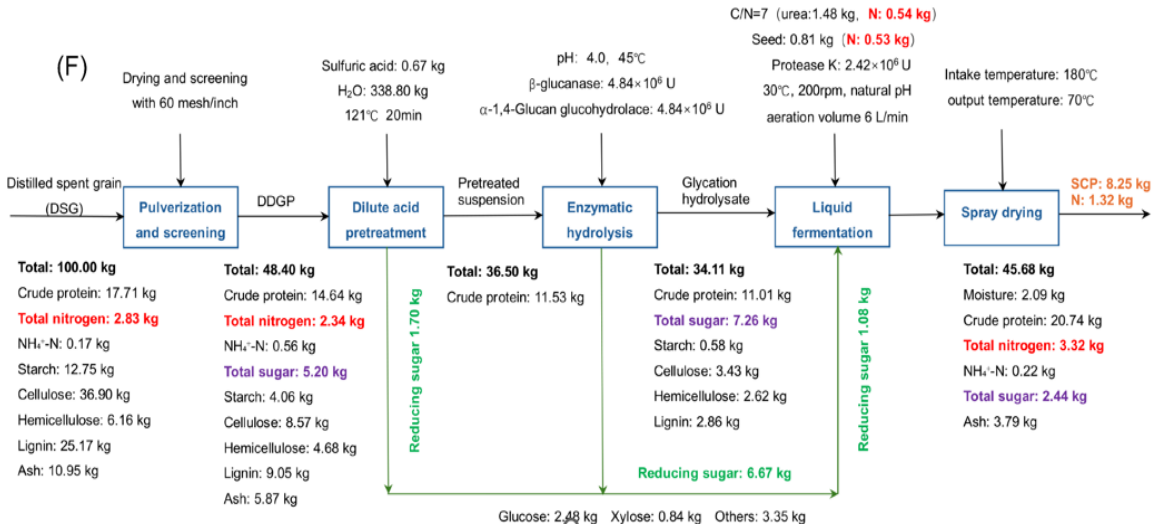

Figure 66. Production of proteins from distiller's grains by HZAU.

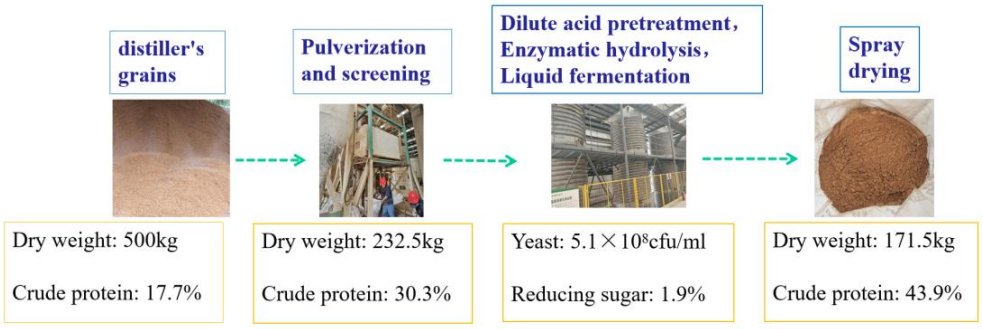

Figure 67. Production of proteins from distiller's grains by SCRG at pilot scale.

5.1.4. Conclusion and perspectives

The future work includes repeating pilot testing, stabilizing production, and preparing test samples in order to conduct animal experiments (**Figure 68**).

Figure 68. Future work: testing yeast proteins for the feeding of animals.

6. Production of PHAs at pilot scale (UNIVR / HBNACOL)

6.1. Production of PHBV from cow manure (UNIVR)

6.1.1. Introduction

Agri-food residues represent unutilised biomass that could be valorised into high-added-value compounds. Polyhydroxyalkanoates (PHAs) are one of the possible high-value products, being an alternative to fossil-based plastics. PHAs are biodegradable polymers produced by more than 300 species of microorganisms endowed with enzymes for the synthesis of these polyesters (Sabapathy et al. 2020). PHAs are accumulated in granules in the cell cytoplasm, where they serve the function of energy and carbon stocks (Cabrera et al. 2021). In the case of limited nutrient conditions, the presence of the carbonosomes allows the bacteria to survive, while other non-PHA-producing species are disadvantaged (Raza et al. 2018).

PHAs can be obtained using pure or mixed microbial cultures (MMC), both processes having advantages and disadvantages. At present, most of the companies that are successfully commercialising PHAs are using pure cultures (Koller and Mukherjee 2022); the Dutch company Paques biomaterials (https://www.paquesbiomaterials.nl/) is the only one known for using MMC. Benefits of pure microbial cultures are the higher amount of PHA that can be accumulated in the bacterial cells of pure cultures, the possibility of obtaining a product of constant composition – given the same feedstock and production parameters – and the easier retrieval of the PHAs from the bacterial cells compared to MMC (Pagliano et al. 2021). However, a consortium of bacteria is more resilient to changes compared to monocultures, it allows for skipping expensive sterilisation steps (4) and for utilising waste feedstock rather than synthetic or food-derived ones, thus reducing operational costs (Colombo et al. 2017).

PHAs are a family of linear polyesters comprising more than 150 types of monomers, which can be combined in different ways, resulting in materials with different properties, from thermoplastics to elastomeric (Laycock et al. 2014). Poly-3-hydroxybutyrate (PHB), for example, is composed only of the monomer 3-(R)-hydroxybutyric acid, and it is typically very brittle and thermally unstable, therefore having limited application as a substitute for traditional plastic (Arcos-Hernández et al. 2013), mostly for the production of hard and creep-resistant items (Koller and Mukherjee 2022). However, the presence of the hydroxyvalerate monomer (HV) in the polymer chain changes the thermal properties, reducing its melting temperature and crystallinity, and raising its flexibility (Arcos-Hernández et al. 2013). This poly(3-hydroxybutyrate-co-3hydroxyvalerate) copolymer (PHBV) is more suitable than PHB for applications such as packaging, biomedical products and tissue engineering. Furthermore, PHAs can be blended with other polymers, inorganic materials, enzymes and plasticisers, lowering the processing temperature and reducing brittleness, further changing the final product's characteristics (Bengtsson et al. 2018). Because of the wider application of PHBV in the market, some experimental works have tried to influence the composition of the PHA produced by the bacteria, to obtain PHBV with different characteristics (Laycock et al. 2014). This has been done with mixed microbial cultures by controlling the carbon source or the timing of its addition, with higher HV content obtained when the volatile fatty acid (VFA) source was propionic or valeric acid rather than acetic or butyric (Wei et

al. 2014), or with variable monomeric distribution when the feedstock composition varied throughout the feeding phase (Arcos-Hernández et al. 2013).

The work of UNIVR within WP4 focuses on **using MMC to produce PHBV at pilot-scale with a set amount of HV monomer (25-35% w/w),** for their use in the production of material for the agricultural sector, in partial substitution of those traditionally obtained from petroleum-based plastic. The aim is to produce PHBV from cow manure and crop residues, following WP3 advances. However, the initial phase of the work involved the use of commercial volatile fatty acids (VFAs) to assess how changes in their relative amounts can influence the percentage of PHA in the bacterial cells, and the amount of HV in the final polymer. The synthetic feedstock will be substituted with VFA-rich fermentate obtained from agri-food residues during the final phases of the pilot-scale operation. Pilot-scale production has been running since M16 and is described in detail in the paragraphs below.

Work at laboratory scale, designed to guide and support pilot-scale production, started in M6 (described in Milestone 14 and RP1). The laboratory-based PHA production ended in M31, but small-scale operations are still in progress to assist with the extraction and purification procedures at pilot-scale, and for the running of anaerobic biodegradability tests of the end-products (these latter experiments are to be performed in the later phases of the project).

6.1.2. General description of the process

A pilot plant for PHA production was set up inside the agricultural cooperative "La Torre" located in Isola della Scala, Verona, Italy. The plant is equipped for VFA and PHA production and is controlled continuously by a programmable logic controlled (PLC) board, allowing the plant to be operated and managed remotely. The plant is organised in the following units, as summarised in **Figure 69**.

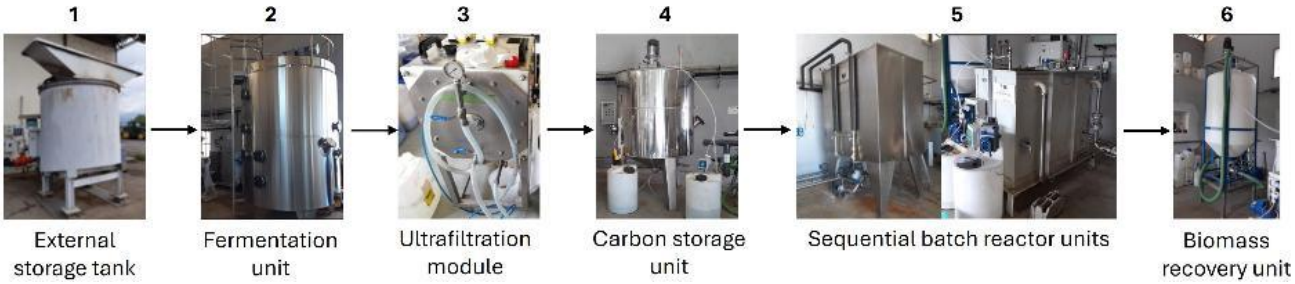

Figure 69. Schematic representation of the units comprising the PHA-production pilot plant.

1. External storage tank for the substrate to be used in the fermentation process. It has a maximum volume of 5.0 m^3 and is equipped with an adjustable stirrer and an internal solution recirculation system.
2. Fermentation unit for the production of a VFA-rich stream to be used in the PHA production process. This bioreactor is made of stainless steel, it has a maximum operating capacity of 5.0 m^3 and it is equipped with a stirrer, temperature sensors and a hot water double jacket for temperature maintenance.
3. Ultrafiltration module for the clarification of the fermented stream used for PHA production. This module is equipped with a 0.2 µm ceramic membrane and has a capacity of 15 L/h. A sieve module of 1 mm porosity is installed before the ultrafiltration module to avoid the blockage of the unit.

4. Carbon storage unit of 2.0 m^3 equipped with a stirrer, which is used to store the VFA-rich liquid after clarification of the carbon source.
5. Sequential batch reactor (SBR) units, consisting of SBR1 and SBR2, both equipped with temperature and oxygen sensors and blowers for air diffusion, and kept at a constant temperature of 25° C. SBR1 (capacity of 2.0 m^3) is intended for the selection of the PHA-producing biomass, while SBR2 (capacity of 1.2 m^3) is used for the accumulation of PHA.
6. Biomass recovery unit, used to recover and concentrate the biomass by flocculation and decantation of the liquid for the subsequent PHA extraction. It is equipped with a stirrer, has a capacity of 1.5 m^3, and is made of resistant plastic.

PHA production started in M16 (March '24) and is still running at M34 (September '25). A total of 13 batches were produced throughout M16-M32, with the timing shown in **Table 37**. Set-up 14 started in M34 and is running at present.

Table 37. PHA-rich biomass production batches.

Set-up	Start	End date	Feedstock	Purificatio	Produced PHA (g)
1	27/2/24	19/3/24	Synthetic	NaOH	800
2	2/4/24	23/4/24	Synthetic	NaOH	N/A
3	24/4/24	13/6/24	Synthetic	NaOH	143
4	13/6/24	25/7/24	Synthetic	NaOH	973
5	26/7/24	28/8/24	Synthetic	NaOH	524
6	29/8/24	9/10/24	Synthetic	NaOH	906
7	13/11/24	28/11/24	Synthetic	NaOH	850
8	28/11/24	12/12/24	Synthetic	NaOH	686
9	12/2/25	25/2/25	Synthetic	NaOH	650
10	27/2/25	10/3/25	Synthetic	NaOH	620
11	28/3/25	7/4/25	Synthetic	NaOH	755
12	14/5/25	27/5/25	Synthetic	NaOH +	In progress
13	19/6/25	1/7/25	Synthetic	NaOH +	In progress
14	5/9/25	In	Real	NaOH +	In progress

1 kg of purified biomass produced in set-ups 10 and 11 was sent to BIOMI in July 2025 for testing the possibility of producing PHBV-based mulching films by blow extrusion, as explained in section 3.2 (**Figure 70**).

Figure 70. The PHBV sent to BIOMI in July 2025.

6.1.3. Feedstock

The substrate used for PHA production during set-ups 1 to 13 was a synthetic mixture (9.7 gCOD/L) of VFAs (acetic 75.0%, propionic 13.0% and butyric acid 12.0%) calibrated for the obtainment of the correct content of HV (25-35%) in the polymer. This feedstock was used for both SBR1 and SBR2. However, the synthetic feedstock for SBR1 was enriched with ammonium bicarbonate and phosphoric acid (with a ratio of 100:5:1 (COD:N:P) or 100:10:1) to ensure the presence of nitrogen and phosphorus macro-nutrients, necessary for the metabolic activities of the microorganisms.

In set-up 14, the system switched to using a real substrate originating from the acidogenic fermentation of agri-food residues and cow manure, using digestate from the anaerobic digestion process as inoculum. The feedstock consisted in materials recovered from a local agricultural cooperative (La Torre, Verpma) and was made up of 50% cattle slurry and 50% corn residues; details of its composition, including the inoculum coming from the anaerobic digester, are described in **Table 38**. Since the setup of 14 has only recently started, no further information is at present available.

Table 38. Inoculum and fermentation feedstocks characterisation for the real substrate used in set-up 14. TS = total solids, VS = volatile solids, COD = chemical oxygen demand.

	TS	VS	VS/TS	COD
	%	%	%	gCOD/KgTS
Inoculum (AD digestate)	6.3±0.0	3.7±0.0	59.0±0.3	26.5±0.3
Cattle slurry	3.0±0.0	2.3±0.0	74.1±0.4	883.4±24.0
Corn residues	33.7±4.6	31.7±4.7	94.1±1.6	772.1±125.9

6.1.4 PHA-producing bacteria selection phase

SBR1 was used for the enrichment of mixed microbial culture with PHA-producing microorganisms (selection phase). The reactor operational parameters are listed in **Table 39**. No settling phase was performed, and the hydraulic retention time was equal to the solid retention time (3 days). The pH was monitored but not controlled, its value oscillating between 8.0 and 9.0. The seed sludge of mixed microbial cultures was collected from a municipal wastewater treatment plant located in Verona (Italy), and it was used as inoculum for the selection reactor at a concentration of 3 gTS/L. The selection of the PHA-storing bacteria was obtained by applying feast and famine (F/F) conditions with a ratio of 0.2, which is reported as one of the most efficient values to establish the optimal conditions to give PHA-accumulating bacteria a competitive advantage over non-accumulators (Reis et al. 2011; Freches and Lemos 2017).

Table 39. Operational parameters for SBR1.

PARAMETER	VALUE
Feast/Famine ratio (F/F)	0.2
Cycle length (h)	6
Feast phase duration (h)	1
Famine phase duration (h)	5
N° cycles/d	4
Hydraulic retention time (d)	3
Selection reactor volume (L)	1,000
Feed volume (L/cycle)	2.33
Feed volume (L/d)	9.32
Feedstock concentration (gCOD/L)	9.7
Organic loading rate (kgCOD/m^3d)	4.1
Temperature (°C)	25
pH	8.0 – 9.0

6.1.5. PHA accumulation phase

SBR2 was used to maximise the PHA content in the bacterial cells (accumulation phase). At the end of the feast phase, the biomass selected in SBR1 was discharged into SBR2, which was kept at 25° C and was equipped with aeration and a dissolved oxygen probe to monitor the substrate uptake. The accumulation was performed following a multi-spike feeding strategy (Valentino et al. 2019), with spikes of 0.5 gCODVFA/L. Each single accumulation phase lasted 5-6 h, with varying numbers of spikes, as a new spike was provided whenever the level of dissolved oxygen in the bulk increased, as this indicates a decline in microbial activity due to carbon exhaustion. At the end of the accumulation phase, the biomass was transferred to the biomass recovery unit, where a polyelectrolyte (SCAEFLOC CL 1908) was added to flocculate all the biomass to allow its separation from the liquid phase. At the end of the sedimentation phase, the biomass was acidified with sulphuric acid (98% w/v) to pH 1-2, to inactivate the cells and avoid the consumption of PHAs by the bacteria for their metabolic activities. The obtained wet biomass was washed with water, and the retrieved pellet was subject to the extraction and purification steps.

6.1.6. PHA extraction and purification

The extraction of PHA from the bacterial biomass was performed following protocols developed by UNIROMA and NID in the frame of WP3 (**Table 40**). Initially, the protocol consisted in applying NaOH to the biomass at the ratio of 4.8 gNaOH/gTS (Salvatori et al. 2025), without considering the final NaOH concentration in the volumes used, which resulted too high (0.6 to 1.0 M, depending on the set-ups). Once it was evident that this high NaOH molarity resulted in decreased PHA purity and quality, the molarity of the final concentration was modified to 0.3 (after testing at laboratory scale), applied to a biomass with the final concentration of 20 gTS/L (Rodrigues et al. 2022). The contact time of NaOH was 4 hours under agitation at room temperature, after which the biomass was washed twice with water, freeze-dried with a Lio 5 P freeze-dryer (5 Pa Srl, Italy), ground with a mortar and pestle and stored at −80 °C. This improved was applied from set-up 11, allowing to obtain PHBV with higher purity (54-65%). From set-up 12, a further purification step with acetic acid was added to achieve better purification. After the washing steps, the biomass was resuspended in water to reach the final concentration of TS of 5% (w/v). Acetic acid (98%, w/w), was applied at the ratio of 0,4 mL/gTS and final concentration of 1,9 % (w/w) and left overnight under agitation at 140 rpm (Rodrigues et al. 2022). The biomass was then washed twice in distilled water, retrieved by centrifugation, lyophilised, ground and stored at −80 °C until further use. At present, we are also evaluating the effect of the treatment with acetic acid; however, precedent tests run at laboratory scale but with the biomass originating from the pilot plant (please read below), suggest an improvement in the polymer's purity after acetic acid application.

The content of hydroxyvalerate (HV) in the polymer was set by the project to be 25-35% for optimal downstream processing; this or a higher value was obtained for the initial 4 batches, but it then decreased, probably due to a lack of propionate in the feedstock. The feedstock composition was corrected twice from set-up 6 to 12, until the correct HV content was obtained again in set-up 12-13.

Part of the biomass originating from set-up 11 was subject to chemical and/or enzymatic treatments at laboratory scale. The chemical treatments have already been discussed, while the enzymatic treatments involved the use of the enzymes alcalase, lysozyme, and phospholipase A2, and their combinations, according to the conditions of **Table 40**. The hydrolyses were performed in replicates in 2 L flasks, with a reaction volume of 500 mL, a biomass to solvent ratio of 5% (w/v), for a total of 4 hours and under agitation at 180 rpm.

Table 40. PHA and HV content of the PHA produced at the pilot plant. analysis of PHA and HV content were performed by UNIROMA. HAc = acetic acid.

Set-up	Purification	Produced PHA (g)	PHA before purification (%)	HV before purification (HV)	PHA after purification (%)	HV after purification (%)
1	NaOH	800	8.4	50.1	2.7	17.5
2	NaOH	N/A	41.3	24.6	6.5	20.4
3	NaOH	143	36.3	27.4	17.0	50.0
4	NaOH	973	3.0	51.0	5.0	40.0
5	NaOH	524	18.0	16.0	2.0	N/A
6	NaOH	906	5.0	8.0	2.0	N/A
7	NaOH	850	30.0	16.0	11.0	16.0
8	NaOH	686	35.0	18.0	10.0	22.0
9	NaOH	650	33.0	16.0	22.0	17.0
10	NaOH	620	33.0	17.0	33.0	16.0
11	NaOH	755	29.0	16.0	54.0-65.0	16.0
12	NaOH + HAc	In progress	26.0	26.0	53.0-63.0	22.0-23.0
13	NaOH + HAc	In progress	16.0	27.0	In progress	In progress
14	NaOH + HAc	In progress	In progress	In progress	In progress	In progress

Table 41. Characteristics of the enzymes and hydrolysis conditions for the extraction and purification protocols tests performed at laboratory scale.

Enzyme	Producer	EC Number	Activity	Temperature (°C)	pH	Enzyme concentration
Alcalase	Novozymes, Denmark	3.4.21.62	2.4 AU-A/g	50 °C	7.5	12.5
Lysozyme	Merck, USA	3.2.1.17	~70,000 U/mg	37 °C	8.0	5.0
Phospholipase A2	Creative Enzymes, USA	3.1.1.4	10,000 U/g	50 °C	5.5	0.02

The results are shown in **Table 42**. The most effective purifications were obtained when using NaOH in conjunction with either the enzyme alcalase (86.4%) or lysozyme (78.9%); however, these protocols were not applied to the pilot-plant production due to the high costs involved in the use of enzymes. Instead, it was opted for the use of NaOH and acetic acid, since the purification protocol applied from set-up 11 with a lower molarity of NaOH allowed to retrieve a polymer with improved characteristics in terms of purity and molecular weight compared to previous set-ups, and the use of acetic acid resulted in further purification. The HV content did not change appreciably within the different treatments, and the molecular weight also appeared not to be particularly influenced by the chemicals and/or enzymes used.

Table 42. Characteristics of the PHAs originating from setup 11 after chemical and/or enzymatic treatments. HAc = acetic acid, H_2O_2 = hydrogen peroxide, PLA = phospholipase A2.

Extraction/purification type	PHA (%)	HV (%)	Mw (kDa)	Mn (kDa)	PDI
Before purification	30.5	22.2	438.65	149.45	2.94
NaOH	51.7	19.0	521.35	244.66	2.13
NaOH + HAc	58.0	20.1	560.19	210.29	2.66
NaOH + HAc + H_2O_2	51.6	19.8	411.27	102.76	4.00
Alcalase	60.4	26.2	491.61	167.56	2.93
Lysozyme	38.8	23.5	392.85	131.53	2.99
NaOH + alcalase	86.4	25.0	411.55	170.74	2.41
NaOH + lysozyme	78.9	20.7	395.22	120.66	2.18
Alcalase + lysozyme	44.6	20.5	423.93	179.71	2.36
NaOH + alcalase + lysozyme	60.4	22.7	337.77	100.32	3.37
PLA2	28.9	20.4	In progress	In progress	In
NaOH + PLA2	33.8	18.3	In progress	In progress	In
Alcalase + lysozyme + PLA2	43.0	20.6	In progress	In progress	In
NAOH + alcalase + lysozyme + PLA2	51.9	19.6	In progress	In progress	In

6.1.7. Analytical techniques for the determination of the polymer purity, HV content and molecular weight

The analysis of PHA and HV content in the obtained biomass was performed in the laboratories of the Department of Chemistry of UNIROMA, a partner of the project. To determine PHA concentration in the biomass, and the content of HV in the polymer, 2-5 mg of dried biomass was hydrolyzed and esterified (via methyl-esterification) into 3-hydroxyacyl methyl esters, and measured using gas chromatography. After preparing the sample, 1 µL of the organic liquid phase was injected into an Agilent 8860 GC equipped with a HP- 5 column (30 m × 320 µm × 0.25 µm). N_2 was used as carrier gas at a flow rate of 10 mL/min. The oven temperature was initially maintained at 100 °C for 1 min, then increased up to 130 °C at a rate of 12 °C/min and further increased up to 250 °C at a rate of 25 °C/min. The flame ionisation detector was maintained at 320 °C. The abundance of hydroxybutyric (HB) and (HV monomers was determined using a PHBV Sigma-Aldrich standard polymer with 12% (w/w) HV content and benzoic acid as an internal standard. The PHA intracellular content (% w/w) in the experimental samples was calculated as a percentage (w/w) of the suspended solids.

The average molecular weight (Mw), number average molecular weight (Mn), and polydispersity index (PDI = Mw/Mn) of the obtained polymer were determined by extracting the polymer from the bacterial cell using chloroform and methanol following Braunegg et al. protocol (1978)(Braunegg et al. 1978). In detail, the biomass was washed with distilled water, centrifuged, freeze-dried, and grounded with a mortar and pestle. The ground biomass was digested at 70 °C for 4 hours with chloroform (50 mL/g biomass); once cooled, filtration was performed using paper filters. Methanol (5 mL/mL chloroform) was added to precipitate PHAs, and after 60 min the precipitate was filtered as previously, recovered, placed on a glass petri dish, and left overnight to allow complete chloroform and methanol

evaporation. The solid polymer obtained with this process was sent to UNIROMA, where it was analysed by Gel Permeation Chromatography equipped with a pump (JASCO PU-4180), a guard column and two columns in series (TSKgel®G6000-HHR TSKGel GMHHR-H), a column oven (JASCO CO-4060) and a refractive index detector (JASCO RI-4030). Chloroform was used as an eluent at a 1 ml/min flow rate. The detector was set at 35 °C, whereas the columns were set at 40 °C. Polystyrene standards (0.013–3.05 × 10 6 g/mol) were used to calibrate the system.

6.1.8 Conclusions and plans for future work

The production of PHBV at pilot-scale using MMC and agri-food residues has not been reported in other studies. Only the company Paques biomaterials, mentioned earlier, produces PHBV with high HV content from organic streams using MMC; this company has only recently established itself (the pilot-plant opened in the spring of 2025), and the organic streams used for PHA production, mainly wastewaters and municipal solid wastes. are different from those of AgriLoop,

Despite evident variations throughout the study, it was possible to obtain a polymer with the desired HV content. This is also a strength of the presented work, since similar results have been reported only at laboratory scale in a few studies (Laycock et al. 2014; Arcos-Hernández et al. 2013; Wei et al. 2014); however, these works focused on producing PHBV with different HV content, rather than reaching a set amount through production.

PHBV production at pilot-scale has been challenging, and it still must be finalised and refined. Various hurdles have been encountered during production, which are listed here:

- Retrieval and concentration of the bacterial biomass (separation from the liquid phase) after the accumulation step, given the high volumes involved. The use of flocculants helped the process, though they must be carefully dosed to avoid unwanted impurities and unpleasant smell in the final product.
- Extraction of PHBV from the bacterial cells with NaOH, while maintaining intact the polymer's properties, which is necessary for downstream applications. The molarity of NaOH and its amount in relation to the TS of the bacterial biomass must be carefully dosed to avoid the polymer's degradation.
- Purification of the polymer. The difficulty of obtaining high purity is probably related to the nature of the feedstock and the use of MMC. At present, the maximum purity that could be achieved with PHBV produced at pilot scale was 65%. This is not ideal for producing flexible PHA-based applications such as mulching films, which require purity up to 99%. For this reason, the mulching films that are being produced within the frame of WP4 will only include a percentage of PHBV produced by UNIVR (up to 30% maximum).

PHA production at pilot scale must terminate well ahead of the end of the project, as the obtained polymers need to be transferred to task 4.1 for end-product testing, and within task 4.2 to BIOMI for the upscaling of two selected end-products (mulching films and rigid applications). These end-products will then be tested at the farm level in close-to-real conditions, and their aerobic and anaerobic biodegradability will be evaluated. For this reason, the pilot-scale production of PHAs should be completed by the end of M37.

Batches with real feedstock are being produced at present. The experience collected at laboratory scale suggests that a filtration step at 0.22 µm is required to allow the bacteria to store significant quantities of PHAs in the cells. However, this filtration step is challenging due to the high volumes of VFA-rich fermentate required for the selection and accumulation phases, as the ultrafiltration module can only sieve 15 L/h.

The enzymatic treatments applied at laboratory scale for the extraction and/or purification of PHAs obtained from MMC have not been used before, to our knowledge. Previous work focused on their use solely on biomass produced by pure cultures, mainly the species Cupriavidus necator and Pseudomonas putida. Therefore, this work highlights an alternative route for the extraction and purification of PHBV, though the cost associated with the use of the enzymes must be considered.

6.2. Production of PHBV using pure cultures (HBNACOL)

6.2.1. Introduction

The work focuses on **PHA high-yielding bacterial strains**, with optimization efforts directed at fermentation technology, fermentation control parameters, and downstream extraction processes. Current work primarily involves **scaling up fermentation processes to an 800L scale**. The process involves inoculating glycerol stock bacterial strains into LB medium at a 0.1% inoculation rate, followed by overnight culture (14–18 hours) at 30°C. This is then transferred to 30L of LB medium at a 5–10% inoculation rate and cultured at 30°C for 4–7 hours. Subsequently, the culture is inoculated into an 800L fermenter containing M9G medium (developed by Nankai University) at a 5–10% inoculation rate. During fermentation, dissolved oxygen is maintained at approximately 30%. A 20 g/L glucose solution is fed at 24 hours and 48 hours, respectively. The fermentation process concludes after 77 hours, after which bacterial cells are harvested via centrifugation.

6.2.2. Materials and method

6.2.2.1. Materials.

Tryptone, Yeast extract, NaCl, $Na_2HPO_4 \cdot 12H_2O$, KH_2PO_4, NH_4Cl, $MgSO_4$, $CaCl_2$, V_{B1}, Glucose, Chloroform, methanol

6.2.2.2. Methods

PHA Fermentation. Streak the glycerol stock onto an LB plate, pick a single colony into LB medium, incubate overnight at 30 ℃, then inoculate 100 mL of fresh LB with 1% of the culture and grow at 30 ℃ for 14 h. Transfer 3% of this culture into 3 L of M9G medium, maintain dissolved oxygen at ~50%, feed 20 g/L glucose at 24 h and 48 h, and terminate fermentation after 60 h.

PHA Extraction. After fermentation, the broth was centrifuged to collect the cells, which were then lyophilized to obtain dry biomass. Chloroform was added to the dry cells for PHA extraction. The extract was filtered through filter paper to remove cell debris, and the filtrate was concentrated by rotary evaporation. Cold methanol was added to precipitate the PHA, which was recovered by filtration and air-dried at room temperature to yield purified PHA. Throughout the process, (1) the yield of dry biomass after lyophilization and (2) the PHA content per unit mass of dry biomass were determined.

6.2.3. Results and discussion

6.2.3.1. Lab-scale fermentation optimization

By adjusting feed rate and dissolved-oxygen levels, the biomass concentration in a 5 L fermenter reached 1.12% (w/w), and the resulting freeze-dried cells contained 39.6% PHA by dry weight (**Table 43**).

Table 43. 5 L fermenter performance: harvested biomass volume, wet-cell weight, and PHA content.

Lot Items	1	2	3	4	5	Mean value
Broth weight（g）	2940	3007	3017	2978	3106	3009
Wet-cell weight（g）	73.5	84.2	90.5	89.3	93.1	86.1
Wet-cell weight(%)	2.5%	2.8%	3.0%	3.0%	3.0%	2.8%
Dry-cell weight(%)	1%	1.12%	1.2%	1.2%	1.2%	1.12%
PHA content (on a dry-cell basis)	-	-	39.9%	38.9%	40%	39.6%

6.2.3.2. Pilot-scale trial

The process was scaled to a 50 L fermenter; dry-cell weight and PHA content matched those of the lab run, stabilizing at ~1.2% and ~40%, respectively, demonstrating linear scalability (**Table 44**).

Table 44. Harvested biomass volume and wet-cell weight from the 50 L fermenter

Lot Items	1	2	3	Mean Value
Broth weight（g）	31.4	30.8	31.2	31.1
Wet-cell weight（g）	0.94	0.92	0.93	0.93
Wet-cell weight(%)	3%	3%	3%	3%
Dry-cell weight(%)	1.2%	1.2%	1.2%	1.2%
PHA content (on a dry-cell basis)	39.6%	39.2%	40%	39.6%

6.2.3.3. 800L Fermentation Trial

The process was scaled to a 800 L fermenter; dry-cell weight and PHA content matched those of the lab run and pilot-scale trial, stabilizing at ~1.3% and ~40%, respectively, demonstrating linear scalability (**Table 45**).

Table 45. Harvested biomass volume and wet-cell weight from the 800 L fermenter

Lot Items	1	2	Mean Value
Broth weight（kg）	577	580	578.5
Wet-cell weight（kg）	18	18.3	18.15
Wet-cell weight(%)	3.1%	3.2%	3.15

Dry-cell weight(%)	1.29%	1.36%	1.33%
PHA content (on a dry-cell basis)	40.1%	39.2%	39.7%

6.2.3.4. PHA Extraction

For different batches of cells, the weights before and after lyophilization were recorded together with the final PHA yield. Table 4 shows that the ratio of dry to wet biomass is approximately 1:2.5, and the PHA output is about 0.124 g per gram of dry cells (Table 42).

The PHA content dropped from 40% before purification to 12% after chloroform purification. This reduction is due to inevitable process losses, which is expected as the purification does not achieve 100% recovery of the PHA from the cells.

Table 46. Dry-to-wet cell ratio and PHA yield per gram of dry cells

Lot Items	1	2	3	4	5	Mean Value
Dry-cell weight（g）	40	39	38	40	42	39.8
PHA yield (on a dry-cell basis)	0.125	0.123	0.125	0.126	0.123	0.124

6.2.2. Conclusion and perspectives

Stable production of PHA has been achieved at an 800 L scale (exceeds the 200L requirement specified in the task document), with a dry cell weight of 1.3% and a PHA content of approximately 40%, consistent with laboratory-level results, validating the feasibility of linear scale-up. After chloroform extraction, the yield reached 12.5 g/100 g of dry cells. Through crude extraction, the PHA yield achieved 40 g/100 g of dry cells. A pilot production line for PHA has now been established. Our future work will likely focus on feedstock diversification and process optimization.

7. Conclusions

This deliverable highlights significant progress in the development of biopolyesters-based materials for agricultural applications, grounded in a frugal design approach that prioritizes real-world user needs and constraints. The results demonstrate the technical feasibility of PHBV-based formulations incorporating cutin, polyphenols, and lignocellulosic fillers, with promising mechanical and functional properties. These findings will directly inform the next stages of WP4, including the upscaling at pilot scale of two selected end-products (mulching films and clips for vineyard), their field testing under real conditions, and biodegradability assessments.

Pilot-scale production and biorefinery schemes are already being implemented. While many goals were reached for plant molecules, MPs and PHAs production at pilot scale, various hurdles have complicated and at times delayed production. However, alternative production routes have been implemented, and the work is on track to deliver production at pilot-scale, which will allow testing of the products in close-to-real conditions.

N°	Dataset name	Open Data	Closed Data	Means of dissemination	Maximum delay before access	Data set access
1	WP4.1_FCAC : Collection of preferences regarding the use of plastics		2 files : 1. Questionnaire about the use of plastic materials by farmers, used for the technical visit in Catalonia in June 2024. 2. Excel file summarizing the data collected during the visits (production site area, type of culture, type of plastic materials used, service life, multiple use or not, disposal after use, free comments).	Conference	Once the deliverable is published	https://doi.org/10.57745/8ZO3CM
2	WP4.1_UNIBO : Cutin/PHBV blends		7 files : 1. Thermogravimetric analysis of cutin from INRAE 2. Thermogravimetric analysis of cutin from TOMAPAINT 3. DSC analysis of the two samples of cutin 4. DSC analysis of the PHBV samples (PHI003 and PHBV Paques) 5. DSC analysis of PHI003 – cutin blends 6. DSC analysis of PHBV Paques – cutin blends 7. Mechanical properties of PHBV-cutin blends	Scientific article, conference	Once the corresponding scientific article is published	https://doi.org/10.57745/RKPR1T

3	WP4.1_UM : Effect of PHAs purity on their processability through thermomechanical treatments		3 files: 1. Description in an excel file of unpurified PHAs used in this deliverable. 2. Information on the shaping behavior of unpurified PHAs using a thermopress. 3. Excel file with the thermal properties of unpurified PHAs powders.	Conference	Once the deliverable is published	https://doi.org/10.57745/VIAI3F
4	WP4.1_UM_2: PHBV/peanut shells biocomposites		13 files : 1. Raw colorimetry data for peanut shells powder (PS-F and PS-UF) 2. Raw granulometic data for peanut shells powders at different steps of the grinding process 3. Size distribution of PS-F and PS-UF, measured by laser granulometry 4. Raw data of contact angle measurements on peanut shells powders (PS-F and PS-UF). 5. DSC curves of PHI002-based injection molded specimens. 6. DSC curves for the PHBV/PS-F 15wt% injection molded composite. 7. DSC curves for the PHBV/PS-UF 15wt% injection molded composite. 8. DSC curves of PHI002: impact of the successive processing steps. 9. DSC curves of PHA/PS-F 15wt% : impact of the process. 10. DSC curves of PHA/PS-UF 15wt% : impact of the process. 11. DSC analysis of biocomposites.	Scientific article, conference, best practical abstract	Once the corresponding scientific article is published	https://doi.org/10.57745/MKVL9F

			12. Tensile curves of biocomposites. 13. Tensile properties of injection molded composite specimens.			
5	WP4.1_UNIVR : Production of PHAs with variable HV content from agricultural residues	2 files : 1. AgriLoop UNIVR laboratory scale database 30 April 2024 2. Text of a communication presented at the 11th international conference on sustainable solid waste management in Rhodes during summer 2024	3 files : 1. An updated version of the database for PHA production at lab-scale (with RP2 data) 2. The database for PHA production at pilot-scale 3. Scientific article in Environmental Science and Pollution Research with lab-scale data	Scientific article, conference	Once the deliverable is published	https://doi.org/10.57745/XLLAI6

References

Afra, Elyas, Saeed Mohammadnejad, and Ahmadreza Saraeyan. 2016. 'Cellulose Nanofibils as Coating Material and Its Effects on Paper Properties'. *Progress in Organic Coatings* 101 (December): 455–60. https://doi.org/10.1016/j.porgcoat.2016.09.018.

Ahankari, Sandeep S., Amar K. Mohanty, and Manjusri Misra. 2011. 'Mechanical Behaviour of Agro-Residue Reinforced Poly(3-Hydroxybutyrate-Co-3-Hydroxyvalerate), (PHBV) Green Composites: A Comparison with Traditional Polypropylene Composites'. *Composites Science and Technology* 71 (5): 653–57. https://doi.org/10.1016/j.compscitech.2011.01.007.

Almasi, Hadi, Babak Ghanbarzadeh, Jalal Dehghannia, Sajad Pirsa, and Mohsen Zandi. 2015. 'Heterogeneous Modification of Softwoods Cellulose Nanofibers with Oleic Acid: Effect of Reaction Time and Oleic Acid Concentration'. *Fibers and Polymers* 16 (8): 1715–22. https://doi.org/10.1007/s12221-015-4294-1.

Almeida, Patrícia V., Licínio M. Gando-Ferreira, and Margarida J. Quina. 2024. 'Tomato Residue Management from a Biorefinery Perspective and towards a Circular Economy'. *Foods* 13 (12): 1873. https://doi.org/10.3390/foods13121873.

Altun, Müslüm, Mithat Çelebi, Sinan Şen, Öznur Kökpınar, and Hanife Songül Kaçoğlu. 2023. 'Characterization of Polyhydroxyalkanoate-based Composites Derived from Waste Cooking Oil and Agricultural Surplus'. *Polymer Composites* 44 (7): 4055–68. https://doi.org/10.1002/pc.27379.

Al-Wandawi, Hussain, Maha Abdul-Rahman, and Kaib Al-Shaikhly. 1985. 'Tomato Processing Wastes as Essential Raw Materials Source'. *Journal of Agricultural and Food Chemistry* 33 (5): 804–7. https://doi.org/10.1021/jf00065a009.

Ambrosio-Martin, Jesús, María José Fabra, Amparo López-Rubio, Giuliana Gorrasi, Andrea Sorrentino, and Jose M. Lagaron. 2016. 'Assessment of Ball Milling as a Compounding Technique to Develop Nanocomposites of Poly(3-Hydroxybutyrate-Co-3-Hydroxyvalerate) and Bacterial Cellulose Nanowhiskers'. *Journal of Polymers and the Environment* 24 (3): 241–54. https://doi.org/10.1007/s10924-016-0767-6.

Amiandamhen, S. O., M. Meincken, and L. Tyhoda. 2020. 'Natural Fibre Modification and Its Influence on Fibre-Matrix Interfacial Properties in Biocomposite Materials'. *Fibers and Polymers* 21 (4): 677–89. https://doi.org/10.1007/s12221-020-9362-5.

Amvrazi, Elpiniki G. 2011. 'Fate of Pesticide Residues on Raw Agricultural Crops after Postharvest Storage and Food Processing to Edible Portions'. In *Pesticides - Formulations, Effects, Fate*. IntechOpen. https://doi.org/10.5772/13988.

Arcos-Hernández, Mónica V., Bronwyn Laycock, Bogdan C. Donose, et al. 2013. 'Physicochemical and Mechanical Properties of Mixed Culture Polyhydroxyalkanoate (PHBV)'. *European Polymer Journal*, Biobased Polymers and Related Materials, vol. 49 (4): 904–13. https://doi.org/10.1016/j.eurpolymj.2012.10.025.

Asim, Nilofar, Marzieh Badiei, and Masita Mohammad. 2021. 'Recent Advances in Cellulose-Based Hydrophobic Food Packaging'. *Emergent Materials* 5. https://doi.org/10.1007/s42247-021-00314-2.

Aulin, Christian, Mikael Gällstedt, and Tom Lindström. 2010. 'Oxygen and Oil Barrier Properties of Microfibrillated Cellulose Films and Coatings'. *Cellulose* 17 (3): 559–74. https://doi.org/10.1007/s10570-009-9393-y.

Avella, M., and M. E. Errico. 2000. 'Preparation of PHBV/Starch Blends by Reactive Blending and Their Characterization'. *Journal of Applied Polymer Science* 77 (1): 232–36. https://doi.org/10.1002/(SICI)1097-4628(20000705)77:1%253C232::AID-APP30%253E3.0.CO;2-Z.

Baiardo, Massimo, Elisa Zini, and Mariastella Scandola. 2004. 'Flax Fibre–Polyester Composites'. *Composites Part A: Applied Science and Manufacturing* 35 (6): 703–10. https://doi.org/10.1016/j.compositesa.2004.02.004.

Bajwa, Usha, and Kulwant Singh Sandhu. 2014. 'Effect of Handling and Processing on Pesticide Residues in Food- a Review'. *Journal of Food Science and Technology* 51 (2): 201–20. https://doi.org/10.1007/s13197-011-0499-5.

Barham, P. J., A. Keller, E. L. Otun, and P. A. Holmes. 1984a. 'Crystallization and Morphology of a Bacterial Thermoplastic: Poly-3-Hydroxybutyrate'. *Journal of Materials Science* 19 (9): 2781–94. https://doi.org/10.1007/BF01026954.

Barham, P. J., A. Keller, E. L. Otun, and P. A. Holmes. 1984b. 'Crystallization and Morphology of a Bacterial Thermoplastic: Poly-3-Hydroxybutyrate'. *Journal of Materials Science* 19 (9): 2781–94. https://doi.org/10.1007/BF01026954.

Basak, Sumanta, Milind Shrinivas Dangate, and Shanmugha Samy. 2024. 'Oil- and Water-Resistant Paper Coatings: A Review'. *Progress in Organic Coatings* 186: 107938. https://doi.org/10.1016/j.porgcoat.2023.107938.

Bengtsson, Simon, Alan Werker, Cindy Visser, and Leon Korving. 2018. *PHARIO. Stepping stone to a value chain for PHA bioplastic using municipal activated sludge | STOWA*. https://www.stowa.nl/publicaties/phario-stepping-stone-value-chain-pha-bioplastic-using-municipal-activated-sludge.

Benítez, José J., Paula M. Castillo, José C. Del Río, et al. 2018. 'Valorization of Tomato Processing By-Products: Fatty Acid Extraction and Production of Bio-Based Materials'. *Materials* 11 (11): 2211. https://doi.org/10.3390/ma11112211.

Benítez, José J., Ana González Moreno, Susana Guzmán-Puyol, José A. Heredia-Guerrero, Antonio Heredia, and Eva Domínguez. 2022. 'The Response of Tomato Fruit Cuticle Membranes Against Heat and Light'. *Frontiers in Plant Science* 12 (January). https://doi.org/10.3389/fpls.2021.807723.

Benítez, José J., Sonja Osbild, Susana Guzman-Puyol, Antonio Heredia, and José A. Heredia-Guerrero. 2020. 'Bio-Based Coatings for Food Metal Packaging Inspired in Biopolyester Plant Cutin'. *Polymers* 12 (4): 942. https://doi.org/10.3390/polym12040942.

Berthet, Marie-Alix, Hélène Angellier-Coussy, Vorleak Chea, Valérie Guillard, Emmanuelle Gastaldi, and Nathalie Gontard. 2015. 'Sustainable Food Packaging: Valorising Wheat Straw Fibres for Tuning PHBV-Based Composites Properties'. *Composites Part A: Applied Science and Manufacturing* 72: 139–47. https://doi.org/10.1016/j.compositesa.2015.02.006.

Berthet, Marie-Alix, Hélène Angellier-Coussy, Valérie Guillard, and Nathalie Gontard. 2016. 'Vegetal Fiber-based Biocomposites: Which Stakes for Food Packaging Applications?' *Journal of Applied Polymer Science* 133 (2): app.42528. https://doi.org/10.1002/app.42528.

Berthet, Marie-Alix, Hélène Angellier-Coussy, Diogo Machado, et al. 2015. 'Exploring the Potentialities of Using Lignocellulosic Fibres Derived from Three Food By-Products as Constituents of Biocomposites for Food Packaging'. *Industrial Crops and Products* 69: 110–22. https://doi.org/10.1016/j.indcrop.2015.01.028.

Berthet, Marie-Alix, Claire Mayer-Laigle, Xavier Rouau, Nathalie Gontard, and Hélène Angellier-Coussy. 2017. 'Sorting Natural Fibres: A Way to Better Understand the Role of Fibre Size Polydispersity on the Mechanical Properties of Biocomposites'. *Composites Part A: Applied Science and Manufacturing* 95 (April): 12–21. https://doi.org/10.1016/j.compositesa.2017.01.011.

Blair, B.F., and M.C. Lamb. 2025. 'Evaluating the Presence of Pesticide Residues and Associated Health Risks in US Peanuts'. *Peanut Science* 52 (1): 70–79. https://doi.org/10.3146/0095-3679-52.1-PS1614.

Bordenave, Nicolas, Stephane Grelier, and Veronique Coma. 2010. 'Hydrophobization and Antimicrobial Activity of Chitosan and Paper-Based Packaging Material'. *Biomacromolecules* 11 (1): 88–96. https://doi.org/10.1021/bm9009528.

Braunegg, G., B. Sonnleitner, and R. M. Lafferty. 1978. 'A Rapid Gas Chromatographic Method for the Determination of Poly-β-Hydroxybutyric Acid in Microbial Biomass'. *European Journal of Applied Microbiology and Biotechnology* 6 (1): 29–37. https://doi.org/10.1007/BF00500854.

Cabrera, Francisco, Álvaro Torres-Aravena, Fernanda Pinto-Ibieta, José Luis Campos, and David Jeison. 2021. 'On-Line Control of Feast/Famine Cycles to Improve PHB Accumulation during Cultivation of Mixed Microbial Cultures in Sequential Batch Reactors'. *International Journal of Environmental Research and Public Health* 18 (23): 12611. https://doi.org/10.3390/ijerph182312611.

Capanema, Nádia S. V., Alexandra A. P. Mansur, Sandhra M. Carvalho, et al. 2018. 'Physicochemical Properties and Antimicrobial Activity of Biocompatible Carboxymethylcellulose-Silver Nanoparticle Hybrids for Wound Dressing and Epidermal Repair'. *Journal of Applied Polymer Science* 135 (6): 45812. https://doi.org/10.1002/app.45812.

Célino, Amandine, Olivier Gonçalves, Frédéric Jacquemin, and Sylvain Fréour. 2014. 'Qualitative and Quantitative Assessment of Water Sorption in Natural Fibres Using ATR-FTIR Spectroscopy'. *Carbohydrate Polymers* 101: 163–70. https://doi.org/10.1016/j.carbpol.2013.09.023.

Chaudhari, Sandeep A., and Rekha S. Singhal. 2015. 'Cutin from Watermelon Peels: A Novel Inducer for Cutinase Production and Its Physicochemical Characterization'. *International Journal of Biological Macromolecules* 79: 398–404. https://doi.org/10.1016/j.ijbiomac.2015.05.006.

Christophliemk, Hanna, Erik Bohlin, Per Emilsson, and Lars Järnström. 2023. 'Surface Analyses of Thin Multiple Layer Barrier Coatings of Poly(Vinyl Alcohol) for Paperboard'. *Coatings* 13 (9): 9. https://doi.org/10.3390/coatings13091489.

Cifarelli, A., I. Cigognini, L. Bolzoni, and A. Montanari. 2016. 'Cutin Isolated from Tomato Processing By-Products: Extraction Methods and Characterization'. 1–20.

Colombo, Bianca, Francesca Favini, Barbara Scaglia, et al. 2017. 'Enhanced Polyhydroxyalkanoate (PHA) Production from the Organic Fraction of Municipal Solid Waste by Using Mixed Microbial Culture'. *Biotechnology for Biofuels* 10 (1): 201. https://doi.org/10.1186/s13068-017-0888-8.

Crétois, R., N. Follain, E. Dargent, et al. 2014. 'Microstructure and Barrier Properties of PHBV/Organoclays Bionanocomposites'. *Journal of Membrane Science* 467: 56–66. https://doi.org/10.1016/j.memsci.2014.05.015.

Cui, Yang, Zhenlan Xu, Shanshan Tang, Yawei Wang, and Guibin Jiang. 2022. 'Organochlorine Pesticides and Other Pesticides in Peanut Oil: Residue Level, Source, Household Processing Factor and Risk Assessment'. *Journal of Hazardous Materials* 429 (May): 128272. https://doi.org/10.1016/j.jhazmat.2022.128272.

Cunha, Ana Gisela, and Alessandro Gandini. 2010. 'Turning Polysaccharides into Hydrophobic Materials: A Critical Review. Part 1. Cellulose'. *Cellulose* 17 (5): 875–89. https://doi.org/10.1007/s10570-010-9434-6.

Dankovich, Theresa A., and You-Lo Hsieh. 2007. 'Surface Modification of Cellulose with Plant Triglycerides for Hydrophobicity'. *Cellulose* 14 (5): 469–80. https://doi.org/10.1007/s10570-007-9132-1.

David, Grégoire. 2019. 'Eco-Conversion de Résidus Lignocellulosiques de l'agriculture En Matériaux Composites Durables à Matrice Biopolyester.' These de doctorat, Montpellier. https://theses.fr/2019MONTG030.

David, Grégoire, Laurent Heux, Stéphanie Pradeau, Nathalie Gontard, and Hélène Angellier-Coussy. 2021. 'Upcycling of Vine Shoots: Production of Fillers for PHBV-Based Biocomposite Applications'. *Journal of Polymers and the Environment* 29 (2): 404–17. https://doi.org/10.1007/s10924-020-01884-8.

Doineau, Estelle, Coline Perdrier, Fanny Allayaud, et al. 2023. 'Designing Poly(3-Hydroxybutyrate-Co-3-Hydroxyvalerate) P(3HB-Co-3HV) Films with Tailored Mechanical Properties'. *Materials Today Communications* 36 (August): 106848. https://doi.org/10.1016/j.mtcomm.2023.106848.

Doineau, Estelle, Fleur Rol, Nathalie Gontard, and Hélène Angellier-Coussy. 2022. 'Physical-Chemical and Structural Stability of Poly(3HB-Co-3HV)/(Ligno-)Cellulosic Fibre-Based Biocomposites over Successive Dishwashing Cycles'. *Membranes* 12 (2): 127. https://doi.org/10.3390/membranes12020127.

Duan, Lifang, Xiaokang An, Xinglu Pan, et al. 2022. 'Residual Levels of Five Pesticides in Peanut Oil Processing and Chips Frying'. *Journal of the Science of Food and Agriculture* 102 (6): 2494–99. https://doi.org/10.1002/jsfa.11590.

Dufresne, Alain, Danièle Dupeyre, and Michel Paillet. 2003. 'Lignocellulosic Flour-reinforced Poly(Hydroxybutyrate-co-valerate) Composites'. *Journal of Applied Polymer Science* 87 (8): 1302–15. https://doi.org/10.1002/app.11546.

Durmuş, Ali, Maybelle Woo, Ahmet Kaşgöz, Christopher W. Macosko, and Michael Tsapatsis. 2007. 'Intercalated Linear Low Density Polyethylene (LLDPE)/Clay Nanocomposites Prepared with Oxidized Polyethylene as a New Type Compatibilizer: Structural, Mechanical and Barrier Properties'. *European Polymer Journal* 43 (9): 3737–49. https://doi.org/10.1016/j.eurpolymj.2007.06.019.

Elmehbad, Noura Y., Nadia A. Mohamed, and Nahed A. Abd El-Ghany. 2024. 'Synthesis of Novel Antimicrobial and Food-Preserving Hydrogel Nanocomposite Films Based on Carboxymethylcellulose'. *Starch - Stärke* 76 (7–8): 2300258. https://doi.org/10.1002/star.202300258.

Escórcio, Rita, Artur Bento, Ana S. Tomé, et al. 2022. 'Finding a Needle in a Haystack: Producing Antimicrobial Cutin-Derived Oligomers from Tomato Pomace'. *ACS Sustainable Chemistry & Engineering* 10 (34): 11415–27. https://doi.org/10.1021/acssuschemeng.2c03437.

European Commission. 2022. *Safe and Sustainable by Design Chemicals and Materials: A European Assessment Framework*. Publications Office of the European Union. https://data.europa.eu/doi/10.2777/86120.

Fasihah Zaaba, Nor, Hanafi Ismail, and Mariatti Jaafar. 2018. 'Recycled Polypropylene/Peanut Shell Powder (RPP/PSP) Composites: Property Comparison before and after Electron Beam Irradiation'. *Polymer Composites* 39 (9): 3048–56. https://doi.org/10.1002/pc.24309.

Freches, André, and Paulo C. Lemos. 2017. 'Microbial Selection Strategies for Polyhydroxyalkanoates Production from Crude Glycerol: Effect of OLR and Cycle Length'. *New Biotechnology* 39: 22–28. https://doi.org/10.1016/j.nbt.2017.05.011.

Gahlawat, Geeta, Preeti Kumari, and Neha Rani Bhagat. 2020. 'Technological Advances in the Production of Polyhydroxyalkanoate Biopolymers'. *Current Sustainable/Renewable Energy Reports* 7 (3): 73–83. https://doi.org/10.1007/s40518-020-00154-4.

Gallardo-Cervantes, Miguel, Yolanda González-García, Aida Alejandra Pérez-Fonseca, et al. 2021. 'Biodegradability and Improved Mechanical Performance of Polyhydroxyalkanoates/Agave Fiber Biocomposites Compatibilized by Different Strategies'. *Journal of Applied Polymer Science* 138 (15): 50182. https://doi.org/10.1002/app.50182.

Garcia-Garcia, Daniel, Alfredo Carbonell-Verdu, Amparo Jordá-Vilaplana, Rafael Balart, and David Garcia-Sanoguera. 2016. 'Development and Characterization of Green Composites from Bio-based Polyethylene and Peanut Shell'. *Journal of Applied Polymer Science* 133 (37): app.43940. https://doi.org/10.1002/app.43940.

Gold, Victor, Alan McNaught, and The International Union of Pure and Applied Chemistry (IUPAC), eds. 2025. *The IUPAC Compendium of Chemical Terminology: The Gold Book*. 5th edn. International Union of Pure and Applied Chemistry (IUPAC). https://doi.org/10.1351/goldbook.

Guan, Feixiang, Zhaoping Song, Furong Xin, et al. 2020. 'Preparation of Hydrophobic Transparent Paper via Using Polydimethylsiloxane as Transparent Agent'. *Journal of Bioresources and Bioproducts* 5 (1): 37–43. https://doi.org/10.1016/j.jobab.2020.03.004.

Guillard, Valérie, Sébastien Gaucel, Claudio Fornaciari, Hélène Angellier-Coussy, Patrice Buche, and Nathalie Gontard. 2018. 'The Next Generation of Sustainable Food Packaging to Preserve Our Environment in a Circular Economy Context'. *Frontiers in Nutrition* 5 (December): 121. https://doi.org/10.3389/fnut.2018.00121.

Guimarães, Tábata C., Everton S. Araújo, María Lucila Hernández-Macedo, and Jorge A. López. 2022. 'Polyhydroxyalkanoates: Biosynthesis from Alternative Carbon Sources and Analytic Methods: A Short Review'. *Journal of Polymers and the Environment* 30 (7): 2669–84. https://doi.org/10.1007/s10924-022-02403-7.

Heredia-Guerrero, José, Jose Benítez, Eva Dominguez, Roberto Cingolani, Athanassia Athanassiou, and Antonio Heredia. 2014. 'Infrared and Raman Spectroscopic Features of Plant Cuticles: A Review'. *Frontiers in Plant Science* 5. https://doi.org/10.3389/fpls.2014.00305.

Hood, Christine, Thamara Laredo, Alejandro G. Marangoni, and Erica Pensini. 2021. 'Water-Repellent Films from Corn Protein and Tomato Cutin'. *Journal of Applied Polymer Science* 138 (33): 50831. https://doi.org/10.1002/app.50831.

Hospodarova, Viola, Eva Singovszka, and Nadezda Stevulova. 2018. 'Characterization of Cellulosic Fibers by FTIR Spectroscopy for Their Further Implementation to Building Materials'. *American Journal of Analytical Chemistry* 9 (6): 6. https://doi.org/10.4236/ajac.2018.96023.

Hu, Zeshan, Xiaoyan Zen, Jian Gong, and Yulin Deng. 2009. 'Water Resistance Improvement of Paper by Superhydrophobic Modification with Microsized CaCO3 and Fatty Acid Coating'. *Colloids and Surfaces A: Physicochemical and Engineering Aspects* 351 (1): 65–70. https://doi.org/10.1016/j.colsurfa.2009.09.036.

Huang, Haibo, Long Mao, Wei Wang, Zhihan Li, and Chengrong Qin. 2023. 'A Facile Strategy to Fabricate Antibacterial Hydrophobic, High-Barrier, Cellulose Papersheets for Food Packaging'. *International Journal of Biological Macromolecules* 236: 123630. https://doi.org/10.1016/j.ijbiomac.2023.123630.

Hubbe, Martin, and Przemyslaw Pruszynski. 2020. 'Greaseproof Paper Products: A Review Emphasizing Ecofriendly Approaches'. *BioResources* 15. https://doi.org/10.15376/biores.15.1.1978-2004.

Hult, Eva-Lena, Jarmo Ropponen, Kristiina Poppius-Levlin, Taina Ohra-Aho, and Tarja Tamminen. 2013. 'Enhancing the Barrier Properties of Paper Board by a Novel Lignin Coating'. *Industrial Crops and Products* 50: 694–700. https://doi.org/10.1016/j.indcrop.2013.08.013.

International Organization for Standardization. 1993. *ISO 527-2:1993: Plastics — Determination of Tensile Properties — Part 2: Test Conditions for Moulding and Extrusion Plastics*. https://file.yizimg.com/305304/2009031608303684.pdf.

Islam, Md., S. Amin, Christopher Brown, Abdul Juraimi, Md. Uddin, and Aziz Arshad. 2022. 'Determination of the Most Efficient Household Technique for the Reduction of Pesticide Residues from Raw Fish Muscles'. *Foods* 11 (9): 1254. https://doi.org/10.3390/foods11091254.

Janowski, Grzegorz, Wiesław Frącz, Łukasz Bąk, et al. 2025. 'Effect of Coffee Grounds Content on Properties of PHBV Biocomposites Compared to Similar Composites with Other Fillers'. *Polymers* 17 (6): 764. https://doi.org/10.3390/polym17060764.

Jeffree, Christopher E. 2006. 'The Fine Structure of the Plant Cuticle'. In *Annual Plant Reviews Volume 23: Biology of the Plant Cuticle*. John Wiley & Sons, Ltd. https://doi.org/10.1002/9780470988718.ch2.

Johansson, Nils, and Joakim Krook. 2021. 'How to Handle the Policy Conflict between Resource Circulation and Hazardous Substances in the Use of Waste?' *Journal of Industrial Ecology* 25 (4): 994–1008. https://doi.org/10.1111/jiec.13103.

Kansal, Dhwani, Syeda Shamila Hamdani, Ruoqi Ping, and Muhammad Rabnawaz. 2020. 'Starch and Zein Biopolymers as a Sustainable Replacement for PFAS, Silicone Oil, and Plastic-Coated

Paper'. *Industrial & Engineering Chemistry Research* 59 (26): 12075–84. https://doi.org/10.1021/acs.iecr.0c01291.

Kansal, Dhwani, Syeda Shamila Hamdani, Ruoqi Ping, Nopphachai Sirinakbumrung, and Muhammad Rabnawaz. 2020. 'Food-Safe Chitosan–Zein Dual-Layer Coating for Water- and Oil-Repellent Paper Substrates'. *ACS Sustainable Chemistry & Engineering* 8 (17): 6887–97. https://doi.org/10.1021/acssuschemeng.0c02216.

Kariyanna, B., Sengottayan Senthil-Nathan, Prabhakaran Vasantha-Srinivasan, et al. 2024. 'Comprehensive Insights into Pesticide Residue Dynamics: Unraveling Impact and Management'. *Chemical and Biological Technologies in Agriculture* 11 (1): 182. https://doi.org/10.1186/s40538-024-00708-4.

Kerckhof, Frederiek-Maarten, Myrsini Sakarika, Marie Van Giel, et al. 2021. 'From Biogas and Hydrogen to Microbial Protein Through Co-Cultivation of Methane and Hydrogen Oxidizing Bacteria'. *Frontiers in Bioengineering and Biotechnology* 9: 733753. https://doi.org/10.3389/fbioe.2021.733753.

Khwaldia, Khaoula. 2010. 'Water Vapor Barrier and Mechanical Properties of Paper-Sodium Caseinate and Paper-Sodium Caseinate-Paraffin Wax Films'. *Journal of Food Biochemistry* 34 (5): 998–1013. https://doi.org/10.1111/j.1745-4514.2010.00345.x.

Khwaldia, Khaoula. 2013. 'Physical and Mechanical Properties of Hydroxypropyl Methylcellulose–Coated Paper as Affected by Coating Weight and Coating Composition'. *Bioresources* 8: 3438–52. https://doi.org/10.15376/biores.8.3.3438-3452.

Kim, Hyo Jeong, Lam Tan Hao, Ga-Hyeun Lee, et al. 2023. 'All-Natural Water-Resistant Paper Coated by Chitosan Nanowhiskers through Hydrophilic-to-Hydrophobic Self-Assembly'. *Progress in Organic Coatings* 182: 107672. https://doi.org/10.1016/j.porgcoat.2023.107672.

Kissa, Erik. 2001. *Fluorinated Surfactants and Repellents, Second Edition,*. CRC Press.

Kjellgren, Henrik, Mikael Gällstedt, Gunnar Engström, and Lars Järnström. 2006. 'Barrier and Surface Properties of Chitosan-Coated Greaseproof Paper'. *Carbohydrate Polymers* 65 (4): 453–60. https://doi.org/10.1016/j.carbpol.2006.02.005.

Koch, Kerstin, and Wilhelm Barthlott. 2009. 'Superhydrophobic and Superhydrophilic Plant Surfaces: An Inspiration for Biomimetic Materials'. *Philosophical Transactions. Series A, Mathematical, Physical, and Engineering Sciences* 367 (1893): 1487–509. https://doi.org/10.1098/rsta.2009.0022.

Koller, Martin, and Anindya Mukherjee. 2022. 'A New Wave of Industrialization of PHA Biopolyesters'. *Bioengineering (Basel, Switzerland)* 9 (2): 74. https://doi.org/10.3390/bioengineering9020074.

Kong, Y., and J. N. Hay. 2003. 'The Enthalpy of Fusion and Degree of Crystallinity of Polymers as Measured by DSC'. *European Polymer Journal* 39 (8): 1721–27. https://doi.org/10.1016/S0014-3057(03)00054-5.

Kunam, Praveen Kumar, Dakuri Ramakanth, Konala Akhila, and Kirtiraj K. Gaikwad. 2024. 'Bio-Based Materials for Barrier Coatings on Paper Packaging'. *Biomass Conversion and Biorefinery* 14 (12): 12637–52. https://doi.org/10.1007/s13399-022-03241-2.

Lammi, Sarah, Nicolas Le Moigne, Djamel Djenane, Nathalie Gontard, and Hélène Angellier-Coussy. 2018. 'Dry Fractionation of Olive Pomace for the Development of Food Packaging Biocomposites'. *Industrial Crops and Products* 120: 250–61. https://doi.org/10.1016/j.indcrop.2018.04.052.

Lavoine, Nathalie, Isabelle Desloges, Bertine Khelifi, and Julien Bras. 2014. 'Impact of Different Coating Processes of Microfibrillated Cellulose on the Mechanical and Barrier Properties of Paper'. *Journal of Materials Science* 49 (7): 2879–93. https://doi.org/10.1007/s10853-013-7995-0.

Laycock, Bronwyn, Monica V. Arcos-Hernandez, Alexandra Langford, et al. 2014. 'Thermal Properties and Crystallization Behavior of Fractionated Blocky and Random Polyhydroxyalkanoate Copolymers from Mixed Microbial Cultures'. *Journal of Applied Polymer Science* 131 (19): app.40836. https://doi.org/10.1002/app.40836.

Le Moigne, Nicolas, Belkacem Otazaghine, Stéphane Corn, Hélène Angellier-Coussy, and Anne Bergeret. 2018. *Surfaces and Interfaces in Natural Fibre Reinforced Composites*. SpringerBriefs in Molecular Science. Springer International Publishing. https://doi.org/10.1007/978-3-319-71410-3.

Le, Phat Thinh, and Khoi Tan Nguyen. 2020. 'Hydrophobizing Cellulose Surfaces via Catalyzed Transesterification Reaction Using Soybean Oil and Starch'. *Heliyon* 6 (11): e05559. https://doi.org/10.1016/j.heliyon.2020.e05559.

Lee, K-Y, F Quero, JJ Blaker, CAS Hill, SJ Eichhorn, and A Bismarck. 2011. 'Surface Only Modification of Bacterial Cellulose Nanofibres with Organic Acids'. *Cellulose* 18: 595–605. https://doi.org/10.1007/s10570-011-9525-z.

Lee, Sung-Eun, Qing X. Li, and Jian Yu. 2006. 'Proteomic Examination of Ralstonia Eutropha in Cellular Responses to Formic Acid'. *Proteomics* 6 (15): 4259–68. https://doi.org/10.1002/pmic.200500824.

Lehermeier, Hans J., John R. Dorgan, and J. Douglas Way. 2001. 'Gas Permeation Properties of Poly(Lactic Acid)'. *Journal of Membrane Science* 190 (2): 243–51. https://doi.org/10.1016/S0376-7388(01)00446-X.

Li, Nan, Sufeng Zhang, Yali Liu, Valentin Nica, and Sergiu Coseri. 2023. 'Surficial Modification of Cellulose with Oleic Acid via Amidation for Developing Water-Resisting Property'. *Industrial Crops and Products* 203: 117214. https://doi.org/10.1016/j.indcrop.2023.117214.

Liang, Shaobo, and Armando G. McDonald. 2014. 'Chemical and Thermal Characterization of Potato Peel Waste and Its Fermentation Residue as Potential Resources for Biofuel and Bioproducts Production'. *Journal of Agricultural and Food Chemistry* 62 (33): 8421–29. https://doi.org/10.1021/jf5019406.

Liu, Bing-Ying, Chao-Hua Xue, Qiu-Feng An, Shun-Tian Jia, and Miao-Miao Xu. 2019. 'Fabrication of Superhydrophobic Coatings with Edible Materials for Super-Repelling Non-Newtonian Liquid Foods'. *Chemical Engineering Journal* 371: 833–41. https://doi.org/10.1016/j.cej.2019.03.222.

Ludueña, L., A. Vázquez, and V. Alvarez. 2012. 'Effect of Lignocellulosic Filler Type and Content on the Behavior of Polycaprolactone Based Eco-Composites for Packaging Applications'. *Carbohydrate Polymers* 87 (1): 411–21. https://doi.org/10.1016/j.carbpol.2011.07.064.

Mahmoodi, Ali, Sajjad Ghodrati, and Manouchehr Khorasani. 2019. 'High-Strength, Low-Permeable, and Light-Protective Nanocomposite Films Based on a Hybrid Nanopigment and Biodegradable PLA for Food Packaging Applications'. *ACS Omega* 4 (12): 14947–54. https://doi.org/10.1021/acsomega.9b01731.

Majoudi, Naji, El-Houssaine Ablouh, Brahim Mazian, et al. 2025. 'Waterproofing of Cellulosic Materials by Hydrophobization with Oleic Acid: Thermochemical Modification and Structural Insights'. *International Journal of Biological Macromolecules* 305: 140936. https://doi.org/10.1016/j.ijbiomac.2025.140936.

Manrich, Anny, Francys K. V. Moreira, Caio G. Otoni, Marcos V. Lorevice, Maria A. Martins, and Luiz H. C. Mattoso. 2017. 'Hydrophobic Edible Films Made up of Tomato Cutin and Pectin'. *Carbohydrate Polymers* 164: 83–91. https://doi.org/10.1016/j.carbpol.2017.01.075.

Marc, Mathilde, Christelle Lopez, Noemie Viller, et al. 2024. 'From Tomato Pomaces Biorefinery to Biobased Shape-Memory Semicrystalline Polyester Networks'. *ACS Sustainable Chemistry & Engineering*, ahead of print. world. https://doi.org/10.1021/acssuschemeng.3c05713.

Marc, Mathilde, Regis Risani, Eric Desnoes, et al. 2021. 'Bioinspired Co-Polyesters of Hydroxy-Fatty Acids Extracted from Tomato Peel Agro-Wastes and Glycerol with Tunable Mechanical, Thermal and Barrier Properties'. *Industrial Crops and Products* 170 (October): 113718. https://doi.org/10.1016/j.indcrop.2021.113718.

Martins, Valter F. R., Manuela E. Pintado, Rui M. S. C. Morais, and Alcina M. M. B. Morais. 2024. 'Recent Highlights in Sustainable Bio-Based Edible Films and Coatings for Fruit and Vegetable Applications'. *Foods* 13 (2): 2. https://doi.org/10.3390/foods13020318.

Matar, Céline, Sébastien Gaucel, Nathalie Gontard, Stéphane Guilbert, and Valérie Guillard. 2018. 'Predicting Shelf Life Gain of Fresh Strawberries "*Charlotte* Cv" in Modified Atmosphere Packaging'. *Postharvest Biology and Technology* 142: 28–38. https://doi.org/10.1016/j.postharvbio.2018.03.002.

Mathel, Vincent, Shazed Aziz, Xiao Guo, et al. 2025. 'Wood/PHAs Biocomposites with Mechanical Properties Comparable to Conventional Plastics: Model-Based Prediction and Experimental Validation'. *Composites Part A: Applied Science and Manufacturing* 194: 108916. https://doi.org/10.1016/j.compositesa.2025.108916.

Matsui, K. N, F. D. S Larotonda, S. S Paes, D. B Luiz, A. T. N Pires, and J. B Laurindo. 2004. 'Cassava Bagasse-Kraft Paper Composites: Analysis of Influence of Impregnation with Starch Acetate on Tensile Strength and Water Absorption Properties'. *Carbohydrate Polymers* 55 (3): 237–43. https://doi.org/10.1016/j.carbpol.2003.07.007.

Mazur, Karolina E., Paulina Jakubowska, Anna Gaweł, and Stanisław Kuciel. 2022. 'Mechanical, Thermal and Hydrodegradation Behavior of Poly (3-Hydroxybutyrate-Co-3-Hydroxyvalerate) (PHBV) Composites with Agricultural Fibers as Reinforcing Fillers'. *Sustainable Materials and Technologies* 31: e00390. https://doi.org/10.1016/j.susmat.2022.e00390.

McNeill, Dayna Colleen, Akhilesh Kumar Pal, Debarshi Nath, et al. 2024. 'Upcycling of Ligno-Cellulosic Nutshells Waste Biomass in Biodegradable Plastic-Based Biocomposites Uses - a Comprehensive Review'. *Composites Part C: Open Access* 14: 100478. https://doi.org/10.1016/j.jcomc.2024.100478.

Meereboer, Kjeld W., Manjusri Misra, and Amar K. Mohanty. 2020. 'Review of Recent Advances in the Biodegradability of Polyhydroxyalkanoate (PHA) Bioplastics and Their Composites'. *Green Chemistry* 22 (17): 5519–58. https://doi.org/10.1039/D0GC01647K.

Mohammed, Mohammed, Msm Rasidi, Aeshah Mohammed, et al. 2022. 'Interfacial Bonding Mechanisms of Natural Fibre-Matrix Composites: An Overview'. *BioResources* 17 (4). https://doi.org/10.15376/biores.17.4.Mohammed.

Montaño-Leyva, Beatriz, Gabriela Ghizzi D. da Silva, Emmanuelle Gastaldi, Patricia Torres-Chávez, Nathalie Gontard, and Hélène Angellier-Coussy. 2013. 'Biocomposites from Wheat Proteins and Fibers: Structure/Mechanical Properties Relationships'. *Industrial Crops and Products* 43: 545–55. https://doi.org/10.1016/j.indcrop.2012.07.065.

Motedayen, Ali Akbar, Mohammadreza Rezaeigolestani, Carole Guillaume, Valérie Guillard, and Nathalie Gontard. 2019. 'Gas Barrier Enhancement of Uncharged Apolar Polymeric Films by Self-Assembling Stratified Nano-Composite Films'. *RSC Advances* 9 (19): 10938–47. https://doi.org/10.1039/C9RA01109A.

Mroczkowska, Marta, David Culliton, Kieran J. Germaine, Manasa Hegde, Edmond F. Tobin, and Adriana Cunha Neves. 2024. 'Valorisation of Tomato Waste as a Source of Cutin for Hydrophobic Surface Coatings to Protect Starch- and Gelatine-Blend Bioplastics'. *Biomass* 4 (3): 990–1004. https://doi.org/10.3390/biomass4030055.

Munch, Mélanie, Patrice Buche, Stéphane Dervaux, et al. 2022. 'Biocomposites from Poly(3-Hydroxybutyrate-Co-3-Hydroxyvalerate) and Lignocellulosic Fillers: Processes Stored in Data Warehouse Structured by an Ontology'. *Data in Brief* 42: 108191. https://doi.org/10.1016/j.dib.2022.108191.

Ninčević Grassino, Antonela, Senka Djaković, Tomislav Bosiljkov, et al. 2020. 'Valorisation of Tomato Peel Waste as a Sustainable Source for Pectin, Polyphenols and Fatty Acids Recovery Using Sequential Extraction'. *Waste and Biomass Valorization* 11 (9): 4593–611. https://doi.org/10.1007/s12649-019-00814-7.

Nygaard, Daiana, Oxana Yashchuk, and Élida Beatriz Hermida. 2025. 'Cupriavidus Necator: A Sustainable Triple Tool for Waste Reduction, Biopolymer Production, and Cost Optimization'. *Cleaner Materials* 17: 100332. https://doi.org/10.1016/j.clema.2025.100332.

Ogihara, Hitoshi, Jing Xie, Jun Okagaki, and Tetsuo Saji. 2012. 'Simple Method for Preparing Superhydrophobic Paper: Spray-Deposited Hydrophobic Silica Nanoparticle Coatings Exhibit High Water-Repellency and Transparency'. *Langmuir* 28 (10): 4605–8. https://doi.org/10.1021/la204492q.

O'Hare, Lesley-Ann, Stuart Leadley, and Bhukan Parbhoo. 2002. 'Surface Physicochemistry of Corona-Discharge-Treated Polypropylene Film'. *Surface and Interface Analysis* 33 (4): 335–42. https://doi.org/10.1002/sia.1217.

Omeje, Kingsley O., Benjamin O. Ezema, Finbarr Okonkwo, et al. 2021. 'Quantification of Heavy Metals and Pesticide Residues in Widely Consumed Nigerian Food Crops Using Atomic Absorption Spectroscopy (AAS) and Gas Chromatography (GC)'. *Toxins* 13 (12): 870. https://doi.org/10.3390/toxins13120870.

Oswald, I, M Villano, A Marchetti, et al. 2024. *First Report on Contaminant Circular Safety: Safety Aspects Related to Contaminants Presence and Possible Transfer from Feedstock to End-*

Products. https://www.agriloop-project.eu/wp-content/uploads/2024/05/D1.7_20240528_INRAE.pdf.

Ouatmani, Toufik, Hayate Haddadi-Guemghar, Lila Boulekbache-Makhlouf, Djamila Mehidi-Terki, Azzedine Maouche, and Khodir Madani. 2022. 'A Sustainable Valorization of Industrial Tomato Seeds (Cv Rio Grande): Sequential Recovery of a Valuable Oil and Optimized Extraction of Antioxidants by Microwaves'. *Journal of Food Processing and Preservation* 46 (1): e16123. https://doi.org/10.1111/jfpp.16123.

Owens, D. K., and R. C. Wendt. 1969. 'Estimation of the Surface Free Energy of Polymers'. *Journal of Applied Polymer Science* 13 (8): 1741–47. https://doi.org/10.1002/app.1969.070130815.

Ozdemir, M., C. U. Yurteri, and H. Sadikoglu. 1999. 'Physical Polymer Surface Modification Methods and Applications in Food Packaging Polymers'. *Critical Reviews in Food Science and Nutrition* 39 (5): 457–77. https://doi.org/10.1080/10408699991279240.

Pagliano, Giorgia, Paola Galletti, Chiara Samorì, Agnese Zaghini, and Cristian Torri. 2021. 'Recovery of Polyhydroxyalkanoates From Single and Mixed Microbial Cultures: A Review'. *Frontiers in Bioengineering and Biotechnology* 9 (February). https://doi.org/10.3389/fbioe.2021.624021.

Palai, Bishwabhusana, Manoranjan Biswal, Smita Mohanty, and Sanjay Kumar Nayak. 2019. 'In Situ Reactive Compatibilization of Polylactic Acid (PLA) and Thermoplastic Starch (TPS) Blends; Synthesis and Evaluation of Extrusion Blown Films Thereof'. *Industrial Crops and Products* 141: 111748. https://doi.org/10.1016/j.indcrop.2019.111748.

Paloyan, Ani, Mane Tadevosyan, Diana Ghevondyan, et al. 2025. 'Biodegradation of Polyhydroxyalkanoates: Current State and Future Prospects'. *Frontiers in Microbiology* 16: 1542468. https://doi.org/10.3389/fmicb.2025.1542468.

Pandiselvam, Ravi, Rathnakumar Kaavya, Anandu Chandra Khanashyam, et al. 2022. 'Research Trends and Emerging Physical Processing Technologies in Mitigation of Pesticide Residues on Various Food Products'. *Environmental Science and Pollution Research* 29 (30): 45131–49. https://doi.org/10.1007/s11356-022-20338-3.

Parvathy, P. A., and Sushanta K. Sahoo. 2021. 'Hydrophobic, Moisture Resistant and Biorenewable Paper Coating Derived from Castor Oil Based Epoxy Methyl Ricinoleate with Repulpable Potential'. *Progress in Organic Coatings* 158: 106347. https://doi.org/10.1016/j.porgcoat.2021.106347.

Paul, Alexander G., Kevin C. Jones, and Andrew J. Sweetman. 2009. 'A First Global Production, Emission, And Environmental Inventory For Perfluorooctane Sulfonate'. *Environmental Science & Technology* 43 (2): 386–92. https://doi.org/10.1021/es802216n.

Pecorini, Gianni, Martina Tamburriello, Erika Maria Tottoli, et al. 2025. 'Transforming Agro-Waste Cutin into Sustainable Materials for Biomedical Innovations'. *Polymers* 17 (6): 742. https://doi.org/10.3390/polym17060742.

Perdoch, Waldemar, Tomasz Nowak, and Konrad Olejnik. 2025. 'Sustainable Hydrophobization of Paper and Packaging for Road Transport of Dangerous Goods – Surface Treatment with Silane-Modified Starch'. *Progress in Organic Coatings* 205: 109312. https://doi.org/10.1016/j.porgcoat.2025.109312.

Perez-Ameneiro, M., G. Bustos, X. Vecino, L. Barbosa-Pereira, J. M. Cruz, and A. B. Moldes. 2015. 'Heterogenous Lignocellulosic Composites as Bio-Based Adsorbents for Wastewater Dye Removal: A Kinetic Comparison'. *Water, Air, & Soil Pollution* 226 (5): 133. https://doi.org/10.1007/s11270-015-2393-7.

Peydecastaing, J., S. Girardeau, C. Vaca-Garcia, and M. E. Borredon. 2006. 'Long Chain Cellulose Esters with Very Low DS Obtained with Non-Acidic Catalysts'. *Cellulose* 13 (1): 95–103. https://doi.org/10.1007/s10570-005-9012-5.

Philippe, Glenn, Nathalie Geneix, Johann Petit, et al. 2020. 'Assembly of Tomato Fruit Cuticles: A Cross-Talk between the Cutin Polyester and Cell Wall Polysaccharides'. *New Phytologist* 226 (3): 809–22. https://doi.org/10.1111/nph.16402.

Phopin, Kamonrat, Sompon Wanwimolruk, Chosita Norkaew, Jaruwat Buddhaprom, and Chartchalerm Isarankura-Na-Ayudhya. 2022. 'Boiling, Blanching, and Stir-Frying Markedly Reduce Pesticide Residues in Vegetables'. *Foods* 11 (10): 1463. https://doi.org/10.3390/foods11101463.

Piercy, Ellen, Peter R Ellis, and Miao Guo. 2024. 'Microbial Upcycling of Food Waste Using Anaerobic Digestion for Energy and Single Cell Protein Production'. *Current Opinion in Food Science* 57: 101173. https://doi.org/10.1016/j.cofs.2024.101173.

Pieters, Kyle, and Tizazu H. Mekonnen. 2024. 'Stable Aqueous Dispersions of Poly(3-Hydroxybutyrate-Co-3-Hydroxyvalerate) (PHBV) Polymer for Barrier Paper Coating'. *Progress in Organic Coatings* 187: 108101. https://doi.org/10.1016/j.porgcoat.2023.108101.

Pignères, Emma, Sébastien Gaucel, Fanny Coffigniez, et al. 2024. 'Deciphering the Respective Roles of Coating Weight and Number of Layers on the Mass Transfer Properties of Polyvinyl Alcohol Coated Cardboards'. *Progress in Organic Coatings* 195: 108627. https://doi.org/10.1016/j.porgcoat.2024.108627.

Polovka, Martin, Júlia Polovková, Katarína Vizárová, Soňa Kirschnerová, Lenka Bieliková, and Milan Vrška. 2006. 'The Application of FTIR Spectroscopy on Characterization of Paper Samples, Modified by Bookkeeper Process'. *Vibrational Spectroscopy* 41 (1): 112–17. https://doi.org/10.1016/j.vibspec.2006.01.010.

Popescu (Stegarus), Diana Ionela, Corina Mihaela Oprita (Cioara), Radu Tamaian, and Violeta-Carolina Niculescu. 2024. 'Consumer Safety and Pesticide Residues: Evaluating Mitigation Protocols for Greengrocery'. *Journal of Xenobiotics* 14 (4): 1638–69. https://doi.org/10.3390/jox14040088.

Radić, Kristina, Emerik Galić, Tomislav Vinković, Nikolina Golub, and Dubravka Vitali Čepo. 2024. 'Tomato Waste as a Sustainable Source of Antioxidants and Pectins: Processing, Pretreatment and Extraction Challenges'. *Sustainability* 16 (21): 21. https://doi.org/10.3390/su16219158.

Rasool, Kashif, Sabir Hussain, Asif Shahzad, et al. 2023. 'Comprehensive Insights into Sustainable Conversion of Agricultural and Food Waste into Microbial Protein for Animal Feed Production'. *Reviews in Environmental Science and Bio/Technology* 22 (2): 527–62. https://doi.org/10.1007/s11157-023-09651-6.

Rastogi, Vibhore Kumar, and Pieter Samyn. 2015. 'Bio-Based Coatings for Paper Applications'. *Coatings* 5 (4): 4. https://doi.org/10.3390/coatings5040887.

Raza, Zulfiqar Ali, Sharjeel Abid, and Ibrahim M. Banat. 2018. 'Polyhydroxyalkanoates: Characteristics, Production, Recent Developments and Applications'. *International Biodeterioration & Biodegradation* 126: 45–56. https://doi.org/10.1016/j.ibiod.2017.10.001.

Reis, M., Maria Albuquerque, M. Villano, and Mauro Majone. 2011. 'Mixed Culture Processes for Polyhydroxyalkanoate Production from Agro-Industrial Surplus/Wastes as Feedstocks'. *Comprehensive Biotechnology* 6: 669–83. https://doi.org/10.1016/B978-0-08-088504-9.00464-5.

Reynoud, Nicolas, Johann Petit, Cécile Bres, et al. 2021. 'The Complex Architecture of Plant Cuticles and Its Relation to Multiple Biological Functions'. *Frontiers in Plant Science* 12 (December). https://doi.org/10.3389/fpls.2021.782773.

Rhim, Jong-Whan, Jun-Ho Lee, and Seok-In Hong. 2006. 'Water Resistance and Mechanical Properties of Biopolymer (Alginate and Soy Protein) Coated Paperboards'. *LWT - Food Science and Technology* 39 (7): 806–13. https://doi.org/10.1016/j.lwt.2005.05.008.

Riederer, M., and L. Schreiber. 2001. 'Protecting against Water Loss: Analysis of the Barrier Properties of Plant Cuticles'. *Journal of Experimental Botany* 52 (363): 2023–32. https://doi.org/10.1093/jexbot/52.363.2023.

Rodrigues, Ana Marta, Rita Dias Guardão Franca, Madalena Dionísio, et al. 2022. 'Polyhydroxyalkanoates from a Mixed Microbial Culture: Extraction Optimization and Polymer Characterization'. *Polymers* 14 (11): 2155. https://doi.org/10.3390/polym14112155.

Rodríguez-Fabià, Sandra, Jonathan Torstensen, Lars Johansson, and Kristin Syverud. 2022a. 'Hydrophobisation of Lignocellulosic Materials Part I: Physical Modification'. *Cellulose* 29 (10): 5375–93. https://doi.org/10.1007/s10570-022-04620-8.

Rodríguez-Fabià, Sandra, Jonathan Torstensen, Lars Johansson, and Kristin Syverud. 2022b. 'Hydrophobization of Lignocellulosic Materials Part II: Chemical Modification'. *Cellulose* 29 (17): 8957–95. https://doi.org/10.1007/s10570-022-04824-y.

Rodríguez-Fabià, Sandra, Jonathan Torstensen, Lars Johansson, and Kristin Syverud. 2022c. 'Hydrophobization of Lignocellulosic Materials Part III: Modification with Polymers'. *Cellulose* 29 (11): 5943–77. https://doi.org/10.1007/s10570-022-04660-0.

Sabapathy, Poorna Chandrika, Sabarinathan Devaraj, Katharina Meixner, et al. 2020. 'Recent Developments in Polyhydroxyalkanoates (PHAs) Production – A Review'. *Bioresource Technology* 306: 123132. https://doi.org/10.1016/j.biortech.2020.123132.

Sakarika, Myrsini, Pieter Candry, Mathilde Depoortere, Ramon Ganigué, and Korneel Rabaey. 2020. 'Impact of Substrate and Growth Conditions on Microbial Protein Production and Composition'. *Bioresource Technology* 317: 124021. https://doi.org/10.1016/j.biortech.2020.124021.

Salvatori, Gaia, Angela Marchetti, Anna Maria Russo, et al. 2025. 'Pilot-Scale Acidogenic Fermentation of Reground Pasta Byproduct for Polyhydroxyalkanoate Production with Mixed Microbial Cultures'. *ACS Sustainable Chemistry & Engineering* 13 (8): 3024–35. https://doi.org/10.1021/acssuschemeng.4c03754.

Santos, Jackson Wesley Silva dos, Vitor Augusto dos Santos Garcia, Anna Cecilia Venturini, Rosemary Aparecida de Carvalho, Classius Ferreira da Silva, and Cristiana Maria Pedroso Yoshida. 2022.

'Sustainable Coating Paperboard Packaging Material Based on Chitosan, Palmitic Acid, and Activated Carbon: Water Vapor and Fat Barrier Performance'. *Foods* 11 (24): 24. https://doi.org/10.3390/foods11244037.

Shahid, Mohammad, Saptarshi Maiti, Ravindra V. Adivarekar, and Shanhu Liu. 2022. 'Biomaterial Based Fabrication of Superhydrophobic Textiles – A Review'. *Materials Today Chemistry* 24: 100940. https://doi.org/10.1016/j.mtchem.2022.100940.

Shanmathy, Mrithula, Monalisha Mohanta, and A. Thirugnanam. 2021. 'Development of Biodegradable Bioplastic Films from Taro Starch Reinforced with Bentonite'. *Carbohydrate Polymer Technologies and Applications* 2 (December): 100173. https://doi.org/10.1016/j.carpta.2021.100173.

Shen, Zhenghui, Araz Rajabi-Abhari, Kyudeok Oh, Guihua Yang, Hye Jung Youn, and Hak Lae Lee. 2021. 'Improving the Barrier Properties of Packaging Paper by Polyvinyl Alcohol Based Polymer Coating—Effect of the Base Paper and Nanoclay'. *Polymers* 13 (8): 1334. https://doi.org/10.3390/polym13081334.

Si, Yifan, Zhiguang Guo, and Weimin Liu. 2016. 'A Robust Epoxy Resins @ Stearic Acid-Mg(OH)2 Micronanosheet Superhydrophobic Omnipotent Protective Coating for Real-Life Applications'. *ACS Applied Materials & Interfaces* 8 (25): 16511–20. https://doi.org/10.1021/acsami.6b04668.

Singh, S, and A Mohanty. 2007. 'Wood Fiber Reinforced Bacterial Bioplastic Composites: Fabrication and Performance Evaluation'. *Composites Science and Technology* 67 (9): 1753–63. https://doi.org/10.1016/j.compscitech.2006.11.009.

Singh, Singam Suranjoy, Amr Zaitoon, Sonu Sharma, Annamalai Manickavasagan, and Loong-Tak Lim. 2022. 'Enhanced Hydrophobic Paper-Sheet Derived from *Miscanthus × Giganteus* Cellulose Fibers Coated with Esterified Lignin and Cellulose Acetate Blend'. *International Journal of Biological Macromolecules* 223: 1243–56. https://doi.org/10.1016/j.ijbiomac.2022.11.066.

Singha, Shuvra, Vasantha Gowda, and Mikael Hedenqvist. 2021. 'Plant Cuticle-Inspired Polyesters as Promising Green and Sustainable Polymer Materials'. *ACS Applied Polymer Materials*, ahead of print. https://doi.org/10.1021/acsapm.1c00585.

Siqueira, Maria C., Gustavo F. Coelho, Márcia R. de Moura, et al. 2014. 'Evaluation of Antimicrobial Activity of Silver Nanoparticles for Carboxymethylcellulose Film Applications in Food Packaging'. *Journal of Nanoscience and Nanotechnology* 14 (7): 5512–17. https://doi.org/10.1166/jnn.2014.8991.

Słowik-Borowiec, Magdalena, and Ewa Szpyrka. 2020. 'Selected Food Processing Techniques as a Factor for Pesticide Residue Removal in Apple Fruit'. *Environmental Science and Pollution Research* 27 (2): 2361–73. https://doi.org/10.1007/s11356-019-06943-9.

Stinga, Camelia. 2008. 'The Use of Chromatogenic Chemistry for the Conception and Realization of Cellulosic Materials, Barrier to Water, Greases and Gas.' Université Joseph Fourier.

Subramani, Thirukkumar, Hemalatha Ganapathyswamy, Vellaikumar Sampathrajan, Amutha Sundararajan, and Murugan Marimuthu. 2022. 'Effect of Simple Processing on Selected Pesticide Residues in Cottonseed (Gossypium Spp.)'. *Journal of Applied and Natural Science* 14 (SI): 176–85. https://doi.org/10.31018/jans.v14iSI.3606.

Tedeschi, Giacomo, Jose Benítez, Luca Ceseracciu, et al. 2018. 'Sustainable Fabrication of Plant Cuticle-Like Packaging Films from Tomato Pomace Agro-Waste, Beeswax, and Alginate'. *ACS Sustainable Chemistry & Engineering* 6. https://doi.org/10.1021/acssuschemeng.8b03450.

Tedeschi, Giacomo, José Jesús Benitez, Luca Ceseracciu, et al. 2018. 'Sustainable Fabrication of Plant Cuticle-Like Packaging Films from Tomato Pomace Agro-Waste, Beeswax, and Alginate'. *ACS Sustainable Chemistry & Engineering* 6 (11): 14955–66. https://doi.org/10.1021/acssuschemeng.8b03450.

Teeri, Tuula T., Harry Brumer, Geoff Daniel, and Paul Gatenholm. 2007. 'Biomimetic Engineering of Cellulose-Based Materials'. *Trends in Biotechnology* 25 (7): 299–306. https://doi.org/10.1016/j.tibtech.2007.05.002.

Terfe, Amare, Seblework Mekonen, and Temima Jemal. 2023. 'Pesticide Residues and Effect of Household Processing in Commonly Consumed Vegetables in Jimma Zone, Southwest Ethiopia'. *Journal of Environmental and Public Health* 2023: 1–12. https://doi.org/10.1155/2023/7503426.

USDA. 2025. 'Peanut Explorer'. https://ipad.fas.usda.gov/cropexplorer/cropview/commodityView.aspx?cropid=2221000&sel_year=2025&rankby=Production.

Valentino, Francesco, Giulia Moretto, Laura Lorini, David Bolzonella, Paolo Pavan, and Mauro Majone. 2019. 'Pilot-Scale Polyhydroxyalkanoate Production from Combined Treatment of Organic Fraction of Municipal Solid Waste and Sewage Sludge'. *Industrial & Engineering Chemistry Research* 58 (27): 12149–58. https://doi.org/10.1021/acs.iecr.9b01831.

Viretto, Amandine, Nathalie Gontard, and Hélène Angellier-Coussy. 2021. 'Urban Parks and Gardens Green Waste: A Valuable Resource for the Production of Fillers for Biocomposites Applications'. *Waste Management* 120: 538–48. https://doi.org/10.1016/j.wasman.2020.10.018.

Wang, Hongxia, Hua Zhou, Adrian Gestos, Jian Fang, and Tong Lin. 2013. 'Robust, Superamphiphobic Fabric with Multiple Self-Healing Ability against Both Physical and Chemical Damages'. *ACS Applied Materials & Interfaces* 5 (20): 10221–26. https://doi.org/10.1021/am4029679.

Wei, Liqing, Nicholas M. Guho, Erik R. Coats, and Armando G. McDonald. 2014. 'Characterization of Poly(3-Hydroxybutyrate-Co-3-Hydroxyvalerate) Biosynthesized by Mixed Microbial Consortia Fed Fermented Dairy Manure'. *Journal of Applied Polymer Science* 131 (11): n/a. https://doi.org/10.1002/APP.40333.

Wennman, Maria, Mårten Hellberg, Anna J. Svagan, and Mikael S. Hedenqvist. 2023. 'A Biobased Binder of Emulsion Type That Provides Unique and Durable Wet Strength and Hydrophobicity to Paper and Nonwoven'. *Industrial Crops and Products* 193: 116126. https://doi.org/10.1016/j.indcrop.2022.116126.

Xiao, Ouli, Minmin Li, Jieyin Chen, Xiaofeng Dai, and Zhiqiang Kong. 2025. 'A Comprehensive Analysis of the Fates of Pesticide Residues in Edible Agricultural Products during Food Processing'. *Journal of Agricultural and Food Chemistry* 73 (30): 18525–44. https://doi.org/10.1021/acs.jafc.5c05285.

Yaashikaa, P. R., P. Senthil Kumar, and Sunita Varjani. 2022. 'Valorization of Agro-Industrial Wastes for Biorefinery Process and Circular Bioeconomy: A Critical Review'. *Bioresource Technology* 343: 126126. https://doi.org/10.1016/j.biortech.2021.126126.

Yadav, Jyoti, Dr Datta, and Vinod Gour. 2014. 'Developing Hydrophobic Paper as a Packaging Material Using Epicuticular Wax: A Sustainable Approach'. *Bioresources* 9: 5066–72. https://doi.org/10.15376/biores.9.3.5066-5072.

Yamoum, Chamaiporn, and Rathanawan Magaraphan. 2017. 'Effect of Peanut Shell Content on Mechanical, Thermal, and Biodegradable Properties of Peanut Shell/Polylactic Acid Biocomposites'. *Polymer Composites* 38 (4): 682–90. https://doi.org/10.1002/pc.23627.

Yang, Xiao Hong, and Wei Ling Zhu. 2007. 'Viscosity Properties of Sodium Carboxymethylcellulose Solutions'. *Cellulose* 14 (5): 409–17. https://doi.org/10.1007/s10570-007-9137-9.

Yaraghi, Nicholas A., and David Kisailus. 2018. 'Biomimetic Structural Materials: Inspiration from Design and Assembly'. *Annual Review of Physical Chemistry* 69: 23–57. https://doi.org/10.1146/annurev-physchem-040215-112621.

Yeats, Trevor H., and Jocelyn K. C. Rose. 2013. 'The Formation and Function of Plant Cuticles'. *Plant Physiology* 163 (1): 5–20. https://doi.org/10.1104/pp.113.222737.

Zaaba, Nor Fasihah, and Hanafi Ismail. 2020. 'The Influence of Different Compounding Sequence and Peanut Shell Powder Loading on Properties of Polylactic Acid/Thermoplastic Corn Starch Biocomposites'. *Journal of Vinyl and Additive Technology* 26 (4): 413–22. https://doi.org/10.1002/vnl.21756.

Zaaba, Nor Fasihah, Hanafi Ismail, and Mariatti Jaafar. 2014. 'The Effects of Modifying Peanut Shell Powder with Polyvinyl Alcohol on the Properties of Recycled Polypropylene and Peanut Shell Powder Composites'. *BioResources* 9 (2): 2128–42.

Zhang, An-An, Parag Prakash Sutar, Qiang Bian, Xiao-Ming Fang, Jia-Bao Ni, and Hong-Wei Xiao. 2022. 'Pesticide Residue Elimination for Fruits and Vegetables: The Mechanisms, Applications, and Future Trends of Thermal and Non-Thermal Technologies'. *Journal of Future Foods* 2 (3): 223–40. https://doi.org/10.1016/j.jfutfo.2022.06.004.

Zhang, Weiwei, Huining Xiao, and Liying Qian. 2014. 'Enhanced Water Vapour Barrier and Grease Resistance of Paper Bilayer-Coated with Chitosan and Beeswax'. *Carbohydrate Polymers* 101: 401–6. https://doi.org/10.1016/j.carbpol.2013.09.097.

Zhang, Wewei, Peng Lu, Liying Qian, and Huining Xiao. 2014. 'Fabrication of Superhydrophobic Paper Surface via Wax Mixture Coating'. *Chemical Engineering Journal* 250: 431–36. https://doi.org/10.1016/j.cej.2014.04.050.

Zhao, Xia, Tao Hu, and Junping Zhang. 2018. 'Superhydrophobic Coatings with High Repellency to Daily Consumed Liquid Foods Based on Food Grade Waxes'. *Journal of Colloid and Interface Science* 515: 255–63. https://doi.org/10.1016/j.jcis.2018.01.034.

Zheng, Chang Ji, Jung-Sung Yoo, Tae-Gyu Lee, Hee-Young Cho, Young-Ho Kim, and Won-Gon Kim. 2005. 'Fatty Acid Synthesis Is a Target for Antibacterial Activity of Unsaturated Fatty Acids'. *FEBS Letters* 579 (23): 5157–62. https://doi.org/10.1016/j.febslet.2005.08.028.